学校代码：10246
学　　号：22210190012

復旦大學

硕 士 学 位 论 文

（学术学位）

膜与 $C^\vee C_1$ 型 DAHA 代数的表示

Branes and Representations of DAHA $C^\vee C_1$

院　　系：　物理学系
专　　业：　物理学
姓　　名：　黄俊康
指 导 教 师：Satoshi Nawata　教授
完 成 日 期：　2025 年 6 月 20 日

Contents

中文摘要

对经典系统的量子化一直都是一个未彻底解决的重要问题。从上世纪量子力学的诞生以来至今，物理学家们从未停止对量子化框架的思考。在将近一百年前，狄拉克提出了量子化的基本公理。然而在这些最简单自然的量子化公理的约束下，人们至今依然没能够找到一个完备且自然的数学框架来描述量子化。几何量子化[1–2]（geometric quantization）是已知的量子化框架之中影响力最大的。该量子化框架要求在预量子化的基础上，选择一个极化方向（polarization），从而完成对量子希尔伯特空间的构建。然而极化方向的选择使得几何量子化的失去了自然性。形变量子化[3–4]（deformation quantization）对观测量代数进行系统的形变研究，能够给出任何经典系统观测量代数的量子形变的广泛结构。然而形变量子化却并不能够对量子希尔伯特空间给出足够信息。

膜量子化[5–6]（brane quantization）是一个非常新的量子化框架。该框架虽然没办法解决通常量子化方案的主要问题，但是却能以深刻的方式沟通多个不同的框架，联系不同的领域。具体来说，膜量子化能够利用二维拓扑 A 模型，将几何量子化与形变量子化两个框架包含其中。形变量子化对应 A 模型中一种特殊的 A 膜（称为正则余迷向 A 膜 canonical coisotropic A-brane）到自身的拓扑弦代数，几何量子化的希尔伯特空间对应于正则迷向 A 膜到其他拉格朗日 A 膜的拓扑弦的空间。前者给出了形变量子化的一种新的理解方式，而后者给出了几何与代数的直接对应。由于正则迷向 A 膜到自身的拓扑弦的代数能够自然作用在它到其他 A 膜的拓扑弦空间上，每一个拉格朗日 A 膜能够与形变量子化代数的一个表示对应起来，因此这给出了用几何方式来理解代数的表示的全新途径。

四维 $\mathcal{N} = 2$ 超对称场论是近三十年理论物理研究的最热门的理论模型之一。上世纪九十年代 Seiberg 和 Witten[7–8]提出了新颖的方法对这些理论在库伦分支（Coulomb branch）上的低能有效理论进行了精确的求解，揭示了四维超对称理论与六维场论、膜理论、拓扑不变量等理论的深刻联系，对各个领域产生了深远的影响。当四维 $\mathcal{N} = 2$ 理论紧致化在圆环上后，库伦分支将被扩充成一个椭圆纤维丛，称为希钦纤维丛[9]（Hitchin fibration）。这个椭圆纤维丛具有超卡勒结构，既等同于一个四穿孔球上的希格斯丛（Higgs bundles）的模空间，也等同于四穿孔球上的平坦联络的模空间。

本研究将膜量子化的框架应用于具有 $SU(2)$ 规范群的希钦纤维丛上，研究

该空间上的全纯函数形变量子化代数的表示与拉格朗日 A 膜之间的一一对应。该希钦纤维丛等同于四穿孔球上的平坦 $SL(2,\mathbb{C})$ 联络模空间，而后者可以被一个三次方程描述

$$-xyz + x^2 + y^2 + z^2 + \theta_1 x + \theta_2 y + \theta_3 z + \theta_4 = 0\,. \tag{1}$$

该空间上的全纯函数的形变量子化代数被 Oblomkov[10]证明为球对称双仿射 Hecke 代数（spherical DAHA）。因此，该空间上的拉格朗日 A 膜与球对称 DAHA 代数的表示具有对应关系。本研究的主要内容是：在几何方面，研究希钦纤维丛空间中可能的拉格朗日子流形，找出对应的 A 膜条件以及 A 膜的体积表达式；在代数方面，利用 Askey-Wilson 多项式研究球对称 DAHA 代数的表示论，分类表示的退化条件（shortening conditions）以及维度；基于两方面的结果，建立 A 膜与表示的一一对应关系。

这项工作具有多个方面的意义：首先，本项目能够给出膜量子化框架直接且不平凡的验证，为量子化理论提供新的实例；其次，本项目对库伦分支的几何与拓扑进行了较细致的分析，加深了我们对库伦分支以及四维场论低能有效理论的理解，还给出了 Argyres-Douglas 共形场论的一种直观的几何理解；最后，本项目建立了库伦分支几何与 DAHA 代数表示之间的对应，同时给两方面的科研提供了新的研究思路，对几何朗兰兹纲领、几何表示论等方向都具有意义，推动了数学与物理、几何与代数之间的交融。

本篇论文的内容主要分为六个章节：§1介绍基本的研究背景；§2介绍膜量子化的基本概念；§3研究希钦纤维丛的几何以及 A 膜；§4研究 DAHA 代数及其表示；§5 建立 A 膜与表示之间的对应；§6给出本研究的主要结论。

本论文的具体结构如下：

在第二章 §2中，我将介绍膜量子化的基本框架。具体来说，在 §2.1中，我将介绍几何量子化的基本概念。一个量子化映射可以简单表述为一个将辛流形上的函数映到一个希尔伯特空间上的算符的映射。该映射需要满足狄拉克公理：（1）线性性（2）将泊松括号映到算符对易子（3）将常值函数映到常数算符。

选定辛流形上的一个预量子线丛及其上的一个 $U(1)$ 联络，我们可以定义一个预量子化映射 $\mathfrak{P}$ 同时满足三条公理。几何量子化在此基础上给该辛流形上赋予了一个额外的极化方向结构，使得希尔伯特空间中的波函数能够被解释为预量子线丛中沿极化方向不变的截面。

在 §2.2中，我将介绍形变量子化的基本概念。一个经典的观测量函数 f 可以被普朗克常量 $\hbar$ 形变成如下形式：

$$f \mapsto \sum_{k=0}^{\infty} f_k \hbar^k\,, \tag{2}$$

其中 f_k 为一系列函数且 $f_0 = f$. 函数之间的乘积可以被形变成为星乘积（star product）

$$f \star g := \sum_{k=0}^{\infty} B_k(f,g)\hbar^k\,, \quad \forall f,g \in C^\infty(M), \tag{3}$$

其中 B_k 为依赖于 f 和 g 的辛流形上的函数。

在 §2.3中，我将介绍膜量子化的基本概念。首先在 §2.3.1中，我将回顾上同调拓扑场论的基本概念，然后复习二维 $\mathcal{N} = (2,2)$ 理论的拓扑 A 类扭曲，并介绍 A 膜的基本概念。然后在 §2.3.2中，我将介绍膜量子化，介绍正则余迷向 A 膜以及拉格朗日 A 膜，介绍正则余迷向 A 膜到自身的拓扑弦代数在其与拉格朗日 A 膜之间的拓扑弦空间上的作用。最后给出本项目主要的对应关系，也就是 A 膜与形变量子化代数的表示的对应关系：

$$\mathbf{R}\mathrm{Hom}(-,\mathfrak{B}_{cc}) : D^b\text{A-Brane}(\mathfrak{X},\omega_{\mathfrak{X}}) \to D^b\mathrm{Rep}(\mathcal{O}^q(\mathfrak{X}))\,. \tag{4}$$

在第三章 §3中，我将具体分析库伦分支的几何以及其中的 A 膜。首先在 §3.1中，我将回顾四维 $\mathcal{N} = 2$ 理论的库伦分支。这些理论的 Seiberg-Witten 曲线可以表示成如下形式：

$$\det(\lambda - \varphi) = 0\,, \tag{5}$$

其中 λ 是其上的全纯 1 形式，φ 是希格斯场。在 §3.1.2中，我将介绍四维 $\mathcal{S}$ 类理论的六维构造。这种构造能够直接给出 Seiberg-Witten 曲线的物理意义。具体来说，六维理论可以通过紧化在 Seiberg-Witten 曲线所覆盖的紫外曲线上得到四维 $\mathcal{S}$ 类理论。在 §3.1.3中，我将介绍希钦系统在紧致化到三维的情况下是如何出现的。

在 §3.2中，我将详细对库伦分支的几何进行分析。具体来说，在 §3.2.1中，我将介绍库伦分支上的拓扑 A 模型，以及其中的正则余迷向 A 膜和拉格朗日 A 膜。希钦纤维丛，或者说是库伦分支，具有超卡勒的结构。这使得我们可以从不同的复结构的角度来分析它的几何。在 §3.2.2中，我将从复结构 J 的角度来分析。在这个复结构下，目标空间等同于四穿孔球上平坦 $SL(2,\mathbb{C})$-联络的模空间。这个空间可以用三次方程来描述，而我将具体分析这个三次曲面的 du Val 奇点。$\mathfrak{g}$ 型奇点出现的条件可以用 D_4 根系的 $\mathfrak{g}$ 型子根系简明地表示为如下形式：

$$t^r = 1\,, \qquad \forall r \in \mathsf{R}(\mathfrak{g}) \hookrightarrow \mathsf{R}(D_4). \tag{6}$$

在 §3.2.3中，我将从复结构 I 的角度来分析。在这个复结构中，这个空间也就是希钦纤维丛，是四穿孔球面上 $SU(2)$ 规范群的希格斯丛的模空间。我将具体分析该希钦奇异纤维的 Kodaira 类型，并说明对应于 Argyres-Douglas 理论的纤维在不同类别的 I_1 奇异纤维重合时出现。在 §3.2.4中，我将分析参数 β_j 和 γ_j

都为 0 的情况下唯一的奇异纤维上的 A 膜。在这种情况下，这个唯一的奇异纤维被称为全局幂零锥（global nilpotent cone）。我将具体分析该纤维的几何与拓扑，并计算其上的 A 膜的体积以及对应的 A 膜条件。该纤维的奇异条件使得其上 A 膜的体积函数产生了穿墙（wall-crossing）的现象，而这种现象对应于仿射 D_4 外尔群的作用。此外，在这种情况下，不同种类 du Val 奇异点能够被直观地解释为全局幂零锥不同分支地退化情况。

在 §3.2.5中，我将分析一般的 γ_j 参数下的奇异纤维。这 $6I_1$ 情况下，只有局部具有相同的单值矩阵的奇异纤维之间才能够连接一个拉格朗日 A 膜。这些 A 膜相互之间相交，形成 D_4Dynkin 图的样式。

在第四章 §4中，我将分析本项目代数方面的工作。具体来说，在 §4.1中，我将介绍 $C^\vee C_1$ 型 DAHA 代数以及其球对称子代数的定义和性质。在 §4.1.1中我将重点分析球对称 DAHA 代数所具有的对称自同构。主要包括：D_4 型外尔群对称性、三阶编织群对称性以及变号对称性。紧接着在 §4.1.2中，我将分析上面的这三种对称性的作用在几何上的表现。由于 DAHA 代数在外尔群作用下不变，我将分析编织群以及变号对称性的作用在二阶同调类上的作用。我们将看到，这两种作用都等同于几何上同调类之间的置换作用。§4.1.3中，我将考虑 DAHA 代数的一个特殊极限。在该极限下，DAHA 代数会退化为 A_1 型 DAHA，对应于单次穿孔环面上的希钦系统的形变量子化，能够与领域中已知的结论进行直接对比。

在 §4.2中，我将介绍 $C^\vee C_1$ 型球对称 DAHA 代数的多项式表示。具体来说，该表示以 Askey-Wilson 多项式作为基底。我将首先介绍 Askey-Wilson 多项式的定义，并给出 DAHA 代数生成元在该多项式上作用的算符形式。然后我将显示构造出作用在 Askey-Wilson 多项式上的升降算符。降算符的退化条件能够将无限长的 Askey-Wilson 多项式序列截断，从而得到由退化条件（shortening conditions）标记的 DAHA 代数的一系列有限维表示。我们将看到，这些退化条件能够统一利用 D_4 根系写成如下形式：

$$q^n = t_1^{-r_1} t_2^{-r_2} t_3^{-r_3} t_4^{-r_4} =: t^{-r}, \qquad r \in \mathsf{R}(D_4) \cup \{(0,0,0,0)\}\,, \tag{7}$$

其中 q 是形变参数，t_j 是 DAHA 代数的四个参数，r_j 代表 D_4 根系中的一个根或零点。因此，每一个有限维表示可以 D_4 根系之中的一个根或零点来标记。

第五章 §5是本研究的最终目标，主要建立了几何方面的 A 膜与代数方面的表示之间的直接对应。具体来说，在 §5.1中，我将把 Askey-Wilson 多项式无限序列作为无限维表示与几何方面目标空间之中的非紧致拉格朗日 A 膜做出对应。令人惊异的是，DAHA 代数的外尔对称性以及编织对称性使得我们能够从一个 Askey-Wilson 多项式序列出发得到总共 24 个不同的多项式序列，而这些多项式序列刚好能够与三次曲面上的 24 条线一一对应。另外，这 24 种多项式表示能够

用 D_4 的向量、旋量以及余旋量三种八维表示的权来标记。这给出了表示与 A 膜对应的一个强力证据。在 §5.2中，我将通过对比 A 膜的体积公式和表示的退化条件，建立有限维多项式表示与紧致 A 膜之间的对应。在 §5.2.1中，我将说明位于希钦系统之中一般的纤维上的 A 膜对应于由零点 $r = (0,0,0,0)$ 标记的有限维表示。在 §5.2.2中，我将说明位于全局幂零锥上的 A 膜对应于 D_4 根系的根。具体来说，全局幂零锥上的二阶同调类 $[\mathbf{D}_j], [\mathbf{V}]$ 上的 A 膜分别对应于由用简单根

$$(-1,-1,-1,-1), (-1,-1,1,1), (-1,1,-1,1), (-1,1,1,-1), (2,0,0,0)$$

标记的有限维 DAHA 代数的表示。我们可以以这些简单根为基底，建立所有 24 个 D_4 根与全局幂零锥上的 A 膜的对应。在 §5.2.3中，我将利用相同的方法建立除了 I_0^* 之外其他的奇异纤维（I_4, I_3, I_2）上的 A 膜与 DAHA 的有限维表示之间的对应。这些 A 膜对应于 D_4 根系的一些子根系中的根标记的表示。在这些讨论之中，$\hbar$ 的值被保持为实数。最后在 §5.2.4中，我将考虑一般的 $\hbar$ 值情况下的对应。一般情况下，希钦系统的纤维不再是拉格朗日子流形。我将给出一般情况下，一个 D_4 根能够有几何对应的条件。然后我将考虑 $\hbar$ 为纯虚数的情况，在这种情况下，拉格朗日的 A 膜将连在不同的奇异纤维之间。

在建立 A 膜与 DAHA 表示的对应的同时，我还将在 §5.2.1到 §5.2.4中建立各种情况下，A 膜与表示之间的态射的对应。具体来说，我们将看到，两个表示之间的态射将在几何上对应于两个 A 膜之间的交点。

最后，在附录 §A中，我总结了本论文使用的主要符号。在 §B中，我总结了 24 种多项式表示与三次曲面上的 24 条线的对应。在 §C中，我给出了全局幂零锥的穿墙现象的具体分析与可视化。在 §D中，我仔细分析了奇异纤维周围的单值矩阵，给出了 Argyres-Douglas 理论对应的奇异纤维出现的条件方程。在此过程之中，我们发现了在参数空间绕 Argyres-Douglas 参数面的不平凡的奇异纤维旋转现象。

关键词：膜量子化；DAHA 代数表示论；拓扑弦论；仿射编织群；四维 $\mathcal{N} = 2$ 超对称场论

中图分类号：O413.1

Abstract

Making use of the brane quantization, we study the polynomial representations of the spherical double affine Hecke algebra (DAHA) of type $C^\vee C_1$. We provide a one-to-one correspondence between Lagrangian A-branes with compact support and finite-dimensional representations of the spherical DAHA, and this provides evidence of derived equivalence between the A-brane category of $\mathrm{SL}(2,\mathbb{C})$-character variety of a four-punctured sphere and the representation category of DAHA of $C^\vee C_1$. We find out the important role played by the D_4 root system in understanding both the geometry and representation theory. In particular, this A-model approach reveals the action of an affine braid group of type D_4 on the category. As a by-product, our geometric investigation offers detailed information about the low-energy effective dynamics of the SU(2) $N_f = 4$ Seiberg-Witten theory.

Keywords: brane quantization; representations of DAHA algebra; topological string theory; affine braid group; 4d $\mathcal{N} = 2$ supersymmetry field theory
CLC code: O413.1

Chapter 1

Introduction

The quantization of classical systems remains an unresolved fundamental problem. Since the advent of quantum mechanics in the previous century, physicists have continuously explored different frameworks for quantization. Nearly a century ago, Dirac proposed the basic axioms of quantization. However, despite these simplest and most natural axioms, a comprehensive and intuitive mathematical framework for describing quantization has yet to be developed. Geometric quantization[1–2] is the most influential of the known quantization frameworks. It requires selecting a polarization direction through prequantization to construct the quantum Hilbert space. However, the need to choose a polarization direction undermines the naturalness of geometric quantization. Deformation quantization[3–4], on the other hand, systematically examines the deformation of observable algebras, revealing broad structures of quantum deformations for any classical observable algebra. However, deformation quantization does not offer enough insight into the quantum Hilbert space.

Brane quantization[5] represents a relatively new quantization framework. While it does not resolve major issues in conventional quantization schemes, it profoundly links various frameworks and interdisciplinary fields. Specifically, brane quantization uses the 2D topological A-model to unify both geometric and deformation quantization. In this framework, deformation quantization corresponds to the algebra of topological strings from a special coisotropic A-brane (the canonical coisotropic A-brane) to itself, while the Hilbert space of geometric quantization corresponds to the space of topological strings between canonical coisotropic A-branes and Lagrangian A-branes. The former provides fresh insights into deformation quantization, while the latter establishes a direct geometric-algebraic correspondence. Since the algebra of topological strings from the canonical coisotropic A-brane to itself naturally acts on the space of topological strings from them to other A-branes, each Lagrangian A-brane corresponds to a representation of the deformation quantization algebra. This establishes a beautiful geometric approach to understanding algebraic representations.

Four-dimensional $\mathcal{N} = 2$ supersymmetric field theories have been one of the most extensively studied theoretical models in physics over the past three decades. In the 1990s, Seiberg and Witten[7–8] pioneered exact solutions for low-energy effective theories on Coulomb branches, revealing profound connections between 4D supersymmetric theories, 6D SCFT, M-theories, and topological invariants, with far-reaching impacts across various disciplines. When compactified on a circle, the Coulomb branch of 4D $\mathcal{N} = 2$ theories extends into an elliptic fibration known as the Hitchin fibration[9]. This hyper-Kähler manifold coincides with both the moduli space of Higgs bundles on a four-punctured sphere and the moduli space of flat connections on the same sphere.

This research applies the brane quantization framework to the $SU(2)$-gauge Hitchin fibration, establishing bijections between representations of the algebra of deforma-

tion quantization of holomorphic function over the Hitchin fibration and Lagrangian A-branes. The Hitchin fibration corresponds to the moduli space of flat $SL(2,\mathbb{C})$ connections on a four-punctured sphere, which is described by the cubic equation:

$$-xyz + x^2 + y^2 + z^2 + \theta_1 x + \theta_2 y + \theta_3 z + \theta_4 = 0\,. \tag{1.1}$$

Oblomkov[10] showed that the deformation quantization algebra of holomorphic functions on this space is the spherical double affine Hecke algebra (DAHA). Therefore, Lagrangian A-branes correspond to representations of the spherical DAHA. Our primary objectives are: geometrically, to explore possible Lagrangian submanifolds in the Hitchin fibration, determine the corresponding A-brane conditions, and derive volume functions; algebraically, to study the representation theory of spherical DAHA via Askey-Wilson polynomials, classify the shortening conditions of representations, and determine their dimensions; and ultimately to establish the correspondence between A-branes and representations.

This work has multiple significances: First, it provides direct, non-trivial verification of brane quantization, offering new examples in quantization theory. Second, a detailed analysis of Coulomb branch geometry and topology enhances our understanding of low-energy effective theories and provides geometric insights into Argyres-Douglas conformal field theories. Finally, establishing the correspondence between A-branes and representations provides novel insights in various directions such as the geometric Langlands program, geometric representation theory, and fosters interdisciplinary connections between mathematics and physics, geometry and algebra.

The thesis is structured in six chapters: §2 introduces the basic concepts of brane quantization; §3 examines the geometry of the Hitchin fibration and A-branes; §4 analyzes DAHA algebra representations; §5 establishes the A-brane/representation correspondences; and §6 presents the key conclusions.

Chapter §2 introduces brane quantization. §2.1 describes geometric quantization: A quantization map sends functions on a symplectic manifold to Hilbert space operators, satisfying Dirac's axioms: (1) Linearity (2) Mapping Poisson brackets to commutators of operators (3) Mapping constant functions to constant operators.

Given a prequantum line bundle with a $U(1)$ connection, the prequantization map $\mathfrak{P}$ satisfies all axioms. Geometric quantization introduces polarization to interpret wavefunctions as polarized sections.

§2.2 presents deformation quantization. §2.3 details brane quantization. §2.3.1 reviews the topological A-twist of 2D $\mathcal{N} = (2,2)$ theories and A-branes. §2.3.2 introduces canonical coisotropic A-branes, Lagrangian A-branes. The central correspondence is:

$$\mathbf{R}\mathrm{Home}(-,\mathfrak{B}_{cc}) : D^b\text{A-Brane}(\mathfrak{X},\omega_{\mathfrak{X}}) \to D^b\mathrm{Rep}(\mathcal{O}^q(\mathfrak{X}))\,. \tag{1.2}$$

Chapter §3 analyzes Coulomb branch geometry. §3.1 reviews Coulomb branches of 4D $\mathcal{N} = 2$ theories. §3.1.2 introduces six-dimensional constructions for 4D class-$\mathcal{S}$ theories, offering direct interpretations of Seiberg-Witten curves. §3.1.3 addresses Hitchin systems under 3D compactification.

§3.2 details Coulomb branch geometry. §3.2.1 describes topological A-models on hyper-Kähler Coulomb branches with canonical coisotropic and Lagrangian A-branes. §3.2.2 analyzes the geometry through complex structure J: the space corresponds to the moduli space of flat $SL(2,\mathbb{C})$ connections on a four-punctured sphere, described by

the cubic equation above. Conditions of du Val singularity can be sorted via D_4 root subsystems:

$$t^r = 1, \qquad \forall r \in \mathsf{R}(\mathfrak{g}) \hookrightarrow \mathsf{R}(D_4). \tag{1.3}$$

§3.2.3 examines the geometry through complex structure I: As the moduli of $SU(2)$ Higgs bundles, we analyze the Kodaira types of Hitchin fibers and point out the cases where the Argyres-Douglas theories appear. §3.2.4 studies A-branes on the global nilpotent cone ($\beta_j = \gamma_j = 0$), calculating volumes and wall-crossing phenomena under affine D_4 Weyl group actions. du Val singularities reflect the degeneration of the global nilpotent cone.

§3.2.5 analyzes generic γ_j parameters. In $6I_1$ configurations, Lagrangian A-branes are suspended between singular fibers with identical monodromy, intersecting as a D_4 Dynkin diagram.

Chapter §4 develops algebraic aspects. §4.1 introduces the $C^\vee C_1$-DAHA and its spherical subalgebras. §4.1.1 explores symmetries: the D_4 Weyl group, braid group, and sign-flips. §4.1.2 interprets these symmetries as permuting the homology classes of the geometry. §4.1.3 considers the A_1-DAHA limit, matching with the known results.

§4.2 presents the representations of spherical DAHA via Askey-Wilson polynomials. We construct the raising and lowering operator, and the lowering operator generates shortening conditions truncating the infinite sequences of polynomials:

$$q^n = t_1^{-r_1} t_2^{-r_2} t_3^{-r_3} t_4^{-r_4} =: t^{-r}, \qquad r \in \mathsf{R}(D_4) \cup (0,0,0,0)\,. \tag{1.4}$$

Chapter §5 establishes A-brane/representation correspondences. §5.1 matches the infinite sequences of Askey-Wilson polynomials with non-compact Lagrangians. Remarkably, the symmetries of DAHA yield 24 polynomial representations corresponding to 24 lines of the affine cubic surface, labeled by the weights of vector, spinor and co-spinor representations of D_4. §5.2 matches compact A-branes with finite-dimensional representations by explicit matching volume formulas and shortening conditions. §5.2.1 associates the A-brane on a generic fiber with the representation marked by D_4 root $(0,0,0,0)$. §5.2.2 matches the A-branes on the global nilpotent cone A-branes to D_4 simple roots.§5.2.3 extends the correspondences to I_4, I_3, I_2 fibers. §5.2.4 generalizes the cases to general $\hbar$ values. In each part, the morphisms between representations are also matched with the morphisms between A-branes, which can be interpreted as the intersections between them.

Appendix §A summarizes the notations. Appendix §B presents the correspondences between 24 polynomial representations and the 24 lines of the affine cubic surface. Appendix §C gives a detailed analysis of the wall-crossing phenomenon. Appendix §D analyzes the monodromies around singular fibers, derives the equation of the surface of parameter points where the Argyres-Douglas theories appear. And we find out a non-trivial monodromy of of the Hitchin fibration around such surface.

Chapter 2

Brane Quantization

It is well-known that the passage from classical physics to quantum physics is not at all a fully solved problem. The standard procedure such as canonical quantization encounters many problems such as the problem of ordering, the problem of global quantization, etc. Therefore, it is important to develop alternative views on the quantization problem in order to provide more hints toward the "ultimate quantization scheme".

A state of a classical mechanical system is described as a point in a phase space, which can be viewed as the cotangent bundle of a configuration space. And the observables are described as functions over the phase space, whose observed values are simply the values of the functions at the state point. Mathematically, the phase space can be generalized to a symplectic manifold M with a symplectic form ω. The symplectic form ω, which is closed and non-degenerate, can be viewed as a generalization of the Poisson bracket, which determines the dynamics of states and observables. The observables then correspond to the algebra of smooth functions $C^\infty(M)$ over M.

On the other hand, the states of a quantum system are described as vectors (or more precisely, rays) in a Hilbert space $\mathcal{H}$. The observables are described as hermitian operators acting on the Hilbert space, with observed values given by the expectation values associated with a state vector. Therefore, the objective of quantization is to, given a symplectic manifold (M, ω), obtain a Hilbert space $\mathcal{H}$ and a map from $C^\infty(M)$ to the space of hermitian operators of $\mathcal{H}$.

In a quantization procedure, the Planck constant $\hbar$ is introduced to parametrize the extent of the quantum deformation. For example, the classical Poisson bracket relation $[q, p]_{\text{P.B.}} = 1$ is quantized to the canonical commutator $[q, p] = i\hbar$. More generally, the classical Poisson brackets between classical observable functions will be deformed by $\hbar$ into a quantum version of algebras of observables.

There are two main frameworks of the above quantization procedure in distinct viewpoints. Geometric quantization[1,11] approaches the quantization problem by naturally generalizing the usual canonical quantization by introducing an additional structure to M called a polarization. The deformation quantization[3–4], on the other hand, gives a generic analysis on the possible deformations of the functions over M.

I will first review the procedures of geometric quantization and deformation quantization in the first two sections. Then I will introduce the scheme of brane quantization[5], which bridges the geometric quantization and deformation quantization, providing an novel viewpoint of quantization from topological string theory. At last, I will state the core idea this project is based on, namely the correspondence between the representations of deformation quantization and the A-branes, which can be viewed as a correspondence between algebra and geometry.

2.1 Geometric quantization

The geometric quantization is one of the proposed scheme in the framework of differential geometry. There are many well written textbooks[12–13] and lecture notes[14–15] about this subject. Let me first review the formulation of classical mechanics by symplectic geometry.

A classical mechanics is described by a cotangent bundle T^*Q of a configuration space Q. If the configuration space is locally parametrized by (generalized) coordinates $q^1, \cdots, q^n$, then the cotangent bundle can be locally parametrized as (q^i, p_j) where $\{p_j\}_{j=1}^n$ are the coefficients of expansion with respect to the local coordinate 1-form $\{dq^j\}$, called conjugate momentums.

Generally, phase spaces T^*Q are generalized to symplectic manifolds (M, ω), with ω a closed non-degenerate 2-form on M called the symplectic form. By the Darboux's theorem, we can always choose the local coordinates $\{(q^i, p_i)\}_{i=1}^n$ on M such that the symplectic form ω can be locally expressed as $\omega = dp_i \wedge dq^i$, where the repeated indices are summed. These coordinates are called Darboux coordinates.

Since closed forms are locally exact, locally there is a 1-form η called symplectic potential such that $\omega = d\eta$, which can be expanded as $\eta = p_i dq^i$. If there is a globally defined symplectic potential, which means that the symplectic form ω is exact, the symplectic manifold is said to be exact.

A smooth function $f \in C^\infty(M)$ induces a natural global vector field X_f over M called the Hamiltonian vector field by the relation

$$df = -i_{X_f}\omega \,, \tag{2.1}$$

where i is the interior product. In a Darboux coordinates, X_f can be expanded as

$$X_f = \frac{\partial f}{\partial p_i}\frac{\partial}{\partial q^i} - \frac{\partial f}{\partial q^i}\frac{\partial}{\partial p_i} \,, \tag{2.2}$$

In particular

$$X_{q^i} = -\frac{\partial}{\partial p_i}, \quad X_{p_i} = \frac{\partial}{\partial q^i}. \tag{2.3}$$

Then it can be verified that

$$[X_f, X_g] = X_{[f,g]_{\text{P.B.}}} \,, \quad \omega(X_f, X_g) = [f, g]_{\text{P.B.}} \,, \tag{2.4}$$

where the Poisson bracket is defined by

$$[f, g]_{\text{P.B.}} := \frac{\partial f}{\partial p_i}\frac{\partial g}{\partial q^i} - \frac{\partial f}{\partial q^i}\frac{\partial g}{\partial p_i} \,. \tag{2.5}$$

2.1.1 Pre-quantization

One of the most astonishing discovery of the formulation of quantum mechanics is the similarity between the Poisson bracket and the quantum commutator. Based on this observation, it is naturally to propose the ansatz of quantization as $[\cdot,\cdot]_{\text{P.B}} \mapsto [\cdot,\cdot]$. In late 1920's, Dirac proposed such kind of scheme of quantization. In this scheme, a quantization is defined as a map $\mathfrak{Q}$ from the space $C^\infty(M)$ of classical observable functions to the space of hermitian operators of a Hilbert space $\mathcal{H}$ such that

1. $\mathfrak{Q}$ is linear: $\mathfrak{Q}(f+g) = \mathfrak{Q}(f) + \mathfrak{Q}(g),\ \forall f, g \in C^\infty(M)$.
2. $[\mathfrak{Q}(f), \mathfrak{Q}(g)] = -i\hbar\mathfrak{Q}([f,g]_{\text{P.B.}}),\ \forall f, g \in C^\infty(M)$.
3. $\mathfrak{Q}(f) = f\text{id}_{\mathcal{H}},\ \forall$ constant $f \in C^\infty(M)$.

From the property (2.4), it is natural to wonder whether the map $f \mapsto -i\hbar X_f$, is a quantization map as required or not. However, though first two conditions hold, it is evident that the third condition is not satisfied since $X_f = 0$ for constant f by definition. But we can modify the answer by defining the *pre-quantization map*

$$\mathfrak{P}(f) := -i\hbar X_f + \left(-i_{X_f}\eta + f\right)\text{id}_{\mathcal{H}},\ \forall f \in C^\infty(M)\ , \tag{2.6}$$

which can then be verified to satisfy all three conditions of Dirac. However, it involves the symplectic potential η, which could be impossible to define globally unless the symplectic manifold is exact.

Even when the symplectic manifold is exact, there is another issue. There is a redundancy in the definition of symplectic potential η. If we shift η by $\eta \mapsto \eta + d\phi$ for arbitrary function $\phi \in C^\infty(M)$, ω will stay the same, so the classical physics is unaltered. While on the other hand, the pre-quantization will change by

$$\mathfrak{P}(f) \mapsto \mathfrak{P}(f) - (i_{X_f}d\phi)\text{id}_{\mathcal{H}},\ \forall f \in C^\infty(M). \tag{2.7}$$

Nevertheless, the issues of global definition and redundancy of η can be resolved simultaneously if we view η, or more conventionally $\eta/\hbar$, as the gauge 1-form of a $U(1)$ connection of some complex line bundle $\mathcal{L}$ over M, called the *pre-quantum line bundle*[2]. Then the redundancy is simply the $U(1)$ gauge transform of connection, and $\omega/\hbar = d(\eta/\hbar)$ can be naturally interpreted as the curvature of the connection. The pre-quantization map can then be written as

$$\mathfrak{P}(f) := -i\hbar\nabla_{X_f} + f,\ \forall f \in C^\infty(M). \tag{2.8}$$

In this formulation, the "pre-quantum Hilbert space" is then naturally a subspace of the space of sections of the line bundle $\mathcal{L}$. We need to define a hermitian inner product $\langle\cdot,\cdot\rangle$ on the section space $\Gamma(\mathcal{L})$, which can be done by requiring a hermitian form $(\cdot,\cdot)$ defined on the line bundle $\mathcal{L}$. Then we can define

$$\langle\psi,\chi\rangle := \int_M (\psi,\chi)\varepsilon\ , \tag{2.9}$$

where ε is the Liouville volume form of M induced from the symplectic form

$$\varepsilon := \frac{1}{(2\pi\hbar)^n}\wedge^n\omega\ , \tag{2.10}$$

for any sections ψ, χ of $\mathcal{L}$. Then the "pre-quantum Hilbert space" $\mathcal{H}$ can be defined as the square-integrable sections of $\mathcal{L}$ with respect to the hermitian inner product above.

In summary, a pre-quantization of a symplectic manifold (M,ω) is to choose a hermitian line bundle $\mathcal{L}$ over M together with a $U(1)$ connection of $\mathcal{L}$ with curvature $\omega/\hbar$. The pre-quantization map is then given by the covariant derivative (2.8).

A symplectic manifold is pre-quantizable if it admits these pre-quantization structures. However, not all symplectic manifolds are pre-quantizable. There is a necessary

condition of the existence of a pre-quantum line bundle called the *Weil integrality condition* requiring that

$$\int_\Sigma \omega \in 2\pi\hbar\mathbb{Z} \tag{2.11}$$

for any closed 2-surface Σ in M. When M is simply-connected, this condition is sufficient as well.

2.1.2 Polarization

A pre-quantization is still not a quantization we want, since there is no natural way to interpret the sections in $\mathcal{H}$ defined above as wave functions. The latter should be a complex function over a configuration subspace of M instead the whole M.

It means that we need to do some restriction on the space of sections, to a subspace of them which only depend on half of the dimensions of M. In order to do this covariantly, we define a *polarization*[2,16] of a symplectic manifold (M, ω) as a sub-bundle P of TM such that:

1. P is closed under the commutator of tangent vectors:
   $[X, Y] \in P,\ \forall X, Y \in P$

2. $\forall m \in M$, P_m is a Lagrangian subspace of $T_m M$.

3. (Some technical condition, which I omit here.)

The second condition implies that P has half the rank of TM. Then we can restrict the sections of $\mathcal{L}$ to the ones s that $\nabla_X s = 0,\ \forall X \in P$, which essentially means that s depends on the directions of P trivially. These sections are called polarized sections, and then we can define the final Hilbert space $\mathcal{H}_P$ of wave functions as the polarized square-integrable sections of the pre-quantum line bundle $\mathcal{L}$.

For consistency, we have to make sure that, the actions of quantum operators will not map a polarized section into a non-polarized one. For any $f \in C^\infty(M)$ and any $X \in P$, we require

$$\nabla_X s = 0 \implies \nabla_X \mathfrak{P}(f) s = 0\,, \tag{2.12}$$

which means that $\nabla_X \nabla_{X_f} = \nabla_{X_f} \nabla_X$. This in turn implies that $[X, X_f] \in P$.

I have introduced the simplest idea of geometric quantization, which still have a lot of issues to resolve. For example, the choice of polarizations is not unique, and there is no guarantee that two different choices give identical quantization. And there are more issues about the preservation of polarization, which I omit here.

2.2 Deformation quantization

Deformation quantization[3] is a scheme which try to derive the generic $\hbar$ deformation of observable functions in $C^\infty(M)$. In order to introduce the deformation quantization, I need to introduce a generalization of symplectic manifolds.

A Poisson structure on a smooth manifold M is a product $[\cdot,\cdot]_{\text{P.B.}} : C^\infty(M) \times C^\infty(M) \to C^\infty(M)$ that is a Lie bracket on $C^\infty(M)$ and satisfies the Leibniz rule

$$[f, gh]_{\text{P.B.}} = [f, g]_{\text{P.B.}} h + g[f, h]_{\text{P.B.}}\,, \tag{2.13}$$

for any $f, g, h \in C^\infty(M)$. A Poisson structure can be equivalently represented by a 2-vector called Poisson bivector $\pi \in \mathfrak{X}^2(M)$ by

$$\pi(df, dg) = [f, g]_{\text{P.B.}} , \tag{2.14}$$

for any $f, g \in C^\infty(M)$. And a Poisson manifold is a smooth manifold with a Poisson structure. Symplectic manifolds can be viewed as special cases of Poisson manifolds with π non-degenerate everywhere, since then we can define the symplectic form ω as the inverse of the Poisson bivector π.

In order to deform the algebra $C^\infty(M)$ of smooth functions, deformation quantization considers the general deformation of a smooth function f in $C^\infty(M)$ to be able to be expanded as

$$f \mapsto \sum_{k=0}^{\infty} f_k \hbar^k , \tag{2.15}$$

for an infinite sequence of $f_k \in C^\infty(M)$ that $f_0 = f$. We call this a formal deformation of f since this sequence is not required to converge.

These kind of deformations form the formal algebra $C^\infty(M)[\![\hbar]\!]$. The function product should also be deformed in some way. The generic deformed product, called a *star product*, is of the form

$$f \star g := \sum_{k=0}^{\infty} B_k(f, g)\hbar^k , \quad \forall f, g \in C^\infty(M), \tag{2.16}$$

for an infinite sequence of bilinear maps B_k that $B_0(f, g) = fg$.

We want the deformed algebra $\left(C^\infty(M)[\![\hbar]\!], \star\right)$ to be the algebra of quantized observables. The quantization ansatz $-i\hbar[\cdot, \cdot]_{\text{P.B.}} \mapsto [\cdot, \cdot]$ implies that we should impose in addition that

$$[f, g] := f \star g - g \star f = -i\hbar[f, g]_{\text{P.B.}} + O(\hbar^2) , \tag{2.17}$$

which means that

$$B_1(f, g) - B_1(g, f) = -i[f, g]_{\text{P.B.}} , \forall f, g \in C^\infty(M). \tag{2.18}$$

The algebra $\left(C^\infty(M)[\![\hbar]\!], \star\right)$ constructed above is called a *deformation quantization* of the Poisson manifold $(M, []_{\text{P.B.}})$. Kontsevich proved that[4], every Poisson manifold has a deformation quantization. This result is called *the Formality Theorem*.

It should be noted that, deformation quantization, though is a systematic way to deform the classical theories, is not really a quantization in the usual sense. In particular, it does not provide a Hilbert space, but concentrates on the algebra of observables. Nevertheless, this also becomes the advantage of deformation quantization, since it does not need to struggle with the definition of Hilbert space as in other quantization scheme such as geometric quantization. For certain complex systems, usual quantization schemes fail, but deformation quantization can provide a useful tool to analyze their quantum behavior.

2.3 Brane quantization

Brane quantization[5], is a relatively new scheme of quantization, which provides a perspective of quantization from the viewpoint of topological string theory. Therefore, let me first give a short review of topological A-model[17–18].

2.3.1 Topological A-model

Firstly, a *cohomological field theory*, or called a topological quantum field theory of Witten type[19], is such a field theory that it possesses a Grassmannian symmetry operator Q that:

1. It is nilpotent: $Q^2 = 0$.
2. Physical operators are (defined to be) Q-closed: $\{Q, \mathcal{O}\} = 0$ for any physical operator $\mathcal{O}$. $\{\cdot, \cdot\}$ is the (anti-)commutator if $\mathcal{O}$ is bosonic(fermionic).
3. Q is not spontaneously broken: $Q|0\rangle = 0$.
4. The energy-momentum tensor is Q-exact: $T_{\mu\nu} = \{Q, G_{\mu\nu}\}$ for some Grassmannian operator $G_{\mu\nu}$.

The first and second properties imply that Q behaves like a BRST operator. The second and third properties imply

$$\langle \mathcal{O}_1 \cdots \{Q, \Lambda\} \cdots \mathcal{O}_n \rangle = 0, \tag{2.19}$$

for any physical operators $\mathcal{O}_1, \cdots \mathcal{O}_n$ and any operator Λ. This means that, it is enough to consider the physical operators up to Q-exact operators. Equivalently, we can view physical operators can then be viewed as in the Q-cohomology of operators. This is the reason why these theories are called cohomological field theories.

The fourth property implies that the theory is independent of the metric of spacetime since

$$\begin{aligned} \frac{\delta}{\delta g^{\mu\nu}} \langle \mathcal{O}_1 \cdots \mathcal{O}_n \rangle &= \frac{\delta}{\delta g^{\mu\nu}} \left(\int \mathcal{D}\varphi \mathcal{O}_1 \cdots \mathcal{O}_n e^{iS[\varphi]} \right) \\ &= i \int \mathcal{D}\varphi \mathcal{O}_1 \cdots \mathcal{O}_n T_{\mu\nu} e^{iS[\varphi]} \\ &= i \langle \mathcal{O}_1 \cdots \mathcal{O}_n \{Q, G_{\mu\nu}\} \rangle = 0 \,, \end{aligned} \tag{2.20}$$

for any physical operators $\mathcal{O}_1, \cdots \mathcal{O}_n$. This is the reason why cohomological field theories are topological field theories.

Integrate $T_{\mu\nu}$ we obtain

$$P_\mu = \{Q, G_\mu\} \,, \tag{2.21}$$

for Grassmannian operator $G_\mu \equiv \int_\Sigma d^{d-1}x G_{0\mu}$ over a spatial slice Σ. Denote the operator-valued 1-form $G \equiv G_\mu dx^\mu$. For any physical scalar local operator $\mathcal{O}^{(0)}$, we have

$$d\mathcal{O}^{(0)} = (\partial_\mu \mathcal{O}^{(0)}) dx^\mu = i[P_\mu, \mathcal{O}^{(0)}] dx^\mu = i[\{Q, G\}, \mathcal{O}^{(0)}] = \{Q, i\{G, \mathcal{O}^{(0)}\}\} \,. \tag{2.22}$$

Let's denote $\mathcal{O}^{(1)} \equiv i\{G, \mathcal{O}^{(0)}\}$, which is an operator-valued 1-form. Then we can do the same thing on $\mathcal{O}^{(1)}$

$$d\mathcal{O}^{(1)} = \partial_\mu \mathcal{O}^{(1)} \wedge dx^\mu = i[P_\mu, \mathcal{O}^{(1)}] \wedge dx^\mu = i[\{Q, G\}, \mathcal{O}^{(1)}] = \{Q, i\{G, \mathcal{O}^{(1)}\}\} \,. \tag{2.23}$$

We can then define $\mathcal{O}^{(k+1)} \equiv i\{G, \mathcal{O}^{(k)}\}$ for all non-negative integer k, then $\mathcal{O}^{(k)}$ is an operator-valued k-form over the space time, which of course vanishes for $k \geq d+1$. They satisfy the descent equation

$$d\mathcal{O}^k = \{Q, \mathcal{O}^{(k+1)}\} \,, \tag{2.24}$$

which means that d, when acting on the sequence of operators, is equivalent to the successive action of G and Q.

However, $\mathcal{O}^{(k)}$ is not a physical operator unless $k = 0$. In order to construct physical ones, we define the integral $\int_\Sigma \mathcal{O}^{(k)}$ of it along a closed k-submanifold Σ. Since

$$\left\{Q, \int_\Sigma \mathcal{O}^{(k)}\right\} = \int_\Sigma \{Q, \mathcal{O}^{(k)}\} = \int_\Sigma d\mathcal{O}^{(k-1)} = 0 \,, \tag{2.25}$$

for any physical local operator $\mathcal{O}^{(0)}$, we have a sequence of physical defect operators $\int_\Sigma \mathcal{O}^{(k)}$ for $k = 1, 2, \cdots, d$.

topological twists of (2,2) sigma model After successfully constructing a cohomological field theory in 4d[19] by a technique called topological twist, Witten continued to apply the same idea to 2d $\mathcal{N} = (2,2)$ non-linear sigma model[17]. Recall that the Lagrangian of a $(2,2)$ non-linear sigma model is given by[20]

$$\begin{aligned} \mathcal{L} &= \int d\theta^{\pm} d\overline{\theta}^{\pm} K(\Phi^i, \overline{\Phi}^{\bar{j}}) \\ &= -g_{i\bar{j}} \partial^\mu \varphi^i \partial_\mu \overline{\varphi}^{\bar{j}} + i g_{i\bar{j}} \overline{\psi}^{\bar{j}}_{\pm} (\nabla_0 \mp \nabla_1) \psi^i_{\pm} + R_{i\bar{j}k\bar{l}} \psi^i_+ \psi^j_- \overline{\psi}^{\bar{j}}_- \overline{\psi}^{\bar{l}}_+ \,, \end{aligned} \tag{2.26}$$

where $\varphi^i, \psi^i_\pm$ are the component fields of the (2,2) chiral multiplet Φ^i, and

$$g_{i\bar{j}} := \frac{\partial^2 K}{\partial \Phi^i \partial \overline{\Phi}^{\bar{j}}} \tag{2.27}$$

$\Gamma^i_{jk}, \nabla_\mu, R_{i\bar{j}k\bar{l}}$ are the Christoffel symbols, covariant derivatives and Riemann tensor with respect to $g_{i\bar{j}}$. So the target space, denoted as $\mathfrak{X}$, is a Kähler manifold with Kähler potential K.

The (2,2) non-linear sigma model enjoys two R-symmetries rotating the left-/right-moving supercharges

$$\begin{aligned} [R_V, Q_\pm] &= Q_\pm, \qquad [R_V, \overline{Q}_\pm] = -\overline{Q}_\pm \,, \\ [R_A, Q_\pm] &= \pm Q_\pm, \qquad [R_A, \overline{Q}_\pm] = \mp \overline{Q}_\pm \,. \end{aligned} \tag{2.28}$$

If the target has vanishing first Chern class, then both R_V and R_A will be anomaly-free. Recall that a cohomological field theory requires a scalar Grassmannian nilpotent symmetry operator Q that the energy-momentum tensor is Q-exact. In particular, the momentum P and Hamiltonian H should be Q-exact. It can be check that, there are only two independent ways to mix supercharges(up to automorphisms of the whole supersymmetry algebra) to obtain such a Q:

$$Q_A := \overline{Q}_+ + Q_-, \quad Q_B := \overline{Q}_+ + \overline{Q}_- \,, \tag{2.29}$$

which can be verified to be nilpotent and H, P are indeed exact:

$$\begin{aligned} H &= \{Q_A, \frac{1}{2}\left(Q_+ + \overline{Q}_-\right)\} = \{Q_B, \frac{1}{2}\left(Q_+ + Q_-\right)\} \,, \\ P &= \{Q_A, \frac{1}{2}\left(\overline{Q}_- - Q_+\right)\} = \{Q_B, \frac{1}{2}\left(Q_- - Q_+\right)\} \,. \end{aligned} \tag{2.30}$$

The Lorentz and R transformations of $\mathcal{Q}_A$, $\mathcal{Q}_B$ are

$$\begin{aligned} [M, \mathcal{Q}_A] &= -\frac{i}{2}\left(\overline{\mathcal{Q}}_+ + \mathcal{Q}_-\right) , \qquad [M, \mathcal{Q}_B] = -\frac{i}{2}\left(\overline{\mathcal{Q}}_+ + \overline{\mathcal{Q}}_-\right) , \\ [R_V, \mathcal{Q}_A] &= -\overline{\mathcal{Q}}_+ + \mathcal{Q}_- , \qquad [R_V, \mathcal{Q}_B] = -\left(\overline{\mathcal{Q}}_+ + \overline{\mathcal{Q}}_-\right) , \\ [R_A, \mathcal{Q}_A] &= -\left(\overline{\mathcal{Q}}_+ + \mathcal{Q}_-\right) , \qquad [R_A, \mathcal{Q}_B] = -\overline{\mathcal{Q}}_+ + \overline{\mathcal{Q}}_- , \end{aligned} \tag{2.31}$$

from which we see that if we define the twisted Lorentz operator

$$M_A := M - \frac{i}{2}R_A , \quad M_B := M - \frac{i}{2}R_V , \tag{2.32}$$

then

$$[M_A, \mathcal{Q}_A] = [M_B, \mathcal{Q}_B] = 0 . \tag{2.33}$$

Therefore, by doing topological twists associated with M_A, M_B, $\mathcal{Q}_A, \mathcal{Q}_B$ are candidates of topological symmetries. Moreover, it can be verified that the energy-momentum tensor of the non-linear sigma model (2.26) is $\mathcal{Q}$-exact, therefore is indeed topological with respect to the two kinds of twists. These two types of topological twists are called *A-twist* and *B-twist*, and the resulting theories are called topological *A-model* and *B-model*.

A-branes In this project, we are mainly interested in the A-twist, resulting in a 2d TQFT with respect to the symmetry charge $\mathcal{Q}_A$. And in order to implement the brane quantization scheme, we have to do a further generalization of the A-model. The topological models constructed above can be viewed as the worldsheet theory of a closed topological string in the target space $\mathfrak{X}$. Now we want to generalize the theory to the worldsheet theory of topological open strings, which means that we need to define proper boundary condition on the worldsheet field theory, in particular, to preserve the topological supersymmetry $\mathcal{Q}_A$ or $\mathcal{Q}_B$. Then the boundary of the open strings situate on topological D-branes, which are called *A-branes* and *B-branes* respectively.

We are mainly interested in the A-branes of the target space $\mathfrak{X}$ with symplectic form $\omega_{\mathfrak{X}}$ associated with the Kähler metric $g_{i\bar{j}}$ defined in the sigma model. It is known that, A-branes can be supported on two kinds of submanifolds of $\mathfrak{X}$. One is the Lagrangian submanifolds M of $\mathfrak{X}$, having half the dimension of $\mathfrak{X}$ and $\omega_{\mathfrak{X}}|_M = 0$, forming the so called *Fukaya category*. This kind of A-branes we refer to as *Lagrangian A-branes*. There is another type of A-branes supported on a co-isotropic submanifold of $\mathfrak{X}$, which is a submanifold filling all of $\mathfrak{X}$. These kind of A-branes we refer as *co-isotropic A-branes*.

We can put both types of A-branes into a single category as objects, and then the topological open strings ending on A-branes can be viewed as the morphisms of this category. This category we refer as the category of A-branes, denoted as A-Brane$(\mathfrak{X}, \omega_{\mathfrak{X}})$.

2.3.2 Brane quantization

Now we are ready to define the scheme of brane quantization[5]. Assume we want to quantize a symplectic manifold (M, ω) with a pre-quantum line bundle $\mathcal{L}$ over M. Firstly, we complexify the symplectic manifold M into a complex manifold $\mathfrak{X}$, and extend ω to a holomorphic 2-form Ω on $\mathfrak{X}$. At the same time, we extend the pre-quantum line bundle into a line bundle over $\mathfrak{X}$, still denoted as $\mathcal{L}$, with connection ReΩ.

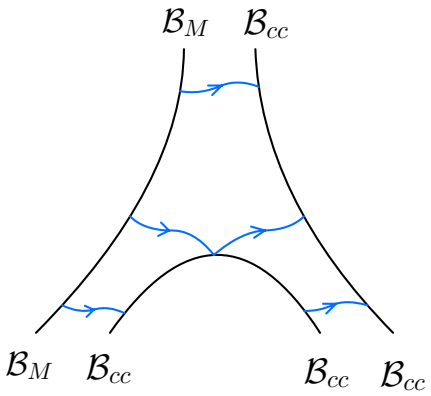

Figure 2-1 The action of $\mathrm{End}(\mathfrak{B}_{cc})$ on $\mathrm{Hom}(\mathfrak{B}_M, \mathfrak{B}_{cc})$.

Now we consider the (2,2) topological A-model with target space the Kähler manifold $(\mathfrak{X}, \omega_{\mathfrak{X}} \equiv \mathrm{Im}\Omega)$. On the other hand, as a (complexified) symplectic manifold, $\mathfrak{X}$ has a deformation quantization $\left(C^\infty(\mathfrak{X})[\![\hbar]\!], \star\right)$ with respect to the symplectic form Ω.

The key idea of brane quantization comes from the observation pointed out by[21–22] that, the pre-quantum line bundle $\mathcal{L}$ determines a unique co-isotropic A-brane $\mathfrak{B}_{cc}$, called *canonical co-isotropic A-brane*, having a special property that the endomorphisms of $\mathfrak{B}_{cc}$ are in 1-to-1 correspondence with the deformation quantization of the algebra of holomorphic functions (with appropriate polynomial growth conditions at infinity) over $\mathfrak{X}$:

$$\mathrm{End}(\mathfrak{B}_{cc}) = \mathcal{O}^q(\mathfrak{X}) \,, \tag{2.34}$$

where $\mathcal{O}^q(\mathfrak{X})$ is the sub-algebra of $C^\infty(\mathfrak{X})[\![\hbar]\!]$ of deformation quantization of holomorphic functions. Therefore, we can inteprete $\mathrm{End}(\mathfrak{B}_{cc})$ as the complexification of the algebra of the quantum operators of original system (M, ω).

Moreover, surpassing deformation quantization, the interpretation above gives in addition the natural Hilbert space associated with M as follows. At the level of category, there is a canonical action of $\mathrm{End}(\mathfrak{B}_{cc})$ on $\mathrm{Hom}(\mathfrak{B}_M, \mathfrak{B}_{cc})$ by right composition. In physics language, this action is depict as the joining of a $(\mathfrak{B}_{cc}, \mathfrak{B}_{cc})$-string with a $(\mathfrak{B}_M, \mathfrak{B}_{cc})$-string, resulting in another $(\mathfrak{B}_M, \mathfrak{B}_{cc})$-string, see Figure 2-1. Then we can naturally interpret $\mathrm{Hom}(\mathfrak{B}_M, \mathfrak{B}_{cc})$ as the Hilbert space associated with M. In this way, we construct the brane quantization of the original symplectic manifold (M, ω)[①].

Another usage of brane quantization, upon which this project is based, is that it provides a correspondence between algebra side and geometry side. To be more specific, the representations of the algebra $\mathcal{O}^q(\mathfrak{X})$ of deformation quantization are related directly to the Lagrangian A-branes inside $\mathfrak{X}$. In rigorou language, it means that brane quantization naturally proposes a derived functor

$$\mathbf{R}\mathrm{Home}(-, \mathfrak{B}_{cc}) : D^b\text{A-Brane}(\mathfrak{X}, \omega_{\mathfrak{X}}) \to D^b\mathrm{Rep}(\mathcal{O}^q(\mathfrak{X})) \,, \tag{2.35}$$

which conjecturally provides a derived equivalence between the category of A-branes and the derived category of $\mathcal{O}^q(\mathfrak{X})$-modules.

① More rigorously, we need to define in addition a hermitian metric of Hilbert space using the complex conjugate involution of $\mathfrak{X}$.

Chapter 3

Geometric Side: Coulomb Branch of 4d $\mathcal{N} = 2$ Theories

I have introduced the scheme of brane quantization in the previous chapter. The first objective of this chapter is to introduce the target space $\mathfrak{X}$ of brane quantization of this project. For many reasons, we are interested in the case where $\mathfrak{X}$ is a sector of vacuum moduli space (called Coulomb branch) of a 4d $\mathcal{N} = 2$ SQCD compactified on S^1. Firstly, this moduli space can indeed be realized as the target space of a 2d A-model by compactifying the 4d theory along a two-dimensional geometry, as I will explain. Secondly, this choice provides us with rich phenomenons such as wall-crossing, action of affine Weyl group, action of braid group etc. . This not only provides a strong verification of the scheme of brane quantization, but also uncovers deep relations to other topics of researches such as the geometric langlands program, Argyres-Douglas theories, BPS states. Thirdly, it turns out that, there are many distinct views toward the geometry of this moduli space. For example, it can be identified with the moduli space of flat connections over a Riemann surface, and it is also identical to the moduli space of Higgs bundles over the Riemann surface. These distinct views provide tools from distinct perspectives to analyze the system, and also pave the way of applications to distinct fields of researches. Lastly, it provides us with a closer view of the IR behavior of the 4d theories, and indeed we find some interesting behavior.

After introducing the target space $\mathfrak{X}$, we then apply the brane quantization to $\mathfrak{X}$. As is mentioned in previous chaper, the brane quantization provides a correspondence between geometry and algebra. In this chapter, I will give an analysis of the geometry, in particular the Lagrangian A-branes, of the target space. Then in the next chapter, I will provide the analysis on the algebraic side.

3.1 Coulomb branch of 4d $\mathcal{N} = 2$ theories

Let me give a quick review of the 4d $\mathcal{N} = 2$ theory, and then introduce the target space $\mathfrak{X}$. Four-dimensional quantum field theories with two complex Weyl supercharges (and their conjugates), which we refer to as 4d $\mathcal{N} = 2$ theories, are one of the most studied class of theories for physicists. In 1994, Nathan Seiberg and Edward Witten gave a seminal study[7–8] of the low-energy effective behavior of the 4d $\mathcal{N} = 2$ super-chromodynamics (SQCD) theories, where they invent a tool called Seiberg-Witten curve to encode the information of the IR theories and determined exactly the quantum corrections to the so called superpotentials. From then on, great advances have been made to understand the mathematics behind Seiberg-Witten approach[23–24] and to generalize the approach to various applications[25–29]. In particular, the S-duality of 4d $\mathcal{N} = 2$ SQCD is generalized by David Gaiotto[27] to obtain a large web of 4d

$\mathcal{N}=2$ theories labeled by Riemannian surfaces, which can also be studied by the tool of Seiberg-Witten curves. The Seiberg-Witten curves can be identified as the spectral curves of a type of completely integrable systems called the Hitchin systems[9,30], which relate the 4d $\mathcal{N}=2$ theories to many distinct systems, providing a deep relation between mathematics and physics.

3.1.1 4d $\mathcal{N}=2$ theories

The theory involved in this project is the 4d $\mathcal{N}=2$ SQCD made up of a vector multiplet $\Phi=(\phi,\lambda_\alpha,\overline{\lambda}_{\dot{\alpha}},A_\mu)$ in the adjoint representation of the gauge group $G=SU(2)$ and $N_f=4$ hypermultiplets $Q_i=(q_i,\psi_i,\tilde{q}_i,\tilde{\psi}_i)$ in the (anti-)fundamental representations. The UV Lagrangian is given by

$$\begin{aligned}\mathcal{L}=\frac{\mathrm{Im}\tau}{4\pi}\int d^4\theta\left(\mathrm{tr}\Phi^\dagger e^{[V,\cdot]}\Phi+Q^{\dagger i}e^V Q_i+\tilde{Q}^i e^{-V}\tilde{Q}_i^\dagger\right)\\ +\int d^2\theta\left(\frac{-i}{8\pi}\mathrm{tr}W_\alpha W^\alpha+\tilde{Q}^i\Phi Q_i+\mu_j^i\tilde{Q}^j Q_i+h.c\right)\end{aligned}\tag{3.1}$$

Expand the Lagrangian into components, then we can read off the scalar potential, which is non-negative as is required by supersymmetry. Therefore, the vacuum configurations are the zero set of the scalar potential. There are two main branches of vacua, the Coulomb branch and the Higgs branch. We are interested in the Coulomb branch, which is determined by the equation

$$[\Phi^\dagger,\Phi]=0\,,\quad Q_i=\tilde{Q}^i=0\,.\tag{3.2}$$

The Coulomb branch can be parametrized by the gauge invariant parameter $u=\langle\mathrm{tr}\Phi^2\rangle\in\mathbb{C}$, thus is also called the u-plane. At each u, the IR effective theory is a sigma model with target the Coulomb branch itself and abelian gauge group $U(1)$, which is completely determined by a holomorphic function $\mathcal{F}(\Phi)$ called the *prepotential*. The effective IR coupling constant can be expressed by a local IR parameter a together with the dual parameter $a_D:=\partial\mathcal{F}/\partial a$ as $\tau(u)=\partial a_D/\partial a$. Therefore, to completely determine the IR physics, all we need is to determine the global behavior of the parameters (a,a_D) over the u-plane. This is not easy since there typically are no global choice of frame (a,a_D). One way to determine the IR physics is to do explicit calculation of the quantum correction to the coupling constant $\tau(u)$, which requires explicit counting (by techniques such as supersymmetric localization) of the instanton solutions, see[31]. The other way is to use the *Seiberg-Witten curves*[7–8].

When the four hypermultiplets are massless, the Seiberg-Witten curve Σ_{massless} is given by[8]

$$y^2=\left(x-e_1(\tau)u\right)\left(x-e_2(\tau)u\right)\left(x-e_3(\tau)u\right)\,,\tag{3.3}$$

with u the parameter of Coulomb branch and $e_i(\tau)$ are roots of the cubic polynomial $4x^3-g_2(\tau)x-g_3(\tau)$ obeying $e_1+e_2+e_3=0$. Note that $g_2(\tau)$ and $g_3(\tau)$ are appropriately normalized Eisenstein series

$$\begin{aligned}g_2(\tau)&=\frac{60}{\pi^4}G_4(\tau)=\frac{60}{\pi^4}\sum_{m,n\in\mathbb{Z}_{\neq0}}\frac{1}{(m\tau+n)^4}\,,\\ g_3(\tau)&=\frac{140}{\pi^6}G_6(\tau)=\frac{140}{\pi^6}\sum_{m,n\in\mathbb{Z}_{\neq0}}\frac{1}{(m\tau+n)^6}\,.\end{aligned}\tag{3.4}$$

The roots e_i can be expressed by the Jacobi theta functions

$$\begin{aligned} e_1 - e_2 &= \vartheta_3{}^4(0,\tau)\,, \\ e_3 - e_2 &= \vartheta_2{}^4(0,\tau)\,, \\ e_1 - e_3 &= \vartheta_4{}^4(0,\tau)\,, \end{aligned} \tag{3.5}$$

where the Jacobi theta functions are defined by

$$\begin{aligned} \vartheta_2(0,\tau) &= \sum_{n\in\mathbb{Z}} q^{\frac{1}{2}(n+1/2)^2}\,, \\ \vartheta_3(0,\tau) &= \sum_{n\in\mathbb{Z}} q^{\frac{1}{2}n^2}\,, \\ \vartheta_4(0,\tau) &= \sum_{n\in\mathbb{Z}} (-1)^n q^{\frac{1}{2}n^2}\,. \end{aligned} \tag{3.6}$$

At generic mass parameters m_j, the Seiberg-Witten curve Σ is obtained in[8], which is

$$\begin{aligned} y^2 = {} & \left(x^2 - c_2^2 u^2\right)\left(x - c_1 u\right) - c_2^2\left(x - c_1 u\right)^2 \sum_i m_i^2 - c_2^2\left(c_1^2 - c_2^2\right)\left(x - c_1 u\right) \sum_{i>j} m_i^2 m_j^2 \\ & + 2c_2\left(c_1^2 - c_2^2\right)\left(c_1 x - c_2^2 u\right) m_1 m_2 m_3 m_4 - c_2^2\left(c_1^2 - c_2^2\right)^2 \sum_{i>j>k} m_i^2 m_j^2 m_k^2, \end{aligned} \tag{3.7}$$

where $c_1 = \frac{3}{2}e_1$ and $c_2 = \frac{1}{2}(e_3 - e_2)$.

The Seiberg-Witten curve Σ at a point u can be rewritten as

$$\det\left(\lambda - \varphi(u)\right) = 0\,, \tag{3.8}$$

which is a complex curve determined by the above equation inside $\mathbb{C}^2$ parametrized by x, z. $\lambda = x dz/z$ is a holomorphic 1-form over Σ called the *Seiberg-Witten differential*. $\varphi(u)$ is an adjoint-valued holomorphic 1-form over Σ depending on the bare masses $m_j, j = 1,2,3,4$ of the hypermultiplets, whose specific form is not important here. $\varphi(u)$ has four poles situated at $z = 0, q \equiv e^{2\pi i \tau_{UV}}, 1, \infty$ with τ_{UV} the coupling constant of the UV theory. The residues at these poles are given by linear combinations of the bare masses[32–34]

$$\left(\frac{m_1+m_2}{2}, \frac{m_1-m_2}{2}, \frac{m_3+m_4}{2}, \frac{m_3-m_4}{2}\right)\,. \tag{3.9}$$

It is easy to show that, Σ is in fact a 2-torus double-branch covering a Riemann surface $C_{0,4}$, i.e. a four-punctured sphere called the *UV curve*, which is parametrized solely by $z \in \mathbb{C}\cup\{\infty\}$. Since $\lambda = x dz/z$ belongs to the cotangent space at each u, we can view Σ as being embedded inside the cotangent bundle $T^*C_{0,4}$ of $C_{0,4}$ with vertical parametrized by x.

The convenience of Seiberg-Witten curve is that, we can view them as being fibered over the u-plane, except for a few singular values. This is a non-trivial torus fibration, for which a local trivialization is to choose a local frame for the tori (γ_A, γ_B). Then the local parameters of IR physics can be obtained by

$$a = \frac{1}{2\pi i}\oint_{\gamma_A} \lambda\,, \quad a_D = \frac{1}{2\pi i}\oint_{\gamma_B} \lambda\,, \quad \tau(u) = \frac{\partial a_D}{\partial a}\,. \tag{3.10}$$

Therefore, we see that the IR coupling $\tau(u)$ can be identified with the period of the torus Σ at u. More generally, for every loop γ in Σ, the integral of the Seiberg-Witten differential λ gives the mass of a BPS particle with electric-magnetic charges (n_e, n_m) and flavour charges f^j

$$M = \frac{1}{2\pi i}\oint_\gamma \lambda = |n_e a + n_m a_D + \sum_{j=1}^{4} f^j m_j| \,. \tag{3.11}$$

In particular, $(1,0)$ corresponds to the W-bosons, $(0,1)$ corresponds to the monopoles, etc..

3.1.2 6d perspective

Now I briefly mention the generalization of the Seiberg-Witten curves to the $\mathcal{N}=2$ theories of class S[27]. The theories of class S are a large family of $\mathcal{N}=2$ superconformal theories constructed by generalizing the S-duality mentioned in[8] to general quiver gauge theories. For simplicity, I only consider the gauge group to be $G = SU(N)$. Each theory of this family is associated with a Riemann surface $C_{g,n}$, i.e. with g genus and n punctures. This complex curve serves as the UV curve, and its Seiberg-Witten curve Σ is a N-fold branch cover over $C_{g,n}$ determined by the same equation (3.8). Similarly, Σ can be viewed as embedded inside the cotangent bundle $T^*C_{g,n}$, and the BPS mass formula can also be obtained by integrating $\lambda = x\frac{dz}{z}$ along a loop on Σ_u

$$M = \frac{1}{2\pi i}\oint_\gamma \lambda = |\sum_{i=1}^{g}(n_i a^i + m_i a_D^i) + \sum_{i=1}^{n} f^i m_i| \,, \tag{3.12}$$

where (a^i, a_D^i) corresponds to the standard loops associated with the i-th genus.

Then it is natural to wonder if there is a direct correspondence between BPS particles and the loops on the Seiberg-Witten curve. The answer is yes[35], since it is known that class S theories can be obtained from 6d $\mathcal{N}=(2,0)$ SCFT compactified on the UV curve $C_{g,n}$[27], which in M-theory can be interpreted as wrapping N M5-branes on $C_{g,n}$. The "wrapping" dimensions of the N M5-branes is exactly the Seiberg-Witten curve Σ covering the UV curve in an N-fold way. On the other hand, there is another type of branes called M2-branes in M-theory, which can end on M5-branes. In particular, they can be suspended between the sheets of Σ over $C_{g,n}$, with constant tension $|dx| \wedge |d\log z|$. Their boundaries are loops on Σ (times time direction), and under projection they becomes strings on $C_{g,n}$ with tension proportional to the distance between two sheets, i.e. x, thus equal exactly to the amplitude of the Seiberg-Witten differential λ. Their masses are therefore given by integrating the tension over the strings, which gives exactly the BPS mass formula. Viewed on the un-compactified 4 dimensions, these strings becomes particles, which are exactly the BPS particles in the effective 4d $\mathcal{N}=2$ theories[36–37].

Moreover, let's consider the reduction from 6d to 4d in more details. It is known that 6d $\mathcal{N}=(2,0)$ SCFT has a single supersymmetry multiplet called the tensor multiplet, which consists of a self-dual 2-form, four Weyl fermions, together with five scalars. When the 6d theory is put on $\mathbb{R}^{3,1}\times C_{g,n}$, the self-dual 2-form will split into the 4d gauge field together with a holomorphic adjoint 1-form φ_H over $C_{g,n}$. The fermions reduces directly to 4d, while 4 scalars out of 5 must vanish if we want the resulting 4d theory to have $\mathcal{N}=2$ supersymmetry. The single scalar left combines with the fermions and gauge field into the 4d $\mathcal{N}=2$ multiplets.

Hitchin systems Now we are especially interested in the holomorphic 1-form field φ_H over $C_{g,n}$. Supersymmetry also requires that it should satisfy the *Hitchin equations*

$$F_A = [\varphi_H, \overline{\varphi}_H] \,, \quad \overline{\nabla}_A \varphi_H = 0 \,, \tag{3.13}$$

where A is a G-connection over $C_{g,n}$ of a holomorphic bundle E and F_A is the curvature associated with A. A solution of Hitchin equations is called a *Higgs bundle*. Define the moduli space of Higgs bundles over $C_{g,n}$ as the space $\mathcal{M}_H(C_{g,n}, G)$ of all solutions (E, A, φ_H) up to certain bundle isomorphisms and gauge redundancy.

The spectral curve associated with a Higgs bundle is defined as a complex curve embedded inside the cotangent bundle $T^*C_{g,n}$ by

$$\det\left(\lambda - \varphi_H\right) = 0 \,, \tag{3.14}$$

where $\lambda = xdz/z$ parameterizing the vertical direction. We see that, the spectral curves of the Hitchin system on the UV curve are in one-to-one correspondence to the Seiberg-Witten curves of the 4d theory. In fact, we can then define the correspondence exactly by

$$\varphi \longleftrightarrow \varphi_H \,. \tag{3.15}$$

The equation of spectral curve can be expanded as

$$\lambda^N + u_2\lambda^{N-2} + u_3\lambda^{N-3} + \cdots + u_N = 0 \,, \tag{3.16}$$

for invariant polynomials $u_i(\varphi_H)$. We see that, distinct curves are labeled by the invariant polynomials. Making use of the correspondence(3.15), these invariant polynomials correspond exactly to the u_i parameters of the u-space. Therefore, we can identify the space of Seiberg-Witten curves with the u-space.

The moduli space of Higgs bundle on $C_{g,n}$, denoted as $\mathcal{M}_H(C_{g,n}, G)$, can then be viewed as a fibration over the u-space by sending each Higgs bundle to its spectral curve (thus to a u point). The fiber of $\mathcal{M}_H(C_{g,n}, G)$ over a u-point can be identified with the space of holomorphic line bundles over the curve Σ at u, which is known to be a complex torus generically. In conclusion, $\mathcal{M}_H(C_{g,n}, G)$ can be viewed as a elliptic fibration over the u-space, which is called the *Hitchin fibration*.

It is known that the moduli space of Higgs bundle carries a hyper-Kähler structure, thus carrying a family of complex structures parameterized by an parameter $\zeta \in \mathbb{C}P^1$ with three independent ones. In the above construction, we have used a complex structure where the Higgs bundles are holomorphic bundles and the Higgs fields are holomorphic 1-forms. We refer to this complex structure as the complex structure I. On the other hand, $A_{\mathbb{C}} := A + i(\varphi + \overline{\varphi})$ forms a $G_{\mathbb{C}}$-connection over $C_{g,n}$, and the Hitchin equation becomes the flatness condition

$$F_{A_{\mathbb{C}}} = dA_{\mathbb{C}} + A_{\mathbb{C}} \wedge A_{\mathbb{C}} = 0 \,. \tag{3.17}$$

Conversely, every flat $G_{\mathbb{C}}$ connection (under certain stability condition) determines a unique Higgs bundle, see[38–39]. Therefore, the moduli space of G-Higgs bundle is identical to the moduli space of $G_{\mathbb{C}}$-flat connections over $C_{g,n}$. This identification is called the non-abelian Hodge correspondence. The latter has also a natural complex structure, which we refer to as the complex structure J. Then the third independent complex structure can be constructed by taking the product $K := IJ$. Let's denote the corresponding three Kähler forms as $\omega_I, \omega_J, \omega_K$, then we can define three 2-forms

$$\Omega_I := \omega_J + i\omega_K \,, \quad \Omega_J := \omega_K + i\omega_I \,, \quad \Omega_K := \omega_I + i\omega_J \,, \tag{3.18}$$

which are holomorphic in complex structure I, J, K respectively, thus are called *holomorphic symplectic forms*.

3.1.3 Reduction to lower dimensions

The moduli space of Higgs bundle can appear from a more physical perspective. We can compactify the 4d $\mathcal{N}=2$ theories over S^1, resulting in a 3d $\mathcal{N}=4$ effective theory. Upon dimension reduction, the 4d gauge fields will split into 3d gauge fields together with periodic scalars as the holonomies of the 4d gauge fields along the compactified S^1. Similarly, the dual gauge fields will also split into the 3d dual gauge fields and dual periodic scalars. At a generic vacuua, the two sets of emerging scalars are paired into tori. Therefore, after compactification on S^1, the Coulomb branch of vacua will be lifted into a elliptic fibration $\mathcal{M}_{\text{Coul}}$ over the u-space. By analyzing the low-energy effective theory on the Coulomb branch, it is easy to see that the Coulomb branch, as the IR target space, has a natural hyper-Kähler structure.

Then it is natural to guess that the Coulomb branch $\mathcal{M}_{\text{Coul}}$ of 3d theory is identical to the moduli space $\mathcal{M}_H(C_{g,n}, G)$ of Higgs bundles. This is indeed the case by the following argument. The 3d theory can be viewed from compactification of 6d $\mathcal{N}=(2,0)$ SCFT first on $C_{g,n}$ then on S^1. If we reverse the order of compactification, the 3d theory can be viewed as 5d $\mathcal{N}=1$ super Yang-Mills theory compactified on the UV curve $C_{g,n}$ with gauge group G. Then the Coulomb branch of 3d theory can be viewed as consisting of the vacuum configurations on the 5d Coulomb branch that is constant along the $\mathbb{R}^{2,1}$ directions. It turns out that the condition of being constant along $\mathbb{R}^{2,1}$ is equivalent to the Hitchin equations[40–41]. Therefore, the Coulomb branch of 3d theory is indeed identical to $\mathcal{M}_H(C_{g,n}, G)$.

There are a few advantages of viewing $\mathcal{M}_H(C_{g,n}, G)$ as the Coulomb branch as 3d theory. For example, the line operators of the 4d $\mathcal{N}=2$ theory under compactification becomes 3d local operators. Consequently, the vacuum expectation values of the line operators corresponds to vacuum expectation values of the corresponding 3d local operators, thus being functions over the Coulomb branch. On the other hand, every half of the supersymmetry is associated with a complex structure of the hyper-Kähler moduli space. Therefore, the 1/2-BPS line operators preserving half of the 4d supersymmetry correspond to holomorphic functions over the Coulomb branch of 3d theory with respect to the associated complex structure.

These 1/2 BPS line operators can be viewed as the worldlines of BPS particles of the 4d theory. Recall that, these BPS particles can be viewed as the reduction of the boundaries of M2-branes on the UV curve. In conclusion, *the algebra of holomorphic functions over the Coulomb branch is given by the algebra of loops over the UV curve* $C_{g,n}$.

3.2 Geometry of Coulomb branch

The moduli space $\mathcal{M}_H(C_{0,4}, SU(2))$ of $SU(2)$ Higgs bundle (in complex structure I), or equivalently the moduli space $\mathcal{M}_{\text{flat}}(C_{0,4}, SL(2,\mathbb{C}))$ of flat $SL(2)$ connections (in complex structure J) over the specific Riemann surface $C_{0,4}$ will be chosen to be our target space $\mathfrak{X}$ of A-model. Let me apply the general discussion of previous section to this specific case in this section.

Denote the four punctures of $C_{0,4}$ as $p_j, j=1,2,3,4$. The moduli space of Higgs

bundles over $C_{0,4}$ is specified by the tame ramification at p_j, which is described by the following conditions on the SU(2) connection A on E and the Higgs field

$$\begin{aligned} A &= \alpha_j \, d\vartheta + \cdots \\ \varphi &= \frac{1}{2}(\beta_j + i\gamma_j)\frac{dz}{z} + \cdots \end{aligned} \tag{3.19}$$

Here, $z = re^{i\vartheta}$ is a local coordinate on a small disk centered at p_j, and the ramification data is a triple $(\alpha_j, \beta_j, \gamma_j) \in \mathfrak{t} \times \mathfrak{t} \times \mathfrak{t}$ where we denote the Cartan subalgebra $\mathfrak{t} \subset \mathfrak{su}(2)$. By expressing them as conjugate to diagonal matrices

$$\begin{aligned} \mathrm{diag}(\alpha_j, -\alpha_j) &\sim \alpha_j \in \mathfrak{t} \, , \\ \mathrm{diag}(\beta_j, -\beta_j) &\sim \beta_j \in \mathfrak{t} \, , \\ \mathrm{diag}(\gamma_j, -\gamma_j) &\sim \gamma_j \in \mathfrak{t} \, , \end{aligned} \tag{3.20}$$

we will often use the triple $(\alpha_j, \beta_j, \gamma_j) \in \mathfrak{t}^3$ interchangeably with the ramification parameters $(\alpha_j, \beta_j, \gamma_j) \in \mathbb{R}^3$ in the following discussions, by a slight abuse of notation.

Since the Higgs field φ is identified with the holomorphic 1-form $\varphi(u)$ in the Seiberg-Witten curve (3.8) with residues given by (3.8). Therefore, we can identify the mass parameters and the ramification parameters by

$$\begin{aligned} &(\beta_1 + i\gamma_1, \beta_2 + i\gamma_2, \beta_3 + i\gamma_3, \beta_4 + i\gamma_4) \\ &\qquad = \left(\frac{m_1 + m_2}{2}, \frac{m_1 - m_2}{2}, \frac{m_3 + m_4}{2}, \frac{m_3 - m_4}{2} \right) . \end{aligned} \tag{3.21}$$

As is mentioned in the previous section, this space is a hyper-Kähler space with three integrable complex structures I, J, K, and the corresponding Kähler forms are given by

$$\begin{aligned} \omega_I &= -\frac{i}{2\pi} \int_{C_{0,4}} |d^2 z| \ \mathrm{Tr}\Big(\delta A_{\bar{z}} \wedge \delta A_z - \delta\bar{\varphi} \wedge \delta\varphi \Big) \, , \\ \omega_J &= \frac{1}{2\pi} \int_{C_{0,4}} |d^2 z| \ \mathrm{Tr}\Big(\delta\bar{\varphi} \wedge \delta A_z + \delta\varphi \wedge \delta A_{\bar{z}} \Big) \, , \\ \omega_K &= \frac{i}{2\pi} \int_{C_{0,4}} |d^2 z| \ \mathrm{Tr}\Big(\delta\bar{\varphi} \wedge \delta A_z - \delta\varphi \wedge \delta A_{\bar{z}} \Big) \, , \end{aligned} \tag{3.22}$$

where it is $\mathcal{M}_H(C_{0,4}, SU(2))$ in complex structure I, $\mathcal{M}_{\mathrm{flat}}(C_{0,4}, SL(2,\mathbb{C}))$ in complex structure J.

The three holomorphic symplectic forms are then given by (3.18). In this situation, as explained in[5], the cohomology classes of $\omega_I, \omega_J, \omega_K$ are proportional to $\alpha_j, \beta_j, \gamma_j$ respectively. Therefore the cohomology class of $\Omega_I = \omega_J + i\omega_K$ is proportional to the combination of moduli $\beta_j + i\gamma_j$ and independent of the other moduli α_j. Therefore, in complex structure I, $\beta_j + i\gamma_j$ are the complex moduli while α_j are the Kähler moduli. Similarly, the complex moduli and Kähler moduli in different complex structures are different, as summarized in Table 3-1.

In a hyper-Kähler manifold, the complex moduli determine the holomorphic functions while the Kähler moduli determine the volumes of the submanifolds.

Complex structure	Complex moduli	Kähler moduli
I	$\beta_j + i\gamma_j$	α_j
J	$\gamma_j + i\alpha_j$	β_j
K	$\alpha_j + i\beta_j$	γ_j

Table 3-1 Complex moduli and Kähler moduli in different complex structures.

3.2.1 A-model on $\mathcal{M}_{\text{flat}}(C_{0,4}, SL(2,\mathbb{C}))$

The primary goal of the analysis of the geometry of the moduli space is to identify the A-branes inside this space. As is mentioned in previous chapter, there are two types of A-branes[42]: the canonical coisotropic brane $\mathfrak{B}_{\text{cc}}$ and the Lagrangian branes $\mathfrak{B}_{\mathbf{L}}$.

canonical coisotropic brane The canonical coisotropic brane is a holomorphic line bundle over the target space itself:

$$\mathfrak{B}_{\text{cc}}: \quad \begin{array}{c} \mathcal{L} \\ \downarrow \\ \mathfrak{X} \end{array} \qquad c_1(\mathcal{L}) = [F/2\pi] \in H^2(\mathfrak{X}, \mathbb{Z}) \,, \tag{3.23}$$

which is parameterized by a single complex parameter $\hbar = |\hbar| e^{i\theta} \in \mathbb{C}^\times$. The curvature F of such a bundle combines with the B-field $B \in H^2(\mathfrak{X}, \mathrm{U}(1))$ of the A-model into a gauge invariant combination $F + B$. This combination is constrained by the relation:

$$\Omega := F + B + i\omega_{\mathfrak{X}} = \frac{\Omega_J}{i\hbar} \,. \tag{3.24}$$

In the brane quantization set up, we choose $\omega_{\mathfrak{X}}$ as the symplectic form of original symplectic manifold, $\Omega = \Omega_J/i\hbar$ as its complexification, the holomorphic symplectic form. Making use of the expression (3.18), at a generic value of $\hbar = |\hbar| e^{i\theta}$, we can express the real and imaginary parts of Ω as

$$\begin{aligned} F + B = \mathrm{Re}\Omega &= \frac{1}{|\hbar|}(\omega_I \cos\theta - \omega_K \sin\theta) \,, \\ \omega_{\mathfrak{X}} = \mathrm{Im}\Omega &= -\frac{1}{|\hbar|}(\omega_I \sin\theta + \omega_K \cos\theta) \,, \end{aligned} \tag{3.25}$$

so the symplectic form $\omega_{\mathfrak{X}}$ depends on the value of $\hbar$. Thanks to the hyper-Kähler structure $\omega_{\mathfrak{X}}^{-1}(F+B) = J$, the brane automatically satisfies the condition $(\omega_{\mathfrak{X}}^{-1}(B+F))^2 = -1$, which is required for a coisotropic A-brane[42]. With this setup, the space of open $(\mathfrak{B}_{\text{cc}}, \mathfrak{B}_{\text{cc}})$-strings gives rise to the deformation quantization of the coordinate ring on $\mathfrak{X}$, holomorphic in J. We will explicitly identify the deformed coordinate ring as the spherical DAHA algebra in the next chapter.

To see the connection between the 4d $\mathcal{N}=2$ theory and the 2d sigma-model, we compactify the 4d $\mathcal{N}=2$ theory on $T^2 \cong S^1 \times S^1_q$, as illustrated in Figure 3-2. This compactification yields a 2d sigma-model $\mathbb{R} \times \mathbb{R}_+ \cong \Sigma \to \mathcal{M}_{\text{flat}}(C_{0,4}, \mathrm{SL}(2,\mathbb{C}))$ on the Coulomb branch. Here, $S^1_q \subset \mathbb{R}^2$ is a circle that encircles the axis of the Ω-background, where the loop operators intersect. By the state-operator correspondence, loop operators in the 4d $\mathcal{N}=2$ theory map to states in $\mathrm{Hom}(\mathfrak{B}_{\text{cc}}, \mathfrak{B}_{\text{cc}})$. Thus, upon the compactification, the canonical coisotropic brane condition $\mathfrak{B}_{\text{cc}}$ naturally emerges from the "axis of the Ω-deformation" $\partial\Sigma$ (or the tip of the cigar, as described in[43]).

Lagrangian A-branes As the target symplectic manifold $(\mathfrak{X}, \omega_{\mathfrak{X}})$ is of quaternionic dimension one, A-branes of the other types are all Lagrangian A-branes, namely it has a Lagrangian submanifold $\mathbf{L}$ as its support, endowed with a flat Spin^c-bundle:

$$\mathfrak{B}_{\mathbf{L}}: \quad \begin{array}{c} \mathcal{L}' \otimes K_{\mathbf{L}}^{-1/2} \\ \downarrow \\ \mathbf{L} \end{array} \tag{3.26}$$

where $K_{\mathbf{L}}^{-1/2}$ is a square root of the canonical bundle of $\mathbf{L}$, which gives rise to a Spin^c structure when $\mathcal{L}'$ is not a genuine line bundle. (See[5–6] for more details.) The subtlety of Spin^c structures appears only when we consider bound states of A-branes, and both $\mathcal{L}'$ and $K_{\mathbf{L}}^{-1/2}$ exist as genuine line bundles in most of the examples in this paper since all the Lagrangian submanifolds considered are of real two dimensions. Additionally, a Lagrangian A-brane must satisfy the flatness condition

$$F' + B|_{\mathbf{L}} = 0 \,, \tag{3.27}$$

where F' is the curvature of $\mathcal{L}'$, and $F'+B$ is the gauge-invariant combination as before.

Then, the space of $(\mathfrak{B}_{\rm cc}, \mathfrak{B}_{\mathbf{L}})$-open string arises from the geometric quantization of $\mathbf{L}$, namely the space of holomorphic sections $\mathfrak{B}_{\rm cc} \otimes \mathfrak{B}_{\mathbf{L}}^{-1}$ over $\mathbf{L}$. Hence, when the support is a compact Lagrangian submanifold, one can employ the B-model perspective to compute the dimension of the representation space $\mathrm{Hom}(\mathfrak{B}_{\mathbf{L}}, \mathfrak{B}_{\rm cc})$ using Hirzebruch-Riemann-Roch formula:

$$\begin{aligned} \dim \mathcal{L} &= \dim \mathrm{Hom}(\mathfrak{B}_{\mathbf{L}}, \mathfrak{B}_{\rm cc}) \\ &= \dim H^0(\mathbf{L}, \mathfrak{B}_{\rm cc} \otimes \mathfrak{B}_{\mathbf{L}}^{-1}) \\ &= \int_{\mathbf{L}} \mathrm{ch}(\mathfrak{B}_{\rm cc}) \wedge \mathrm{ch}(\mathfrak{B}_{\mathbf{L}}^{-1}) \wedge \mathrm{Td}(T\mathbf{L}) \,, \end{aligned} \tag{3.28}$$

where $\mathrm{Td}(T\mathbf{L})$ is the Todd class of the tangent bundle of $\mathbf{L}$. Since $\mathbf{L}$ is real two-dimensional in our case, the Todd class $\mathrm{Td}(T\mathbf{L})$ is equal to $\mathrm{ch}(K_{\mathbf{L}}^{-1/2})$. Thus, the dimension formula is simplified to

$$\dim \mathcal{L} = \int_{\mathbf{L}} \mathrm{ch}(\mathfrak{B}_{\rm cc}) = \int_{\mathbf{L}} \frac{F+B}{2\pi} \,, \tag{3.29}$$

for a real two-dimensional Lagrangian $\mathbf{L}$. In this way, we can explicitly provide the dimension of a finite-dimensional representation corresponding to a Lagrangian A-brane with compact support.

On the other hand, the volume of a Lagrangian submanifold $\mathbf{L}$ is is defined as the integration of the Kähler form ω_I over $\mathbf{L}$

$$\mathrm{vol}_I(\mathbf{L}) := \int_{\mathbf{L}} \frac{\hbar}{2\pi} \mathrm{Im}\Omega = \int_{\mathbf{L}} \frac{\omega_I}{2\pi} \,. \tag{3.30}$$

3.2.2 Geometry in complex structure J: cubic surface

In order to find the Lagrangian A-branes in the target space, we first need to have enough knowledge of the geometry of the target space. Thank to its hyper-Kähler structure, we

can view the geometry from different perspectives. In this subsection, I will describe the geometry in complex structure J. In the next subsection, I will view the geometry from complex structure I.

The moduli space of flat $SL(2,\mathbb{C})$ connections are specified by the monodromy M_j around the puncture p_j, which is conjugate to

$$M_j \sim \exp\left(-2\pi\left(\gamma_j + i\alpha_j\right)\right) \tag{3.31}$$

while β_j is a Kähler parameter in this complex structure. These monodromies satisfy

$$\mathcal{M}_{\text{flat}}(C_{0,4}, \mathrm{SL}(2,\mathbb{C})) = \langle M_1, M_2, M_3, M_4 \in \mathrm{SL}(2,\mathbb{C}) \mid M_1M_2M_3M_4 = \mathrm{Id}\rangle / \mathrm{SL}(2,\mathbb{C}) , \tag{3.32}$$

where the quotient by $\mathrm{SL}(2,\mathbb{C})$ is taken with respect to conjugation. See Figure 3-1.

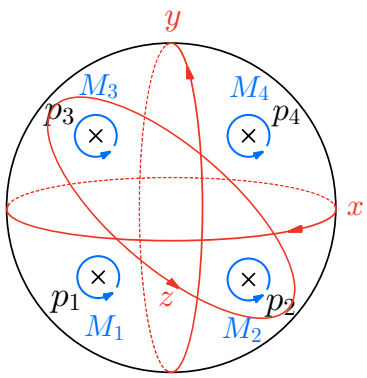

Figure 3-1 BPS loops on the UV curve $C_{0,4}$ generate the ring of holomorphic functions over the moduli space $\mathcal{M}_{\text{flat}}(C_{0,4}, SL(2,\mathbb{C}))$.

To describe the moduli space geometrically, we introduce holonomy variables as holomorphic functions on $\mathcal{M}_{\text{flat}}(C_{0,4}, \mathrm{SL}(2,\mathbb{C}))$:

$$\begin{aligned} &x = -\operatorname{Tr}(M_1M_2) , \quad y = -\operatorname{Tr}(M_1M_3) , \quad z = -\operatorname{Tr}(M_2M_3) , \\ &\overline{t_j} = \operatorname{Tr}(M_j) = \exp\left(-2\pi(\gamma_j + i\alpha_j)\right) , \qquad (j = 1,2,3,4) . \end{aligned} \tag{3.33}$$

These variables are subject to the trace identity[44]:

$$f(x,y,z) = -xyz + x^2 + y^2 + z^2 + \theta_1 x + \theta_2 y + \theta_3 z + \theta_4 = 0 , \tag{3.34}$$

where

$$\begin{aligned} \theta_1 &= \overline{t_1}\,\overline{t_2} + \overline{t_3}\,\overline{t_4} , \\ \theta_2 &= \overline{t_1}\,\overline{t_3} + \overline{t_2}\,\overline{t_4} , \\ \theta_3 &= \overline{t_1}\,\overline{t_4} + \overline{t_2}\,\overline{t_3} , \\ \theta_4 &= \overline{t_1}^2 + \overline{t_2}^2 + \overline{t_3}^2 + \overline{t_4}^2 + \overline{t_1}\,\overline{t_2}\,\overline{t_3}\,\overline{t_4} - 4 . \end{aligned} \tag{3.35}$$

Then the moduli space $\mathcal{M}_{\text{flat}}(C_{0,4}, \mathrm{SL}(2,\mathbb{C}))$ can be viewed as an affine variety determined by the cubic equation (3.34). It is not hard to observe that, the parameters θ_i of the cubic equation are in fact the characters of the SO(8) representations, which can be attributed to the SO(8) flavor symmetry present in the 4d $\mathcal{N} = 2$ SU(2) theory with $N_f = 4$.

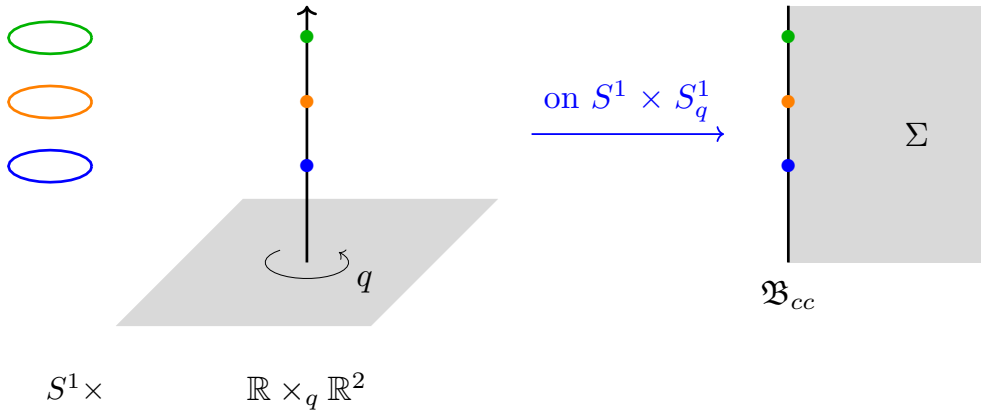

Figure 3-2 An algebra of line operators (colored circles) in a 4d $\mathcal{N} = 2$ theory becomes non-commutative in the Ω-background $S^1 \times \mathbb{R} \times_q \mathbb{R}^2$, which provides deformation quantization of holomorphic coordinate ring of the Coulomb branch. The 4d $\mathcal{N} = 2$ theory compactified on $S^1 \times S^1_q$ is described by 2d A-model $\Sigma \to \mathcal{M}_C$ on the Coulomb branch where the boundary condition at $\partial\Sigma$ is given by $\mathfrak{B}_{cc}$. Here $\mathbb{R}^2 \supset S^1_q$ is the circle generating the Ω-deformation.

As is mentioned in the previous section, the holonomy variables x, y, z can be interpreted as vacuum expectation values of loop operators along S^1 in the 4d $\mathcal{N} = 2$ theory. In the class $\mathcal{S}$ construction, two M5-branes wrap the four-punctured sphere $C_{0,4}$, with the punctures realized by intersections of co-dimension two with other M5-branes. A line operator in the 4d $\mathcal{N} = 2$ theory is realized by an M2-brane attaching to a one-cycle on $C_{0,4}$[36–37], and the one-cycles x, y, z in Figure 3-1 correspond to fundamental Wilson, 't Hooft, and dyonic loop operators, respectively:

$$\begin{aligned} x &\longleftrightarrow \text{Wilson loop}\,, \\ y &\longleftrightarrow \text{'t Hooft loop}\,, \\ z &\longleftrightarrow \text{dyonic loop}\,. \end{aligned} \tag{3.36}$$

Consequently, the algebra of loop operators gives rise to the coordinate ring $\mathcal{O}(\mathcal{M}_{\text{flat}}(C_{0,4}, \text{SL}(2,\mathbb{C})))$ of the Coulomb branch holomorphic in complex structure J[29].

deformation quantization of coordinate ring As is proved in[10], the deformation quantization of the coordinate ring $\mathcal{O}(\mathcal{M}_{\text{flat}}(C_{0,4}, \text{SL}(2,\mathbb{C})))$ with respect to the holomorphic symplectic form Ω_J is an algebra called the spherical double affine hecke algebra (spherical DAHA) $S\ddot{H}_{q,t}$ of type $C \vee C_1$, which will be introduced in detail in Chapter 4. Now let me give a physical verification of such a conclusion.

One can introduce the Ω-background $S^1 \times \mathbb{R} \times_q \mathbb{R}^2$, which effectively introduces a potential around the origin of the Ω-deformation. As illustrated in Figure 3-2, the loop operators are localized along the axis of the Ω-deformation and are forced to cross each other as they exchange positions. Consequently, the algebra of loop operators becomes non-commutative, providing a physical realization of the deformation quantization of the coordinate ring[43,45–49].

The deformation quantization we consider is with respect to the holomorphic symplectic form $\Omega_J = \omega_K + i\omega_I$ of complex structure J (also known as the Atiyah-Bott-

Goldman symplectic form), which is given by

$$\Omega_J = -\frac{1}{2\pi}\frac{dx\wedge dy}{\partial f/\partial z} = -\frac{1}{2\pi}\frac{dx\wedge dy}{2z-xy+\theta_3}. \tag{3.37}$$

In terms of the holomorphic symplectic form Ω_J, the Poisson brackets of the generators of the coordinate ring are given by

$$\begin{aligned}\{x,y\} &= -2\pi(2z-xy+\theta_3)\,,\\ \{y,z\} &= -2\pi(2x-yz+\theta_1)\,,\\ \{z,x\} &= -2\pi(2y-zx+\theta_2)\,.\end{aligned} \tag{3.38}$$

Using the algebraic relation of the spherical DAHA $\ddot{SH}_{q,t}$ in (4.12), one can show that, with $q=e^{2\pi i\hbar}$, the Poisson brackets can be obtained by

$$\left.\frac{[-,-]}{i\hbar}\right|_{\hbar\to 0} = \{-,-\}\,, \tag{3.39}$$

where $[x,y]=xy-yx$ is the ordinary commutator (not the q-commutator). This verifies that the spherical DAHA $\ddot{SH}_{q,t}$ is indeed the deformation quantization of the coordinate ring with respect to the holomorphic symplectic form Ω_J:

$$\ddot{SH}_{q,t} \cong \mathcal{O}^q(\mathcal{M}_{\text{flat}}(C_{0,4},\mathrm{SL}(2,\mathbb{C})))\,. \tag{3.40}$$

In other words, the spherical DAHA $\ddot{SH}_{q,t}$ is the algebra of loop operators in the 4d $\mathcal{N}=2$ SU(2) gauge theory with $N_f=4$ hypermultiplets on the Ω-background[33,50].

Another perspective comes from the Kauffman bracket skein algebra[51–52] of a Riemann surface, which also provides a deformation quantization of the coordinate ring of the character variety on the surface with respect to Ω_J[53–54]. Indeed, the algebraic relations (4.12) and (4.15) for $\ddot{SH}_{q,t}$ can also be derived as the skein algebra $\mathrm{Sk}(C_{0,4})$ of a four-punctured sphere in[55]. This perspective has been explored extensively in the literature[56–59]; see also[6]§2.5 for discussions on the relationship between skein algebras/modules and brane quantization. Accordingly, we will not go into the details here, referring instead to these sources.

du Val singularities and D_4 root system The affine cubic surface (3.34) has been the subject of study since the 19th century, with a history spanning over a century[60–61]. Notably, the character variety $\mathfrak{X}=\mathcal{M}_{\text{flat}}(C_{0,4},\mathrm{SL}(2,\mathbb{C}))$ naturally arises in the isomonodromic deformation problem of Painlevé VI equation[62]. The non-abelian Hodge correspondence identifies $\mathfrak{X}$ with the corresponding moduli space of Higgs bundles. Following developments in Seiberg-Witten theory[8], this space has been intensively investigated even from physics perspective. Nonetheless, this paper further investigates $\mathfrak{X}$, uncovering its new aspects. As demonstrated in[6], Hitchin fibration is the key to understanding compact Lagrangian submanifolds in $\mathfrak{X}$. Moreover, the remainder of this subsection aims to reveal intrinsic connections between the geometry of $\mathfrak{X}$ and the root system of type D_4.

The root system of type D_4 appears naturally in the classification of du Val singularities of the character variety $\mathfrak{X}$. For specific values of the monodromy parameters t, the character variety $\mathfrak{X}$ develops du Val singularities (a.k.a. ADE singularities) around

which the space is locally $\mathbb{C}^2/\Gamma_{ADE}$ with Γ_{ADE} being a finite subgroup of SU(2) classified by the ADE types. These singularities arise when the discriminant of the cubic equation (3.34) vanishes[63]:

$$\Delta(t) = \left[\prod_{\epsilon_1\epsilon_2\epsilon_3=1}\left(\overline{t_4} + \sum_{j=1}^{3}\epsilon_j\overline{t_j}\right) - \prod_{j=1}^{3}(\overline{t_j}\,\overline{t_4} - \overline{t_k}\,\overline{t_l})\right]^2 \prod_{j=1}^{4}(\overline{t_j}^2 - 4)\,, \tag{3.41}$$

where $\epsilon_j = \pm 1$, and (j,k,l) is the positive permutation of $(1,2,3)$ for any j. In fact, the discriminant can be expressed in a remarkably concise way, using the set $\mathsf{R}(D_4)$ of the D_4 roots:

$$\Delta(t) = \prod_{r\in\mathsf{R}(D_4)}(t^r - 1)\,, \tag{3.42}$$

where $t^r = t_1^{r_1}t_2^{r_2}t_3^{r_3}t_4^{r_4}$. (See Appendix A for the notation of the D_4 roots.) Furthermore, the specific ADE type of each singularity can be identified by embedding the corresponding root system into $\mathsf{R}(D_4)$. Taking into account the multiplicity of singularities, a singularity of type $\mathfrak{g}$ emerges when

$$t^r = 1\,, \qquad \forall r \in \mathsf{R}(\mathfrak{g}) \hookrightarrow \mathsf{R}(D_4) \tag{3.43}$$

where $\mathfrak{g}$ is a Lie subalgebra of D_4 so that $\mathsf{R}(\mathfrak{g})$ is the subset of $\mathsf{R}(D_4)$[64]. In this manner, we can consistently classify the conditions and types of du Val singularities using the root system of type D_4, as summarized in Table 3-2.

Types	Conditions of t	Examples
A_1	$t^r = 1,\ \forall r \in \mathsf{R}(A_1) \hookrightarrow \mathsf{R}(D_4)$	$t_1^2 = 1$ or $t_1t_2t_3t_4 = 1$
$A_1^{\oplus 2}$	$t^r = 1,\ \forall r \in \mathsf{R}(A_1^{\oplus 2}) \hookrightarrow \mathsf{R}(D_4)$	$t_1^2 = t_2^2 = 1$
A_2	$t^r = 1,\ \forall r \in \mathsf{R}(A_2) \hookrightarrow \mathsf{R}(D_4)$	$t_1^2 = t_1t_2t_3t_4 = 1$
$A_1^{\oplus 3}$	$t^r = 1,\ \forall r \in \mathsf{R}(A_1^{\oplus 3}) \hookrightarrow \mathsf{R}(D_4)$	$t_1^2 = t_1t_2t_3t_4 = t_1t_2t_3t_4^{-1} = 1$
A_3	$t^r = 1,\ \forall r \in \mathsf{R}(A_3) \hookrightarrow \mathsf{R}(D_4)$	$t_1^2 = t_2^2 = t_1t_2t_3t_4 = 1$
$A_1^{\oplus 4}$	$t^r = 1,\ \forall r \in \mathsf{R}(A_1^{\oplus 4}) \hookrightarrow \mathsf{R}(D_4)$	$t_1^2 = t_2^2 = t_3^2 = t_4^2 = 1,\ t_1t_2t_3t_4 = -1$
D_4	$t^r = 1,\ \forall r \in \mathsf{R}(D_4)$	$t_1 = t_2 = t_3 = t_4 = 1$

Table 3-2 Classification of du Val singularities and the corresponding conditions on t. Each row represents a type of singularity characterized by the embedding of a sub-root system into $\mathsf{R}(D_4)$. The second column specifies the conditions on t, where $t^r = 1$ holds for all roots r in the respective sub-root system. The third column provides illustrative examples of these conditions. The type of the sub-root system matches that of the du Val singularity.

3.2.3 Geometry in complex structure I: Hitchin fibration

In this subsection, I will analyze the geometry from the perspective of Hitchin system, where I will show the important role of D_4 root system again. And I will describe how the du Val singularities appear from this perspective.

As is mentioned in the last chapter, in complex structure I, the Hitchin moduli space admits the Hitchin fibration over the Hitchin base $\mathcal{B}_H$[9]:

$$\begin{aligned} h : \mathcal{M}_H(C_{0,4}, \mathrm{SU}(2)) &\to \mathcal{B}_H = H^0(C_{0,4}, K_C^{\otimes 2}) \,. \\ (E, \varphi) &\mapsto \mathrm{Tr}(\varphi^2) \end{aligned} \tag{3.44}$$

It is a completely integrable system so that generic fibers are abelian varieties (sometimes called "Liouville tori") and they are holomorphic Lagrangian with respect to Ω_I, namely Lagrangian submanifolds of type (B, A, A). For our case where $G = \mathrm{SU}(2)$ and the base curve is $C_{0,4}$, the Hitchin moduli space is of quaternionic dimension one, and a generic fiber $\mathbf{F}$ of the Hitchin fibration is topologically a two-torus. The Hitchin base $\mathcal{B}_H$ is identified with the u-plane that parametrizes the complex structure u of the Seiberg-Witten curve(3.7).

At special points of the u-plane where the Seiberg-Witten curve(3.7) becomes singular, a Hitchin fiber degenerates into a singular fiber. The geometry of the moduli space undergoes significant changes as the ramification parameters (3.19) at the four punctures are varied, leading to changes in the types of singular fibers.

The appearance of these singular fibers on the Coulomb branch can be understood physically as the result of certain charged BPS particles becoming massless in the low-energy effective theory of SU(2) $N_f = 4$ SQCD[7–8]. In the 6d perspective, singular Seiberg-Witten curves correspond to the case where two branch points coincide. Then some M2-brane suspended on the M5-brane wrapping along some loop will shrink to a point, therefore resulting in a massless M2-brane thus a massless BPS particle in 4d.

Each singular fiber has an associated monodromy matrix in $\mathrm{SL}(2, \mathbb{Z})$, which encodes how the homology cycles of the elliptic curve transform around the singularity. The specific type of massless BPS particle is determined by the monodromy matrix around the singular fiber, once an electromagnetic frame is chosen. More precisely, if the particle becoming massless at u_* has charge (n_m, n_e), then its charge remains invariant under the monodromy matrix M associated with u_*:

$$(n_m, n_e) \cdot M = (n_m, n_e) \,. \tag{3.45}$$

Kodaira types of singular fibers The possible types of singular fibers in an elliptic fibration have been systematically classified by Kodaira[65–66]. The types of Kodaira singular fibers in the Hitchin fibration can be determined from the Seiberg-Witten curve (3.7) through two steps. The first step is to convert the Seiberg-Witten curve (3.7) into the Weierstrass form $y^2 = x^3 + a(u)x + b(u)$[65,67]. The second step is to find a vanishing locus $u = u_*$ of its discriminant

$$\mathfrak{D}(u_*) := -16\left(4a(u_*)^3 + 27b(u_*)^2\right) , \tag{3.46}$$

where u_* is the location of a singular fiber at the Hitchin base $\mathcal{B}_H$. The vanishing orders of $a(u)$, $b(u)$, and $\mathfrak{D}(u)$ at this specific u_* determine the Kodaira type of the singular fiber.

It turns out that the resulting classification can be conveniently summarized by the usage of affine D_4 Dynkin diagram. Each type of singular fiber forms a chain of $\mathbb{CP}^1$ components (also known as rational curves or (-2)-curves) connected according to the structure of an affine ADE Dynkin diagram (except for Kodaira type II). Consequently, the intersection matrix of a singular fiber matches the corresponding affine Cartan matrix, up to an overall sign difference. While the analysis of the Seiberg-Witten curve

(3.7) with the ramification parameters γ_j, as described above, determines the configurations of singular fibers, the relationship between singular fibers and affine root systems provides a systematic way to classify the types of singular fibers. To see that, given the ramification parameters γ_j, we define the evaluation map as

$$\mathrm{ev}_\gamma : \mathsf{R}(D_4) \to \mathbb{R}\ ;\ r = (r_1, r_2, r_3, r_4) \mapsto \gamma_1 r_1 + \gamma_2 r_2 + \gamma_3 r_3 + \gamma_4 r_4\ . \tag{3.47}$$

The kernel of this linear map precisely gives the root system associated with the singular fibers. Physically, it encodes the breaking patterns of the flavor symmetry group $\mathrm{SO}(8)$ of the 4d SQCD for given mass parameters. By combining the analysis of the Seiberg-Witten curve with this root system approach, we can straightforwardly classify the possible configurations of the Hitchin fibrations. In the case where, given the kernel condition, the positions of singular fibers are generic, seven configurations appear as γ_j vary. These configurations are summarized in Table 3-3.

ord($\mathfrak{D}$)	Kodaira types	Conditions	Examples in γ_j	Examples in mass m_j
$(1,1,1,1,1,1)$	$6I_1$	$\mathrm{Ker}_{\mathrm{ev}_\gamma} = \emptyset$	$(\gamma_1,\gamma_2,\gamma_3,\gamma_4)$	(m_1,m_2,m_3,m_4)
$(2,1,1,1,1)$	$(I_2, 4I_1)$	$\mathrm{Ker}_{\mathrm{ev}_\gamma} \cong \mathsf{R}(A_1)$	$(\gamma_1,\gamma_2,\gamma_3,0)$ $(\gamma_1,\gamma_2,\gamma_3,\gamma_1+\gamma_2+\gamma_3)$	(m_1,m_2,m_3,m_3)
$(2,2,1,1)$	$(2I_2, 2I_1)$	$\mathrm{Ker}_{\mathrm{ev}_\gamma} \cong \mathsf{R}(A_1)^{\oplus 2}$	$(\gamma_1,\gamma_2,\gamma_1,\gamma_2)$ $(\gamma_1,\gamma_2,0,0)$	(m_1,m_2,m_1,m_2) $(m_1,m_2,0,0)$
$(2,2,2)$	$3I_2$	$\mathrm{Ker}_{\mathrm{ev}_\gamma} \cong \mathsf{R}(A_1)^{\oplus 3}$	$(\gamma_1,0,0,0)$ $(\gamma_1,\gamma_1,\gamma_1,\gamma_1)$	$(m_1,m_1,0,0)$
$(3,1,1,1)$	$(I_3, 3I_1)$	$\mathrm{Ker}_{\mathrm{ev}_\gamma} \cong \mathsf{R}(A_2)$	$(\gamma_1,\gamma_2,\gamma_1+\gamma_2,0)$	(m_1,m_2,m_2,m_2)
$(4,1,1)$	$(I_4, 2I_1)$	$\mathrm{Ker}_{\mathrm{ev}_\gamma} \cong \mathsf{R}(A_3)$	$(\gamma_1,\gamma_1,0,0)$	(m_1,m_1,m_1,m_1) $(m_1,0,0,0)$
(6)	I_0^*	$\mathrm{Ker}_{\mathrm{ev}_\gamma} \cong \mathsf{R}(D_4)$	$(0,0,0,0)$	$(0,0,0,0)$

Table 3-3 The "generic" configurations of Kodaira singular fibers in the Hitchin fibration of $\mathcal{M}_H(C_{0,4}, \mathrm{SU}(2))$, along with conditions on the evaluation map kernel $\ker \mathrm{ev}_\gamma$. The table also lists the associated multiplicity ord($\mathfrak{D}$) of the discriminant (3.46), and examples of the corresponding parameters γ_j and m_j where the mass parameters and monodromy parameters are related by (3.21), where $\beta_i = 0$ is assumed for simplicity. The evaluation map ev_γ is defined in (3.47). The singular fibers can be read off from affine root system $\mathrm{Ker}_{\mathrm{ev}_\gamma}$, as detailed in the conditions column, with specific examples of γ_j and m_j values provided for each case.

However, Table 3-3 is *not* exhaustive as the root system does *not* uniquely determine the Kodaira types. To classify all possible configurations of the Hitchin fibration, it is helpful to revisit the physical interpretation of the singular fibers. For generic mass parameters, the Hitchin fibration contains six I_1 singular fibers ($6I_1$), which can be divided into two classes based on their distinct monodromies. In a preferred electro-magnetic frame, four of these singular fibers, with base points denoted by p_i for $i = 1,2,3,4$, have monodromies given by

$$M_q = T = \begin{pmatrix} 1 & 1 \\ 0 & 1 \end{pmatrix}\ . \tag{3.48}$$

At these points, known as quark singularities, the $(n_m, n_e) = (0,1)$-cycle $S^1 \subset T^2$ is pinched in a Hitchin fiber so that a quark with charge $(n_m, n_e) = (0,1)$ becomes

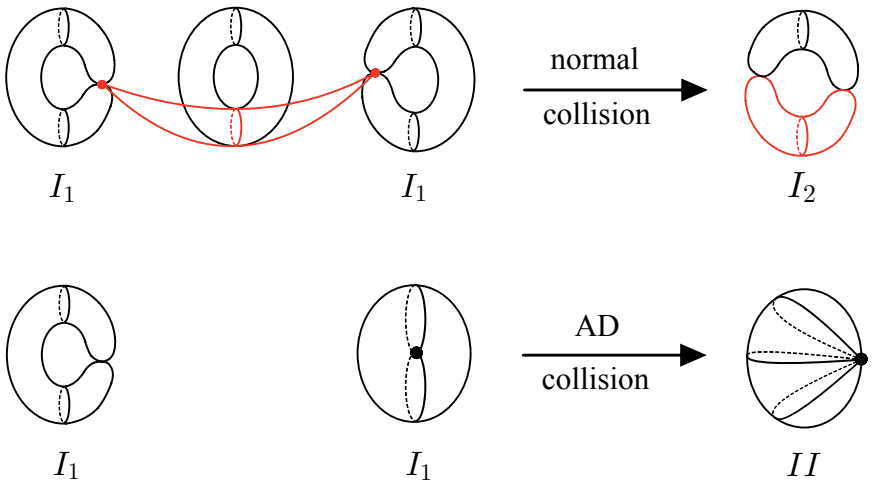

Figure 3-3 Two types of collisions of I_1 fibers. When two I_1 are of the same type, there is a cycle suspended between them, drawn in red. After the collision, an I_2 fiber appears where the suspended cycle becomes a (red) fiber cycle. When two I_1 are of distinct types, there is no cycle directly suspended between them, and collision will result in a II type singular fiber.

massless. The remaining two singular fibers, with base points denoted by p_i for $i = 5, 6$, have monodromies given by

$$M_d = T^2 S T S^{-1} T^{-2} = \begin{pmatrix} -1 & 4 \\ -1 & 3 \end{pmatrix} , \tag{3.49}$$

where the standard generators of $\mathrm{SL}(2, \mathbb{Z})$ are given by

$$T = \begin{pmatrix} 1 & 1 \\ 0 & 1 \end{pmatrix} , \qquad S = \begin{pmatrix} 0 & 1 \\ -1 & 0 \end{pmatrix} . \tag{3.50}$$

At these points, known as dyon singularities, the $(n_m, n_e) = (1, -2)$-cycle $S^1 \subset T^2$ is pinched in a Hitchin fiber so that a dyon with charge $(n_m, n_e) = (1, -2)$ becomes massless. Then, direct calculation shows that the combined monodromy satisfies

$$M_q^2 M_d M_q^2 M_d = \begin{pmatrix} -1 & 0 \\ 0 & -1 \end{pmatrix} \tag{3.51}$$

which corresponds to the monodromy for the I_0^* singular fiber, as expected at infinity.[①]

There are two possible scenarios when two I_1 fibers collide to form a singular fiber. The first possibility is a collision of two I_1 fibers with monodromies of the same type. We refer to this as a *normal collision*. Since the same one-cycle $S^1 \subset T^2$ becomes trivial for both singular fibers, there exists a two-cycle suspended between these singular fibers, as illustrated in Figure 3-3. Generally, when such fibers collide, an additional fiber cycle emerges. As a result, a normal collision of two I_1 fibers produces an I_2

① In[8], an electro-magnetic frame is chosen such that there are four quark (M_q), one monopole (M_m), and one dyon (M_d) singularities, satisfying:

$$M_q^4 M_m M_d = \begin{pmatrix} -1 & 0 \\ 0 & -1 \end{pmatrix} . \tag{3.52}$$

For convenience, we have adopted a different frame here.

singular fiber. By appropriately tuning the parameters γ_j, one can successively collide additional I_1 fibers, leading to higher singular types as listed in Table 3-3.

The second possibility involves a collision of two I_1 fibers with monodromies of different types. With a specific choice of the UV coupling constant τ and the mass parameters of the Seiberg-Witten curve (3.7), a quark singularity and a dyon singularity can collide, resulting in the monodromy

$$M_d \cdot M_q = \begin{pmatrix} -1 & 3 \\ -1 & 2 \end{pmatrix} \sim \begin{pmatrix} 1 & 1 \\ -1 & 0 \end{pmatrix}, \tag{3.53}$$

which corresponds to the monodromy of Kodaira type II. At this point, mutually non-local degrees of freedom become massless simultaneously, as discussed in[68–69]. The resulting low-energy theory is known as the (A_1, A_2) Argyres-Douglas (AD) theory. Geometrically, AD points are characterized by the collision of singular fibers with monodromy of distinct types. We refer to this as an *AD collision*.

Further collisions involving the (A_1, A_2) AD point and quark singularities give rise to singular fibers of Kodaira types III and IV, corresponding to the (A_1, A_3) and (A_1, D_4) AD theories[69], respectively. These account for the remaining configurations of the Hitchin fibration. Figure 3-4 classifies all possible Kodaira singular fibers in $\mathcal{M}_H(C_{0,4}, \mathrm{SU}(2))$ and illustrates how, starting from the $6I_1$ configuration, singular fibers undergo collisions and evolve into fibers of higher types as the ramification parameters γ_j are tuned, ultimately culminating in the I_0^* singular fiber. Note that the kernel of the evaluation map (3.47) is the root system associated with the singular fibers even with these "exceptional" cases. Nonetheless, such collisions require a specific choice of the UV coupling constant τ. A detailed analysis of these AD points in the Hitchin moduli space is presented in Appendix D.

affine Weyl group of type D_4 A key insight into understanding this geometry under the change of the ramification parameters comes from its connection to the D_4 root system. Among physics literature, the geometry of the Hitchin moduli space for a curve with tame ramifications has been studied in great detail in[26]. One of the key insights there is the action of the affine Weyl group on the second (co)homology group of the Hitchin moduli space. Consider the case where all ramification points correspond to full punctures, and the triples $(\alpha_j, \beta_j, \gamma_j) \in (\mathfrak{t}_j)^3$ take generic values. Following the notation of[26], we denote the corresponding moduli space as $\mathcal{M}_H(\alpha_1, \beta_1, \gamma_1; \dots; \alpha_s, \beta_s, \gamma_s; G)$. In this setting, the second integral homology group can be identified with the (generalized) affine root lattice:

$$H_2(\mathcal{M}_H(\alpha_1, \beta_1, \gamma_1; \dots; \alpha_s, \beta_s, \gamma_s; G), \mathbb{Z}) \cong \mathbb{Z}\langle e \rangle \oplus \bigoplus_{j=1}^{s} \mathsf{Q}_j(\mathfrak{g}), \tag{3.54}$$

where e is the generator of the second homology group $H_2(\mathbf{V}, \mathbb{Z}) \cong \mathbb{Z}\langle e \rangle$ of the moduli space $\mathbf{V}$ of G-bundles. Consequently, the (generalized) affine Weyl group $\dot{W}^s \cong (W \ltimes \mathsf{t}(\mathsf{Q}^\vee))^s$ acts naturally on the second homology group. Here, $\mathsf{Q}^\vee$ represents the coroot lattice, which acts via affine translations t, given explicitly by:

$$\mathsf{t}(r_j^\vee)(\tilde{r}_j) = \tilde{r}_j - (\tilde{r}_j, r_j^\vee)e, \quad j \in \{1, \dots, s\}. \tag{3.55}$$

In our case, where $G = \mathrm{SU}(2)$ and the Riemann surface is a four-punctured sphere $C_{0,4}$, it is well known that the flavor symmetry is enhanced from $\mathrm{SU}(2)^4$ to the $\mathrm{SO}(8)$

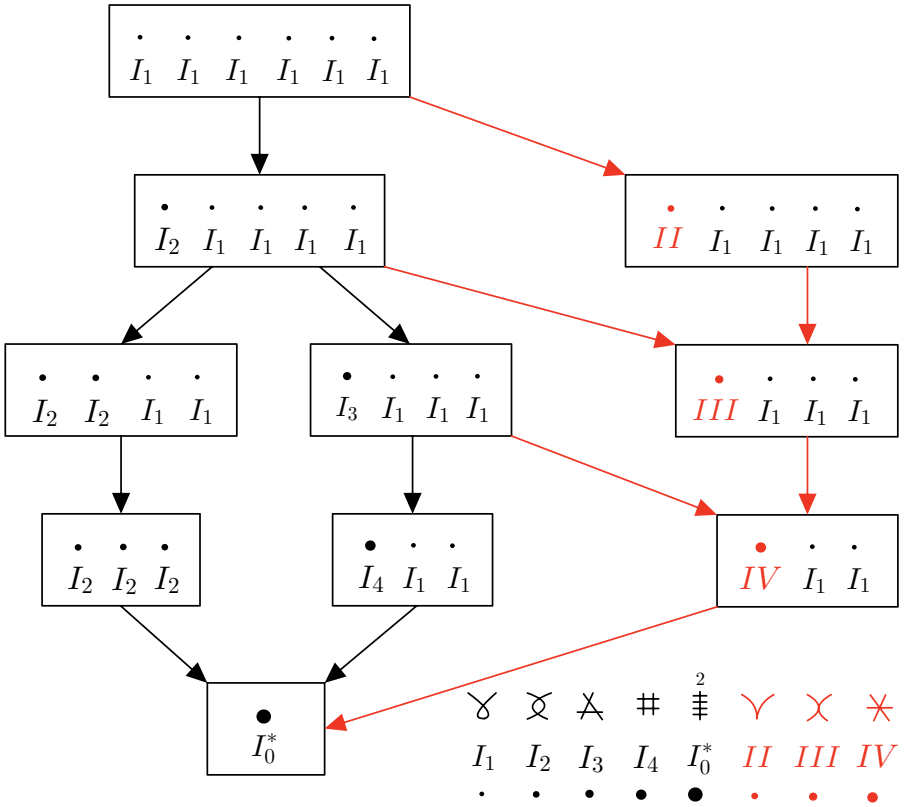

Figure 3-4 Classification of Kodaira singular fibers and their transitions under continuous variations of mass parameters. Seven configurations contain only I_k-type or I_0^*-type singular fibers, referred to as "generic" configurations, which are interconnected by black arrows representing normal collisions. The remaining three configurations involve II, III, and IV types of singular fibers, corresponding to Argyres-Douglas points, and are denoted as "exceptional" configurations. These transitions are depicted with red arrows, indicating the presence of collisions of Argyres-Douglas type. The geometry of singular fibers is schematically illustrated at the bottom right, where each line represents a $\mathbb{CP}^1$ component.

group[8]. As a result, the space of ramification parameters $(\alpha_j, \beta_j, \gamma_j) \in (\mathfrak{t}_j)^3$ at the four punctures, where each parameter takes values in the Cartan subalgebra $\mathfrak{t}_j$ of $\mathrm{SU}(2)$, can be naturally identified with the Cartan subalgebra of the Lie algebra of type D_4:

$$\prod_{j=1}^{4} \mathfrak{t}_j^{(\alpha)} \times \mathfrak{t}_j^{(\beta)} \times \mathfrak{t}_j^{(\gamma)} \cong \mathfrak{t}_{D_4}^{(\alpha)} \times \mathfrak{t}_{D_4}^{(\beta)} \times \mathfrak{t}_{D_4}^{(\gamma)} \,. \tag{3.56}$$

Moreover, the second integral homology group of the moduli space can be identified with the affine root lattice of type D_4:

$$\mathbb{Z}\langle e \rangle \oplus \bigoplus_{j=1}^{4} \mathsf{Q}_j(A_1) \cong \dot{\mathsf{Q}}(D_4) \cong H_2(\mathcal{M}_H(C_{0,4}, \mathrm{SU}(2)), \mathbb{Z}) \,, \tag{3.57}$$

on which the affine Weyl group of type D_4 acts:

$$\dot{W}(D_4) \cong W(D_4) \ltimes \mathfrak{t}(\mathsf{Q}_{D_4}^\vee) \,. \tag{3.58}$$

The affine Weyl group also acts on the ramification parameters (α, β, γ)

$$\frac{\mathfrak{t}_{D_4}^{(\alpha)} \times \mathfrak{t}_{D_4}^{(\beta)} \times \mathfrak{t}_{D_4}^{(\gamma)}}{\dot{W}(D_4)} \cong \frac{T_{D_4}^{(\alpha)} \times \mathfrak{t}_{D_4}^{(\beta)} \times \mathfrak{t}_{D_4}^{(\gamma)}}{W(D_4)}, \tag{3.59}$$

where the affine translation $\mathfrak{t}(Q_{D_4}^\vee)$ acts non-trivially only on the α-space. The quotient of the affine translation (3.55) can be identified with the periodicity

$$\alpha_j \sim \alpha_j + 1\,. \tag{3.60}$$

As we will see below, a point of the space $T_{D_4} \times \mathfrak{t}_{D_4} \times \mathfrak{t}_{D_4}$ represents the cohomology classes of the Kähler forms in the second cohomology group $H^2(\mathcal{M}_H, \mathbb{R})$ of the corresponding moduli space:

$$\left(\left[\frac{\omega_I}{2\pi}\right], \left[\frac{\omega_J}{2\pi}\right], \left[\frac{\omega_K}{2\pi}\right]\right) \in T_{D_4} \times \mathfrak{t}_{D_4} \times \mathfrak{t}_{D_4}\,. \tag{3.61}$$

In fact, the connection between the affine Weyl group of type D_4 and this system also has an extensive history. It was first discovered in[70] that a group of Bäcklund transformations of Painlevé VI equation is isomorphic to $\dot{W}(D_4)$. For our purposes, the modern treatment of the relation between the geometry of the cubic surface (3.34) and the affine Weyl group $\dot{W}(D_4)$ is provided in[64].

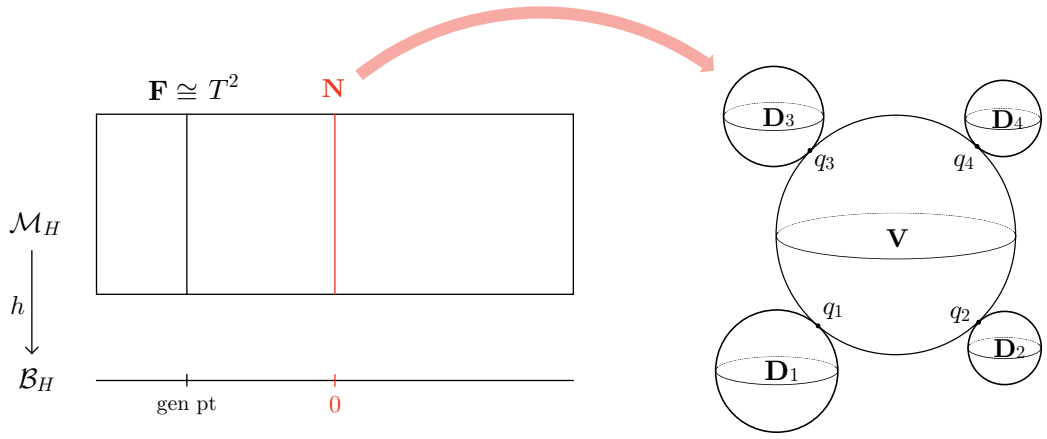

Figure 3-5 The schematic figure of the Hitchin fibration $\mathcal{M}_H \to \mathcal{B}_H$ when the ramification parameters α_j are generic, and the others are zero $\beta_j = \gamma_j = 0$, $(j = 1, 2, 3, 4)$. A generic fiber **F** is topologically a two-torus, and the global nilpotent cone **N** at the origin of the Hitchin base $\mathcal{B}_H$ is a singular fiber of Kodaira type I_0^*, which is illustrated on the right.

3.2.4 Global nilpotent cone

Let us examine the geometry of the Hitchin moduli space under the condition that the ramification parameters α_j are generic while the others are set to zero, $\beta_j = \gamma_j = 0$ $(j = 1, 2, 3, 4)$. Under these assumptions, the Hitchin fibration $h : \mathcal{M}_H(C_p, \mathrm{SU}(2)) \to \mathcal{B}_H$ in (3.44) possesses a singular fiber only at the origin of the base, $\mathbf{N} = h^{-1}(0)$, which is referred to as the *global nilpotent cone*. The global nilpotent cone **N** is a singular fiber of Kodaira type I_0^*[71], characterized by a configuration of five irreducible components,

each of which is topologically $\mathbb{CP}^1$, arranged in the shape of the affine D_4 Dynkin diagram:

$$\mathbf{N} = \mathbf{V} \cup \bigcup_{j=1}^{4} \mathbf{D}_j \,, \tag{3.62}$$

where $\mathbf{V}$ represents the moduli space of SU(2)-bundles on the four-punctured sphere $C_{0,4}$, and $\mathbf{D}_j$ $(j = 1, 2, 3, 4)$ are known as the exceptional divisors. (See Figure 3-5.)

At generic values of α_j, each irreducible component of the global nilpotent cone serves as a generator of the second integral homology group, $H_2(\mathcal{M}_H, \mathbb{Z}) \cong \mathbb{Z}^{\oplus 5}$. Using the basis $\{[\mathbf{D}_1], [\mathbf{D}_2], [\mathbf{D}_3], [\mathbf{D}_4], [\mathbf{V}]\}$, the intersection pairing between these homology classes is represented by the Cartan matrix of the affine D_4 Dynkin diagram, up to an overall minus sign:

$$Q = \begin{pmatrix} -2 & 0 & 0 & 0 & 1 \\ 0 & -2 & 0 & 0 & 1 \\ 0 & 0 & -2 & 0 & 1 \\ 0 & 0 & 0 & -2 & 1 \\ 1 & 1 & 1 & 1 & -2 \end{pmatrix} . \tag{3.63}$$

With this bilinear pairing defined by the intersection form, the second homology group $H_2(\mathcal{M}_H, \mathbb{Z})$ can be identified with the root lattice of the affine D_4 Lie algebra. In this identification, the irreducible components correspond to the simple roots of the affine D_4 root system. Furthermore, these components also satisfy a fiber-class relation in $H_2(\mathcal{M}_H, \mathbb{Z})$:

$$[\mathbf{F}] = 2[\mathbf{V}] + \sum_{j=1}^{4} [\mathbf{D}_j] \,, \tag{3.64}$$

where $[\mathbf{F}]$ denotes the homology class of a generic fiber of the Hitchin fibration[71].

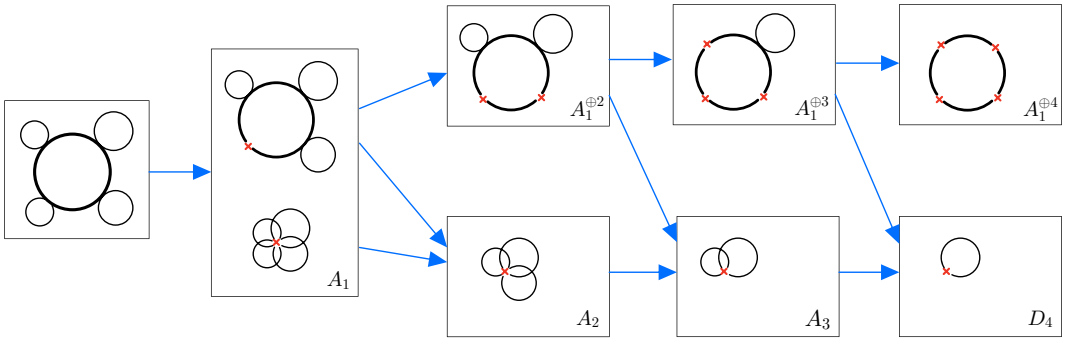

Figure 3-6 When $\beta_j = \gamma_j = 0$, du Val singularities emerge as the volumes of $\mathbf{V}$ or $\mathbf{D}_j$ shrink to zero. These vanishing volumes are indicated by red crosses on the corresponding diagrams. The blue arrows represent transitions where a single volume contracts to zero, leading to successive enhancements of the singularity type. The progression illustrates the hierarchy of du Val singularities, starting from A_1 and culminating in higher types such as $A_1^{\oplus 4}$ and D_4.

Now let's determine the volumes (3.30) of the classes identified above:

$$\mathrm{vol}_I(\mathbf{V}) := \int_{\mathbf{V}} \frac{\omega_I}{2\pi} \,, \qquad \mathrm{vol}_I(\mathbf{D}_j) = \int_{\mathbf{D}_j} \frac{\omega_I}{2\pi} \,. \tag{3.65}$$

As a characteristic of the Hitchin fibration, due to its complete integrability, the period of $\omega_I/2\pi$ over a general fiber $\mathbf{F}$ is one:

$$\mathrm{vol}_I(\mathbf{F}) = \int_{\mathbf{F}} \frac{\omega_I}{2\pi} = 1 \,. \tag{3.66}$$

As a result of the relation (3.64), we have the constraint

$$2\mathrm{vol}_I(\mathbf{V}) + \sum_{j=1}^{4} \mathrm{vol}_I(\mathbf{D}_j) = 1 \,. \tag{3.67}$$

The relation between the ramification parameters α_j and the volumes of the irreducible components in the global nilpotent cone is subtle and involves the wall-crossing phenomenon. As illustrated in Figure 3-6, when an irreducible component $\mathbf{V}$ or $\mathbf{D}_j$ shrinks to zero, the Higgs bundle is no longer stable, and the Hitchin moduli space develops a du Val singularity. These singularities correspond to special points in the Kähler moduli space, which are located at codimension-one loci, referred to as walls. As seen in (3.41), du Val singularities appear precisely at the zeros of the discriminant

$$t^r = 1 \,, \quad \forall r \in \mathsf{R}(D_4) \,. \tag{3.68}$$

Since we are now considering the case $\gamma_j = 0$, with $t_j = e^{-2\pi(\gamma_j + i\alpha_j)}$, the locations of the walls (3.68) in the Kähler moduli space are therefore specified by

$$\sum_{j=1}^{4} r_j \alpha_j = n, \qquad \forall r \in \mathsf{R}(D_4), \quad \forall n \in \mathbb{Z} \,. \tag{3.69}$$

These walls align with the set of reflection hyperplanes for the affine D_4 weight lattice at level one[64]. In an affine root system, the reflection of an affine weight λ at level one with respect to an affine root $\dot{r} = r - n\delta$

$$s_{\dot{r}}(\lambda) = s_r\left(\lambda - \frac{n}{2} r\right) \tag{3.70}$$

corresponds to a reflection over the hyperplane specified by (3.69), generating the affine Weyl group $\dot{W}(D_4)$. Therefore, a chamber surrounded by the walls in (3.69) corresponds to a Weyl alcove of type D_4.

A du Val singularity arises when a two-cycle shrinks to zero volume, whose condition (3.69) is linear in the Kähler parameters α_j. This implies that the volume of a compact two-cycle depends linearly on α_j. This linearity can be numerically verified by the integration of $\omega_I/2\pi$ over $\mathbf{V}$ in the relevant domain where the variables x, y, z in the cubic surface (3.34) are real. Starting from this observation, we can make some statements about the volumes of the cycle.

Assuming that the volumes of compact two-cycles are linear in α_j, the configurations of the walls in (3.68), along with the normalization in (3.66) uniquely determine the volumes of the cycles. Given a point α_j of the Kähler moduli space, the volumes of the two-cycles $\mathbf{V}$ and $\mathbf{D}_j$ ($j = 1, 2, 3, 4$) are equal to twice the distance from this point to the corresponding walls, as illustrated in Figure 3-7. The factor of two arises from the length of a root $r \in \mathsf{R}(D_4)$. Since the walls can be identified with the set of reflection hyperplanes for the affine D_4 Weyl group, the set of volumes agrees with the concept of the basis for the affine root system D_4[72].

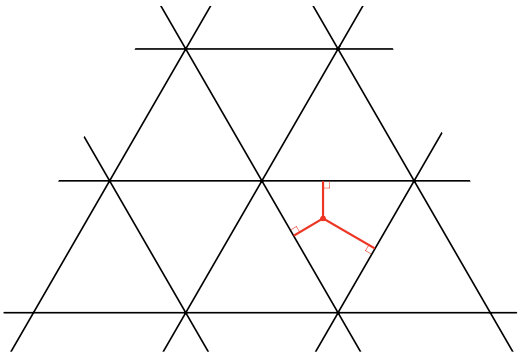

Figure 3-7 A schematic illustration of the volumes of compact two-cycles in the Kähler moduli space. The black lines represent reflection hyperplanes, and each triangle corresponds to a Weyl alcove, which is a chamber in the moduli space. The volumes of the two-cycles are twice the distances (depicted by the lengths of the red lines) from a given parameter point to the walls of the chamber containing it.

This identification immediately indicates a wall-crossing phenomenon of the volume functions in the Kähler moduli space. Whenever the α_j parameters cross the wall defined by the vanishing loci of an affine root r, the basis of roots is transformed by the Weyl reflection s_r.

$$s_{r_a}(r_b) = r_b - \dot{A}_{ba} r_a \tag{3.71}$$

where $\dot{A}_{ba}$ is the affine D_4 Cartan matrix. As a result, the volume functions exhibit a discontinuity, with their dependence on the Kähler parameters α_j jumping by the affine Weyl reflection. The detailed study of the chamber structures and the appearance of du Val singularities is presented in Appendix C.

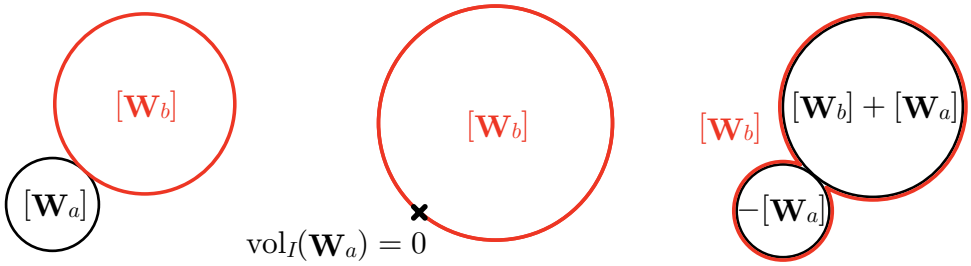

Figure 3-8 When crossing the wall defined by $\mathrm{vol}_I(\mathbf{W}_a) = 0$, there is a basis transformation of the second homology, governed by the Picard-Lefschetz monodromy transformation $T_{\mathbf{W}_a}$ defined in (3.72). This figure illustrates the action of $T_{\mathbf{W}_a}$ on the homology classes $[\mathbf{W}_a]$ and $[\mathbf{W}_b]$ when their intersection number satisfies $[\mathbf{W}_a] \cdot [\mathbf{W}_b] = 1$ where $[\mathbf{W}_a]$ is inverted and $[\mathbf{W}_b]$ shifts by $[\mathbf{W}_a]$. The middle diagram represents the configuration at the moment of wall-crossing, where the volume of $\mathbf{W}_a$ vanishes. This transformation reflects the geometric change in the homology basis due to the vanishing cycle.

This wall-crossing phenomenon admits geometric interpretation. When crossing a wall defined by $\mathrm{vol}_I(\mathbf{W}_a) = 0$ for $[\mathbf{W}_a] \in H_2(\mathcal{M}_H, \mathbb{Z})$, the Picard-Lefschetz (PL) monodromy transformation[73–74] changes a base of the second homology due to the vanishing cycle $[\mathbf{W}_a]$ as

$$T_{\mathbf{W}_a}([\mathbf{W}_b]) = [\mathbf{W}_b] + ([\mathbf{W}_a] \cdot [\mathbf{W}_b])[\mathbf{W}_a] \,, \qquad [\mathbf{W}_b] \in H_2(\mathcal{M}_H, \mathbb{Z}) \,. \tag{3.72}$$

The sign difference from (3.71) results from the sign difference between the intersection form (3.63) and the affine Cartan matrix $\dot{A}_{ba}$. Therefore, writing $T_j \equiv T_{\mathbf{D}_j}$ for $(j = 1,2,3,4)$, the PL transformation geometrically realizes the affine Weyl reflection in (3.71) in the second homology classes, subject to the following relations:

$$\begin{aligned} T_j T_k &= T_k T_j \,, \\ T_j T_{\mathbf{V}} T_j &= T_{\mathbf{V}} T_j T_{\mathbf{V}} \,, \\ T_j^2 &= T_{\mathbf{V}}^2 = \mathrm{id} \,, \end{aligned} \tag{3.73}$$

for any pair $(j,k = 1,2,3,4)$. In conclusion, the PL transformation gives a concrete example of the affine Weyl group action on the second integral homology class of the Hitchin moduli space[26].

The remainder of this subsection focuses on visualizing the wall inside the Kähler moduli space, specifying a chamber, and explicitly writing down the volume function. Using the periodicity $\alpha_j \to \alpha_j + 1$, we can restrict α_j to the range $[-\frac{1}{2}, \frac{1}{2}]$. In addition, the Weyl group invariance $\alpha_j \to -\alpha_j$ of the cubic equation implies that parameter space is symmetric with respect to four $\alpha_j = 0$ walls. In total, all the walls of (3.68) divide the parameter space into 24×2^5 chambers, where the factor 2^5 corresponds to the sign changes of α_j. Consequently, it suffices to study the region where α_j is restricted to $[0, \frac{1}{2}]$, which contains 24 chambers. This subset of the parameter space forms a 4-dimensional hypercube, which we denote as Cube.

To visualize the 24 chambers in Cube, we can fix the value of α_1 and examine a 3-dimensional cross-section of the hypercube, represented as a 3-cube in Figure 3-9. This 3-cube is subdivided into 23 distinct regions, each corresponding to a unique chamber in Cube. The mapping between these regions and the chambers is injective, meaning no two regions correspond to the same chamber. However, one chamber remains "invisible" in this visualization. If we instead cut along $\frac{1}{2} - \alpha_1$, the central chamber $WXYZ$ is replaced by the previously hidden chamber..

In the subsequent analysis, we focus on the central chamber $WXYZ$, as depicted in Figure 3-9, with $\alpha_1 \in [0, \frac{1}{4}]$. The other chambers can be analyzed similarly. The central chamber is the region defined by the following constraints:

$$\begin{aligned} \alpha_1 + \alpha_2 + \alpha_3 + \alpha_4 &\le 1 \,, \\ -\alpha_1 - \alpha_2 + \alpha_3 + \alpha_4 &\ge 0 \,, \\ -\alpha_1 + \alpha_2 - \alpha_3 + \alpha_4 &\ge 0 \,, \\ -\alpha_1 + \alpha_2 + \alpha_3 - \alpha_4 &\ge 0 \,, \end{aligned} \tag{3.74}$$

together with the restriction $\alpha_1 \in [0, \frac{1}{4}]$. The four constraints in (3.74) correspond to the four walls XYZ, WYZ, WZX, WXY of this tetrahedron. From the identification between the volume functions and the basis of the affine root system, we deduce the explicit volume functions in this chamber:

$$\begin{aligned} \mathrm{vol}_I(\mathbf{D}_j) = \Big(&1 - \alpha_1 - \alpha_2 - \alpha_3 - \alpha_4,\ -\alpha_1 - \alpha_2 + \alpha_3 + \alpha_4, \\ &-\alpha_1 + \alpha_2 - \alpha_3 + \alpha_4,\ -\alpha_1 + \alpha_2 + \alpha_3 - \alpha_4\Big), \\ \mathrm{vol}_I(\mathbf{V}) = &\ 2\alpha_1 \,, \end{aligned} \tag{3.75}$$

where the normalization in (3.67) is appropriately applied.

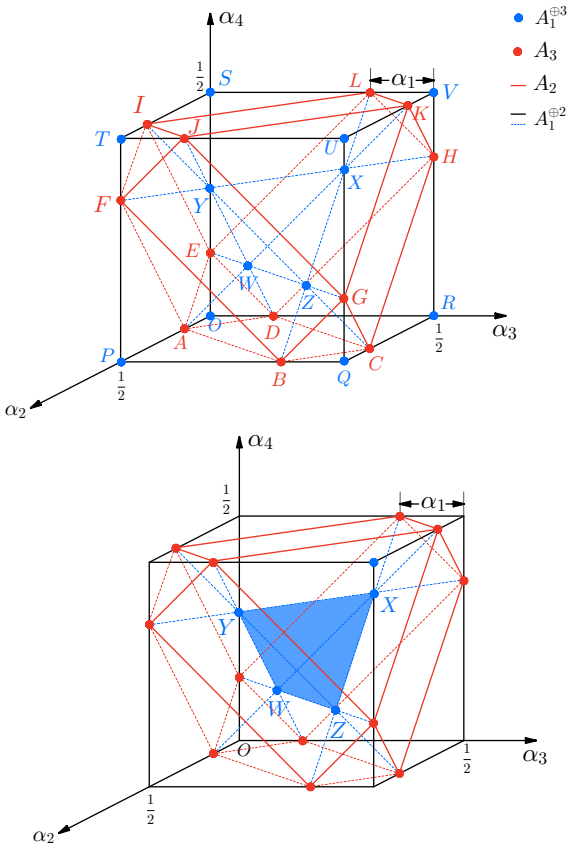

Figure 3-9 (Left): The cross section of the Kähler moduli space Cube at a fixed $\alpha_1 \in [0, \frac{1}{4}]$, and its chamber structure. W is at $(\alpha_1, \alpha_1, \alpha_1)$ and X, Y, Z have one coordinate α_1 and two $\frac{1}{2} - \alpha_1$; A, D, E have two coordinates 0 one α_1 and $B, C, F, G, H, I, J, K, L$ have one coordinate 0, one $\frac{1}{2}$ and one $\frac{1}{2} - \alpha_1$. Every plane in the 3-cube corresponds to a wall where an A_1 type singularity develops, and other singularities are marked out. The $A_1^{\oplus 4}$ and D_4 singularities can be seen only for specific α_1.
(Right): The center chamber with $\alpha_1 \in [0, \frac{1}{4}]$, shaded in blue, is the tetrahedron $WXYZ$ determined by the constraints (3.74).

In fact, we can define the simple roots of the D_4 root system with a suitable choice of positive roots as

$$\{e^1, e^2, e^3, e^4\} = \{(-1,-1,1,1), (-1,1,-1,1), (-1,1,1,-1), (2,0,0,0)\}\,, \tag{3.76}$$

Then, the highest root is expressed by $\theta = e^1 + e^2 + e^3 + 2e^4 = (1,1,1,1)$. Using these roots, the volume functions can be concisely written as

$$\Big(\mathrm{vol}_I(\mathbf{D}_1), \mathrm{vol}_I(\mathbf{D}_2), \mathrm{vol}_I(\mathbf{D}_3), \mathrm{vol}_I(\mathbf{D}_4), \mathrm{vol}_I(\mathbf{V})\Big) = \Big(1 - \theta\cdot\alpha,\ e^1\cdot\alpha,\ e^2\cdot\alpha,\ e^3\cdot\alpha\,,\ e^4\cdot\alpha\Big)\,, \tag{3.77}$$

where $r \cdot \alpha = \sum_{j=1}^4 r_j \alpha_j$ is the Euclidean inner product. As drawn in Figure 3-10, the homology class of each irreducible component of the I_0^* singular fiber corresponds to an affine D_4 root as

$$[\mathbf{D}_1] \leftrightarrow e^0 = \delta - \theta\,, \quad [\mathbf{D}_2] \leftrightarrow e^1\,, \quad [\mathbf{D}_3] \leftrightarrow e^2\,, \quad [\mathbf{D}_4] \leftrightarrow e^3\,, \quad [\mathbf{V}] \leftrightarrow e^4\,, \tag{3.78}$$

where δ is the imaginary root and the case $\delta \cdot \alpha = 1$ is assumed for the volume function. Using the relation of the second homology classes, the homology class $[\mathbf{F}]$ of a generic

Hitchin fiber indeed corresponds to the imaginary root δ.

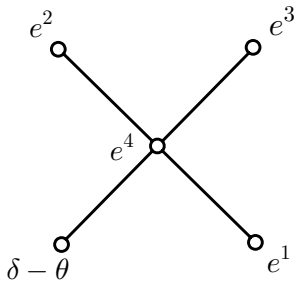

Figure 3-10 Simple roots of affine D_4 root system.

3.2.5 Generic Hitchin fibrations

As the parameters γ_j vary, the Hitchin fibration over the u-plane exhibits increasingly intricate behavior. In this subsection, we aim to identify the generators of the second homology group and compute their volumes. This investigation also provides insights into how the geometry of the target space $\mathfrak{X}$ evolves as the parameters (α_j, γ_j) are varied. We focus specifically on the central chamber $WXYZ$, defined in (3.74), where the parameters (α_j, γ_j) can be freely adjusted. By selecting sufficiently generic parameters, we ensure that the geometry avoids developing du Val singularities. Consequently, the second homology group $H_2(\mathcal{M}_H, \mathbb{Z})$ and its intersection form Q remain invariant as the γ_j parameters are turned on. Therefore, $H_2(\mathcal{M}_H, \mathbb{Z})$ can still be identified with the affine D_4 root lattice, as described in (3.57).

When the parameters γ_j are turned on, the global nilpotent cone of type I_0^* splits into other singular fibers, and the homology generators $[\mathbf{V}]$, $[\mathbf{D}_j]$ $(j = 1, 2, 3, 4)$ are not manifest in the Hitchin fibration. Nevertheless, they still span a basis of the second homology group at generic γ_j.

Recall the definition (3.30) of the volumes of 2-cycles, which is a linear function of the Kähler parameter α_j. In order to determine the volumes when γ_j are non-zero, we can consider a holomorphic version of volume:

$$\mathrm{vol}(\mathbf{W}) := \int_{\mathbf{W}} \frac{\Omega_J}{2\pi i} \,. \tag{3.79}$$

Due to the holomorphicity of Ω_J, the volumes depend solely on the complex moduli $\gamma_j + i\alpha_j$. When $\gamma_j = 0$ for all j, this coincides with the usual volume function vol_I. Thus when γ_j are turned on, the holomorphic volumes can be obtained by simply replacing α_j with $\alpha_j - i\gamma_j$.

For the center chamber, the holomorphic volumes can then be directly written down from (3.77) as:

$$\begin{aligned}&\Big(\mathrm{vol}(\mathbf{D}_1), \mathrm{vol}(\mathbf{D}_2), \mathrm{vol}(\mathbf{D}_3), \mathrm{vol}(\mathbf{D}_4), \mathrm{vol}(\mathbf{V})\Big)\\ &= \Big(1 - \theta \cdot (\alpha - i\gamma),\ e^1 \cdot (\alpha - i\gamma),\ e^2 \cdot (\alpha - i\gamma),\ e^3 \cdot (\alpha - i\gamma),\ e^4 \cdot (\alpha - i\gamma)\Big),\end{aligned} \tag{3.80}$$

where e^i and θ represent the simple roots and the highest root, respectively, as defined in (3.76).

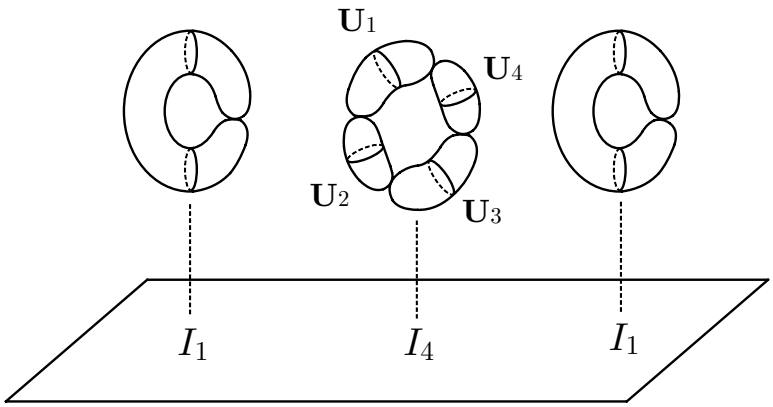

Figure 3-11 Cycles in Kodaira type $(I_4, 2I_1)$.

An I_k singular fiber consists of k $\mathbb{CP}^1$ components arranged in a necklace shape where we denote irreducible components by $\mathbf{U}_a$ for $a = 1, \ldots, k$. For instance, see Figure 3-11 for the I_4 singular fiber. To determine the volume function for these cycles, it is necessary to find the relationship between $[\mathbf{U}_a]$ and the basis $\{[\mathbf{D}_j], [\mathbf{V}]\}$. This can be done by simply using the structure of the affine root system.

The intersection form between the cycles $\mathbf{U}_a$ in an I_k singular fiber corresponds to the Cartan matrix of the affine root system A_{k-1}, up to an overall minus sign. This correspondence allows us to identify the second homology group of an I_k singular fiber with the affine A_{k-1} root lattice, where the homology classes $[\mathbf{U}_a]$ serve as the simple roots of the root lattice. Consequently, specifying the relationships between $[\mathbf{U}_a]$ and the basis $\{[\mathbf{D}_j], [\mathbf{V}]\}$ reduces to finding an embedding of an affine sub-root lattice $\dot{\mathsf{R}}(\mathfrak{g})$ into the affine D_4 root lattice $\dot{\mathsf{R}}(D_4)$.

Importantly, the embedding of $\dot{\mathsf{R}}(\mathfrak{g}) \hookrightarrow \dot{\mathsf{R}}(D_4)$ is not unique. This non-uniqueness arises because different choices of γ parameters can produce the same Hitchin fibration pattern. However, each embedding of the root system uniquely determines the γ parameters that generate the fibration pattern, up to cyclic permutations. Conversely, a fixed set of γ parameters uniquely determines the corresponding embedding of the affine subroot system.

To illustrate this interplay, we will conduct a detailed case study of the fibration configurations listed in Table 3-3. This analysis will clarify how specific embeddings of $\dot{\mathsf{R}}(\mathfrak{g}) \hookrightarrow \dot{\mathsf{R}}(D_4)$ correspond to the γ parameters and their corresponding Hitchin fibration patterns.

Type $(I_4, 2I_1)$

Let us consider the fibration pattern $(I_4, 2I_1)$, as shown in Figure 3-11. In this case, the singular fiber of type I_1 consists of a single irreducible component, and its homology class is simply the fiber class $[\mathbf{F}]$. So a generic fiber has volume 1 for any choice of (γ_j, α_j). On the other hand, the I_4 singular fiber has four components: $\{[\mathbf{U}_1], [\mathbf{U}_2], [\mathbf{U}_3], [\mathbf{U}_4]\}$. The intersection form of these components coincides with the Cartan matrix of the affine

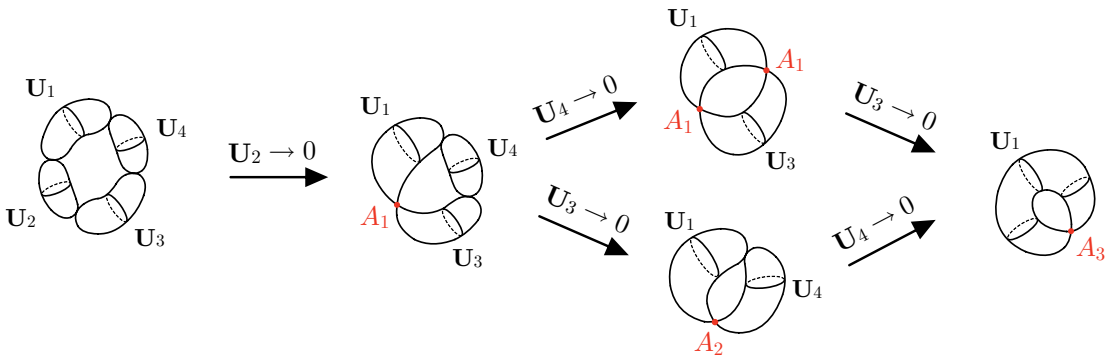

Figure 3-12 du Val singularities developed on I_4 fiber by shrinking cycles to points. $\mathbf{U}_a \to 0$ means that $\mathbf{U}_a$ shrinks to a point.

A_3 root system up to an overall sign, which is:

$$Q_{I_4} = \begin{pmatrix} -2 & 1 & 0 & 1 \\ 1 & -2 & 1 & 0 \\ 0 & 1 & -2 & 1 \\ 1 & 0 & 1 & -2 \end{pmatrix} \tag{3.81}$$

Therefore, the components $[\mathbf{U}_a]$ correspond to the simple roots of the affine A_3 root system. To compute the volumes of these cycles, we need to express their homology classes $[\mathbf{U}_a]$ in terms of the basis of $H_2(\mathcal{M}_H, \mathbb{Z})$. Although the data available now do not allow for a unique determination of these homology classes, we can infer that this setup specifies an embedding of the A_3 root system into the D_4 root system. One such possible embedding is given by:

$$[\mathbf{U}_1] = [\mathbf{V}] + [\mathbf{D}_1], \quad [\mathbf{U}_2] = [\mathbf{D}_2], \quad [\mathbf{U}_3] = [\mathbf{V}] + [\mathbf{D}_3], \quad [\mathbf{U}_4] = [\mathbf{D}_4]. \tag{3.82}$$

Next, since all of these components $[\mathbf{U}_a]$ are Lagrangian with respect to the symplectic form ω_K, consistency requires that we choose the parameters γ_j such that the integral of ω_K over each component vanishes. This condition is encoded in the following system of linear equations:

$$\begin{aligned} -\gamma_1 + \gamma_2 + \gamma_3 + \gamma_4 &= 0\,, \\ -\gamma_1 - \gamma_2 + \gamma_3 + \gamma_4 &= 0\,, \\ \gamma_1 + \gamma_2 - \gamma_3 + \gamma_4 &= 0\,, \\ -\gamma_1 + \gamma_2 + \gamma_3 - \gamma_4 &= 0\,. \end{aligned} \tag{3.83}$$

The solution to this system is $(\gamma_1, \gamma_2, \gamma_3, \gamma_4) = (\gamma_1, 0, \gamma_1, 0)$, which matches the conditions for the fibration configuration $(I_4, 2I_1)$ derived from the Seiberg-Witten curve, as classified in Table 3-3. From the homology class relation (3.82), we deduce the explicit volume formulas for the irreducible components of the cycles:

$$\begin{aligned} \mathrm{vol}_I(\mathbf{U}_1) &= 1 - (-\alpha_1 + \alpha_2 + \alpha_3 + \alpha_4), \\ \mathrm{vol}_I(\mathbf{U}_2) &= -\alpha_1 - \alpha_2 + \alpha_3 + \alpha_4, \\ \mathrm{vol}_I(\mathbf{U}_3) &= \alpha_1 + \alpha_2 - \alpha_3 + \alpha_4, \\ \mathrm{vol}_I(\mathbf{U}_4) &= -\alpha_1 + \alpha_2 + \alpha_3 - \alpha_4. \end{aligned} \tag{3.84}$$

When one or more of these volumes vanish, du Val singularities emerge. The conditions for such singularities align precisely with the classifications in Table 3-2, and these phenomena can be visualized geometrically in Figure 3-12.

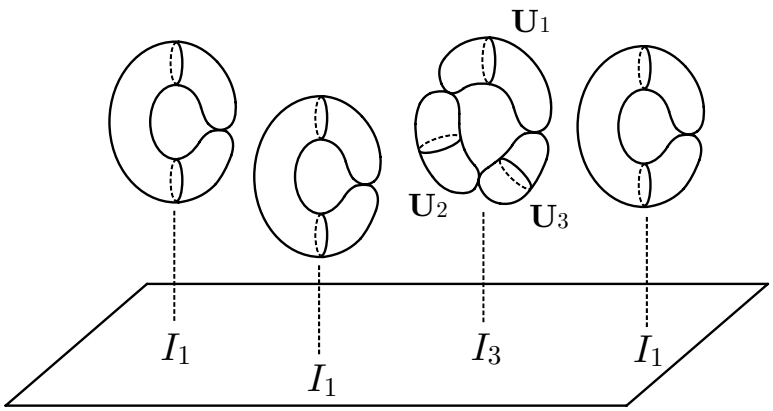

Figure 3-13 Cycles in Kodaira type $(I_3, 3I_1)$.

We can approach the analysis from the opposite direction by first specifying a choice of γ parameters. For illustration, we select the γ parameters as $(\gamma_1, \gamma_2, \gamma_3, \gamma_4) = (\gamma_1, 0, \gamma_1, 0)$. Since this choice of γ_j gives $\mathrm{Ker}\,(\mathrm{ev}_\gamma) = \mathsf{R}(A_3)$, this implies that the homology classes of the Lagrangian cycles with respect to ω_K span an affine A_3 root lattice in $H_2(\mathcal{M}_H, \mathbb{Z})$. Given a choice (3.74) of the chamber in the α parameter space, (equivalently a choice of positive roots in the root lattice), $\mathrm{Ker}\,(\mathrm{ev}_\gamma) = \mathsf{R}(A_3) \subset \mathsf{R}(D_4)$ uniquely specifies an embedding of $\dot{\mathsf{R}}(A_3) \hookrightarrow \dot{\mathsf{R}}(D_4)$. This will give the relation between the homology classes $[\mathbf{U}_a]$ and the basis of $H_2(\mathcal{M}_H, \mathbb{Z})$, which is exactly (3.82). A similar analysis is applied to the other cases.

Type $(I_3, 3I_1)$

Let us now consider the $(I_3, 3I_1)$ case, as in Figure 3-13. Denote the components of I_3 singular fiber as $[\mathbf{U}_1], [\mathbf{U}_2], [\mathbf{U}_3]$. The intersection form coincides with the affine A_2 Cartan matrix.

$$Q_{I_3} = \begin{pmatrix} -2 & 1 & 1 \\ 1 & -2 & 1 \\ 1 & 1 & -2 \end{pmatrix} \tag{3.85}$$

Thus, the components $[\mathbf{U}_a]$ can be interpreted as the simple roots of the affine A_2 root system. To compute their volumes, we express $[\mathbf{U}_a]$ in the basis of $H_2(\mathcal{M}_H, \mathbb{Z})$. Although the data do not uniquely determine these homology classes, it specifies an embedding of the affine A_2 root system into the affine D_4 root system, such as:

$$[\mathbf{U}_1] = [\mathbf{V}] + [\mathbf{D}_1] + [\mathbf{D}_2]\,, \qquad [\mathbf{U}_2] = [\mathbf{V}] + [\mathbf{D}_4]\,, \qquad [\mathbf{U}_3] = [\mathbf{D}_3]\,. \tag{3.86}$$

The Lagrangian conditions of cycles impose the following conditions on γ_j

$$\begin{aligned} 2\gamma_2 &= 0, \\ \gamma_1 + \gamma_2 + \gamma_3 - \gamma_4 &= 0, \\ -\gamma_1 + \gamma_2 - \gamma_3 + \gamma_4 &= 0, \end{aligned} \tag{3.87}$$

with solution taking the form $(\gamma_1, \gamma_2, \gamma_3, \gamma_4) = (\gamma_1, 0, \gamma_3, \gamma_1 + \gamma_3)$. It coincides with one of the conditions when $(I_3, 3I_1)$ singular type occurs as in Table 3-3. Integrating

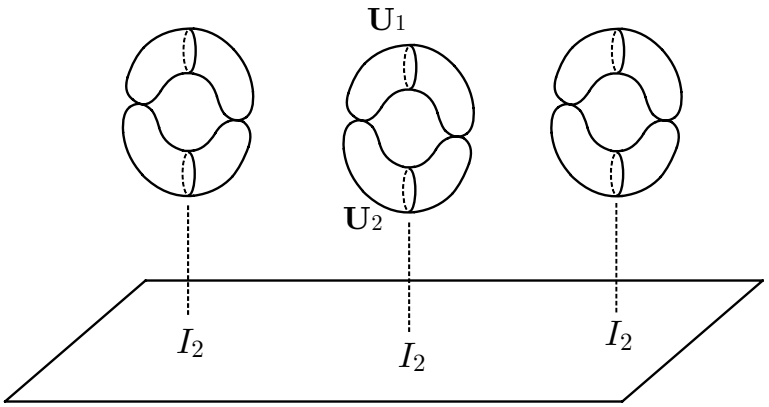

Figure 3-14 Cycles in Kodaira type $3I_2$.

the volume form over these cycles, one finds that

$$\begin{aligned} \mathrm{vol}_I(\mathbf{U}_1) &= 1 - 2\alpha_2 \\ \mathrm{vol}_I(\mathbf{U}_2) &= \alpha_1 + \alpha_2 + \alpha_3 - \alpha_4, \\ \mathrm{vol}_I(\mathbf{U}_3) &= -\alpha_1 + \alpha_2 - \alpha_3 + \alpha_4. \end{aligned} \tag{3.88}$$

We can further analyze the singularities through the behavior of the volume function. When a single volume vanishes, the cubic surface develops an A_1 singularity. In contrast, when two volumes vanish simultaneously, the singularity enhances to A_2.

Type $(I_2, 4I_1)$, $(2I_2, 2I_1)$ and $3I_2$

We now analyze the cases $(I_2, 4I_1)$, $(2I_2, 2I_1)$, and $3I_2$, as depicted in Figures 3-15 and 3-14. Each I_2 fiber consists of two components, denoted as $\{[\mathbf{U}_1], [\mathbf{U}_2]\}$. These components correspond to the simple roots of the affine A_1 root system, with their intersection matrix matching the Cartan matrix of affine A_1 (up to an overall sign):

$$Q_{I_2} = \begin{pmatrix} -2 & 2 \\ 2 & -2 \end{pmatrix} \tag{3.89}$$

The homology classes of the components $[\mathbf{U}_a]$ can be expressed in terms of the basis of $H_2(\mathcal{M}_H, \mathbb{Z})$, providing an embedding of the affine A_2 root system into the affine D_4 root system:

$$[\mathbf{U}_1] = [\mathbf{V}] + [\mathbf{D}_1] + [\mathbf{D}_2]\,, \qquad [\mathbf{U}_2] = [\mathbf{V}] + [\mathbf{D}_3] + [\mathbf{D}_4]\,, \tag{3.90}$$

In this case, the Lagrangian condition enforces $\gamma_2 = 0$, which corresponds to the $(I_2, 4I_1)$ singularity type. Integrating the volume form over these cycles yields:

$$\begin{aligned} \mathrm{vol}_I(\mathbf{U}_1) &= 1 - 2\alpha_2, \\ \mathrm{vol}_I(\mathbf{U}_2) &= 2\alpha_2. \end{aligned} \tag{3.91}$$

When $\alpha_2 = 0$ or $\frac{1}{2}$, one A_1 singularity is developed.

For the $(2I_2, 2I_1)$ case, the singular fiber corresponds to a reducible affine $A_1 \oplus A_1$ root system. Each component $[\mathbf{U}_a]$ corresponds to a simple root of this system. By an

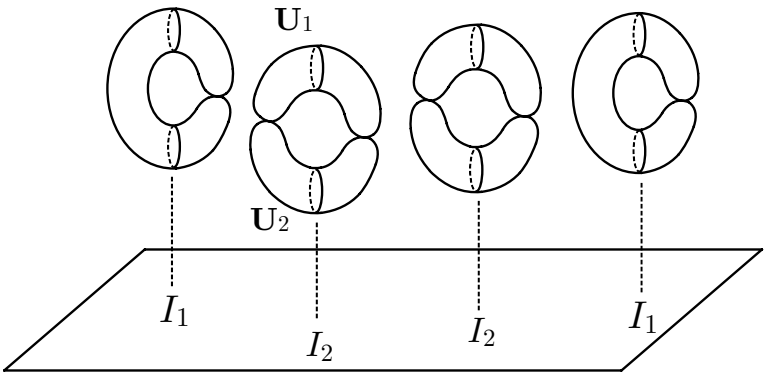

Figure 3-15 Cycles in Kodaira type $(2I_2, 2I_1)$.

embedding of the affine $A_1 \oplus A_1$ root system into the affine D_4 root system, we can express $[\mathbf{U}_a]$ in terms of the basis of $H_2(\mathcal{M}_H, \mathbb{Z})$:

$$\begin{aligned} [\mathbf{U}_1^{(1)}] &= [\mathbf{V}] + [\mathbf{D}_1] + [\mathbf{D}_2] \,, \qquad [\mathbf{U}_2^{(1)}] = [\mathbf{V}] + [\mathbf{D}_3] + [\mathbf{D}_4] \,, \\ [\mathbf{U}_1^{(2)}] &= [\mathbf{V}] + [\mathbf{D}_1] + [\mathbf{D}_3] \,, \qquad [\mathbf{U}_2^{(2)}] = [\mathbf{V}] + [\mathbf{D}_2] + [\mathbf{D}_4] \,, \end{aligned} \tag{3.92}$$

The lagrangian condition imposes $\gamma_2 = \gamma_3 = 0$. The volume for the first I_2 cycles is the same as (3.91). The volume cycles of the second fiber can also be achieved by straightforward calculation via (3.75).

$$\begin{aligned} \mathrm{vol}_I(\mathbf{U}_1^{(2)}) &= 1 - 2\alpha_3, \\ \mathrm{vol}_I(\mathbf{U}_2^{(2)}) &= 2\alpha_3. \end{aligned} \tag{3.93}$$

For the $3I_2$ case, the singular fibers correspond to a reducible affine root system $A_1 \oplus A_1 \oplus A_1$, which is the same as the one taken in[6]. With the same analysis as before, we can take an embedding of the root lattice such that

$$\begin{aligned} [\mathbf{U}_1^{(1)}] &= [\mathbf{V}] + [\mathbf{D}_1] + [\mathbf{D}_2] \,, \qquad [\mathbf{U}_2^{(1)}] = [\mathbf{V}] + [\mathbf{D}_3] + [\mathbf{D}_4] \,, \\ [\mathbf{U}_1^{(2)}] &= [\mathbf{V}] + [\mathbf{D}_1] + [\mathbf{D}_3] \,, \qquad [\mathbf{U}_2^{(2)}] = [\mathbf{V}] + [\mathbf{D}_2] + [\mathbf{D}_4] \,, \\ [\mathbf{U}_1^{(3)}] &= [\mathbf{V}] + [\mathbf{D}_1] + [\mathbf{D}_4] \,, \qquad [\mathbf{U}_2^{(3)}] = [\mathbf{V}] + [\mathbf{D}_2] + [\mathbf{D}_3] \,, \end{aligned} \tag{3.94}$$

Then, the Lagrangian condition implies that $\gamma_2 = \gamma_3 = \gamma_4 = 0$. The volume of the components in the first two singular fibers is the same as the one in (3.93). For the third singular fiber, the volume is given by:

$$\begin{aligned} \mathrm{vol}_I(\mathbf{U}_1^{(3)}) &= 1 - 2\alpha_4, \\ \mathrm{vol}_I(\mathbf{U}_2^{(3)}) &= 2\alpha_4. \end{aligned} \tag{3.95}$$

Type $6I_1$

Up to this point, we study homology classes of irreducible components in Kodaira singular fibers. However, as illustrated in Figure 3-3, there exist two-cycles suspended between two Kodaira singular fibers at a generic γ_j. We study two-cycles suspended

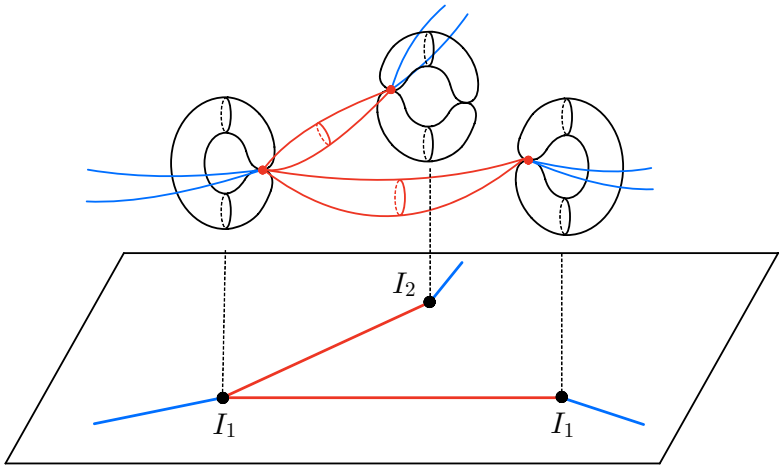

Figure 3-16 The cycles in the second homology of the Hitchin total space can be represented by a diagram on the u-plane. Singular fibers are represented as marked points along with their Kodaira types. Suspended cycles are represented by the lines connecting marked points.

between two Kodaira singular fibers in more detail below, and we also identify generators of the second integral homology groups in each configuration of the Hitchin fibrations. This analysis will be useful for the A-model approach to the representation theory of $\ddot{SH}_{q,t}$.

First, let us consider the case $6I_1$ with generic ramification parameters. The homology class of an I_1 singular fiber in $H_2(\mathcal{M}_H, \mathbb{Z})$ is equivalent to the class $[\mathbf{F}]$ of a generic fiber, while the second homology satisfies $H_2(\mathcal{M}_H, \mathbb{Z}) \cong \mathbb{Z}^{\oplus 5}$, as previously established. Therefore, there must exist additional homology generators in the Hitchin moduli space in the case of $6I_1$ singularities. To identify these generators, we begin by showing that for any class $[\mathbf{W}] \in H_2(\mathcal{M}_H, \mathbb{Z})$, there exists a suitable representative $\mathbf{W}$ such that its projection $h(\mathbf{W})$ onto the Hitchin base $\mathcal{B}_H$, via the fibration described in (3.44), satisfies one of the following conditions:

(1) a point
(2) a (piece-wise) line between Kodaira singular points

If the projection $h(\mathbf{W})$ is two-dimensional, then $\mathbf{W}$ intersects the Hitchin fibers at discrete points due to dimensionality. However, since the Hitchin base $\mathcal{B}_H$ is a complex plane $\mathbb{C}$, a representative of $[\mathbf{W}]$ can be homotopically deformed such that its projection to $\mathcal{B}_H$ reduces to either a point or a one-dimensional curve (with or without endpoints) in $\mathcal{B}_H$. In the former case, where the projection is a point, a representative of $[\mathbf{W}]$ is supported entirely on a single Hitchin fiber, corresponding to condition (1) above. In the latter case, a representative of $[\mathbf{W}]$ intersects a generic Hitchin fiber along $S^1 \subset T^2 \cong \mathbf{F}$, again by dimensionality. If we denote the projection to $\mathcal{B}_H$ again by $h(\mathbf{W})$ (abusing notation), this curve $h(\mathbf{W})$ can end at points where the S^1 collapses to a trivial cycle in a Hitchin fiber, which occurs only at singular fibers. Note that for a singular fiber with monodromy M, the (n_m, n_e)-cycle subject to (3.45) collapses to a trivial cycle. As a result, a representative of $[\mathbf{W}]$ can always be deformed such that its projection to $\mathcal{B}_H$ is either a composition of lines connecting Kodaira singular points (see Figure 3-16) or a point in $\mathcal{B}_H$. Therefore, the statement holds.

The two-cycles satisfying condition (1) will be referred to as *fiber* (two-)cycles, while those satisfying condition (2) will be called *suspended (two-)cycles*. As seen in Figure

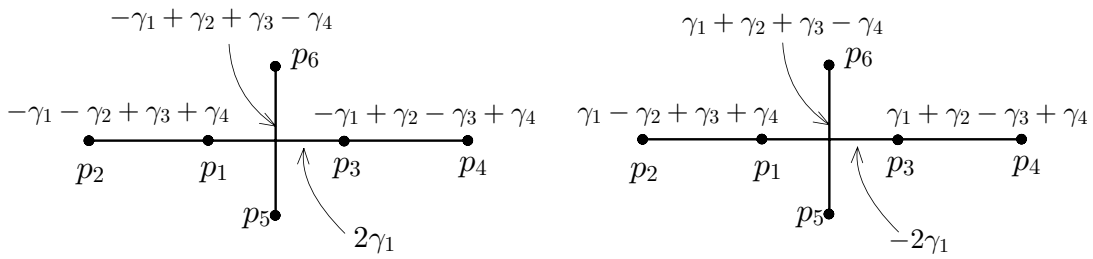

Figure 3-17 The generators of the second homology of the Hitchin total space for the $6I_1$ case. Singular fibers at p_i are all of type I_1, and suspended cycles are projected onto lines between these points. The cycle suspended between p_1 and p_3 intersects with the one suspended between p_5 and p_6 once. Two examples of length assignments are related by a PL transformation (3.72) with respect to the cycle suspended $[\mathbf{W}_{13}]$ between p_1 and p_3.

3-3, there exists a suspended cycle between the two I_1 singular fibers of the same type. In the case of the configuration $6I_1$, these suspended cycles as well as the homology class $[\mathbf{F}]$ of a generic fiber generate the second homology group $H_2(\mathcal{M}_H, \mathbb{Z})$, forming the affine D_4 root lattice (3.57):

$$\dot{\mathsf{Q}}(D_4) \cong \mathsf{Q}(D_4) \oplus \mathbb{Z}\langle\delta\rangle, \tag{3.96}$$

where the homology class of a generic fiber serves as the imaginary root δ. Hence, the homology classes represented by the suspended cycles span the root lattice $\mathsf{Q}(D_4)$ with the intersection form given by the Cartan matrix of type D_4 (up to an overall sign).

From the analysis above, suspended cycles can be represented as line segments connecting six marked points p_i on the u-plane, corresponding to the loci of the I_1 singular fibers. We denote the cycle associated with the line segment between p_i and p_j as $\mathbf{W}_{ij}$. Recalling that four marked points p_i ($i = 1, 2, 3, 4$) are quark singularities while two marked points p_i ($i = 5, 6$) are dyon singularities. Since suspended cycles can exist between singular fibers of the same type, a consistent method to assign the cycles is illustrated in Figure 3-17. Note that additional cycles, which wind around singular fibers, also exist. These winding cycles are discussed in Appendix D, where they are explicitly shown to be homologous to the suspended cycles depicted in Figure 3-17.

The homology classes of the suspended cycles are determined by embedding the D_4 root system into the affine D_4 root lattice, along with specifying a chamber in the γ-space. Let us begin by considering a specific chamber:

$$\{\gamma \in \mathfrak{t}^{(\gamma)}_{D_4} \mid e^i \cdot \gamma > 0,\ i = 1, 2, 3, 4\}. \tag{3.97}$$

In this chamber, the homology classes of the suspended cycles are identified as follows:

$$[\mathbf{W}_{13}] = [\mathbf{V}], \quad [\mathbf{W}_{12}] = [\mathbf{D}_2], \quad [\mathbf{W}_{34}] = [\mathbf{D}_3], \quad [\mathbf{W}_{56}] = [\mathbf{D}_4]. \tag{3.98}$$

Therefore, (3.80) tells us the volumes of these suspended cycles defined in (3.79) are

$$\Big(\mathrm{vol}(\mathbf{W}_{12}), \mathrm{vol}(\mathbf{W}_{34}), \mathrm{vol}(\mathbf{W}_{56}), \mathrm{vol}(\mathbf{W}_{13})\Big) = \Big(e^1 \cdot (\alpha - i\gamma), e^2 \cdot (\alpha - i\gamma),\ e^3 \cdot (\alpha - i\gamma)\ , e^4 \cdot (\alpha - i\gamma)\Big) \tag{3.99}$$

The imaginary part of the volume in (3.99) has a geometric interpretation. By comparing these volumes with the conditions for the Kodaira singular fibers (as detailed

in Table 3-3), we observe that a new Kodaira singular fiber appears precisely when the imaginary part of a volume vanishes. Geometrically, this corresponds to the collision of two I_1 fibers, as shown schematically in Figure 3-3. Consequently, the imaginary part of the volume serves as a measure of the "distance" between two I_1 singular fibers. The left-hand panel of Figure 3-17 visually represents these distances in the central chamber.

It is important to emphasize that the embedding of the D_4 root system into the affine D_4 root lattice does not uniquely specify the homology classes of the suspended cycles. Wall-crossing phenomena allow transitions between different bases of their homology classes. As seen in (3.59), the γ-space receives only the Weyl group $W(D_4)$ rather than the affine Weyl group $\dot{W}(D_4)$ since the affine translation acts on the γ-space trivially. Thus, the walls in the γ-space are determined by the discriminant loci given by

$$\sum_{j=1}^{4} r_j \gamma_j = 0, \qquad \forall r = (r_1, r_2, r_3, r_4) \in \mathsf{R}(D_4), \tag{3.100}$$

where $\mathsf{R}(D_4)$ denotes the D_4 root system. These walls correspond to the reflection hyperplanes of the D_4 weight lattice. As a result, each chamber in the γ-space, bounded by these walls, corresponds to a Weyl chamber of type D_4. In Figure D-3, we schematically represent these walls by black lines.

The volume in (3.99) is proportional to the distance from the chamber boundaries, where the chamber is specified by (3.97). This relation indicates a wall-crossing phenomenon for the volume functions in the γ-space. When γ_j crosses a wall defined by a root r, the basis of the root undergoes a Weyl reflection s_r:

$$s_{r_a}(r_b) = r_b - A_{ba} r_a \,, \tag{3.101}$$

where A_{ba} is the D_4 Cartan matrix. Consequently, the volume functions exhibit a discontinuity, with their dependence on γ_j jumping according to the Weyl reflection. Since the wall-crossing is governed by Weyl reflections, the PL transformation defined by (3.72) still provides the basis transformation of the second homology classes once crossing a wall. The wall-crossing of the volume functions with respect to the cycle $[\mathbf{W}_{13}]$ is depicted in Figure 3-17.

To better understand the physical interpretation of the volume function, we examine the $\alpha_j = 0$ limit and express the volumes in terms of the mass parameters m_j as defined in (3.21). In this case, the volumes of the relevant 2-cycles are given by:

$$\begin{aligned} \mathrm{vol}(\mathbf{W}_{12}) &= m_1 - m_3, \\ \mathrm{vol}(\mathbf{W}_{13}) &= -m_1 - m_2, \\ \mathrm{vol}(\mathbf{W}_{34}) &= m_2 + m_4, \\ \mathrm{vol}(\mathbf{W}_{56}) &= m_2 - m_4. \end{aligned} \tag{3.102}$$

These expressions illustrate how the mass parameters dictate the geometric volumes of the cycles, encapsulating both their physical and geometric significance.

This result can also be derived in the string theory framework of Seiberg-Witten theory, using the complex structure I instead of J. Using the isomorphism $\mathrm{SU}(2) \cong \mathrm{Sp}(1)$, the $\mathrm{Sp}(1)$ theory with $N_f = 4$ can be realized by considering a D3-brane in the presence of four D7-branes and an O7$^-$-plane in Type IIB string theory[75]. The four D7-branes carry electric charges $(n_m, n_e) = (0, 1)$. A notable result from[76] shows that the O7$^-$-plane splits into two 7-branes with charges $(n_m, n_e) = (1, 0)$ and $(n_m, n_e) =$

$(1, -2)$. Remarkably, the charges of these 7-branes agree perfectly with those of the massless BPS particles on the u-plane in the 4d $\mathcal{N} = 2$ theory.

In this framework, the mass (or equivalently, the central charge) of a BPS string stretched between the i-th and j-th 7-branes has a clear geometric interpretation. It is determined by integrating the holomorphic symplectic form Ω_I over the 2-cycle connecting the two I_1 singular fibers associated with the 7-branes[76]:

$$\left| \int_{\mathbf{W}_{ij}} \frac{\Omega_I}{2\pi} \right| = |m_a \pm m_b| \,, \tag{3.103}$$

where m are the mass parameters of the 4d theory. The precise relation between $\mathbf{W}_{ij}$ and the masses depends on a choice of chamber and electromagnetic frame of BPS particles, which we do not specify here. Nevertheless, our analysis in (3.102) is consistent with the result of[76] in the complex structure I, provided $\beta_j = 0$. Consequently, the hyper-Kähler structure ensures a unified and consistent connection between the analyses in the complex structures I and J.

Chapter 4
Algebraic Side: DAHA of Type $C^\vee C_1$

This project exploits the tool of brane quantization on the target space of the moduli space $\mathcal{M}_{\text{flat}}(C_{0,4}, SL(2,\mathbb{C}))$ of flat $SL(2,\mathbb{C})$-connections over a four-punctured sphere. In Chapter 3, I have given a detailed analysis of the geometry of such a target space from distinct perspective. In particular, the Lagrangian A-branes are identified and their A-brane conditions and volumes are determined explicitly. In this chapter, I will give the analysis on the algebraic side. In §3.2.2, I have mentioned that, the deformation quantization of the coordinate ring of holomorphic functions over the target space is the spherical DAHA of type $C \vee C_1$. In §4.1, I will review the definitions and properties of the DAHA of type $C^\vee C_1$. In particular, we will find out how the braid group B_3 arises at the level of algebra, which will play an important role in the later chapters. In §4.2, I will explain how DAHA acts on the Askey-Wilson polynomials. And in §4.2, I will construct the finite-dimensional representations from the action on Askey-Wilson polynomials, which will be used to construct the correspondec between representations and branes in the later chapter.

4.1 DAHA of type $C^\vee C_1$

The DAHA of type $C^\vee C_1$, denoted as $\ddot{H}_{q,t}$, can be defined from the fundamental group of a fourth-punctured sphere

$$\pi_1\left(S^2\backslash\{p_1,p_2,p_3,p_4\}\right) = \langle T_0, T_0^\vee, T_1, T_1^\vee \mid T_0^\vee T_0 T_1 T_1^\vee = 1\rangle, \tag{4.1}$$

where the generators are denoted as $T_0, T_0^\vee, T_1, T_1^\vee$. To define $\ddot{H}_{q,t}$, we need to deform the relation between generators into

$$T_0^\vee T_0 T_1 T_1^\vee = q^{-\frac{1}{2}}, \tag{4.2}$$

by a q parameter and then impose four additional relations (called Hecke relations[77])

$$\begin{aligned}(T_0 + iq^{\frac{1}{2}}t_1)(T_0 + iq^{-\frac{1}{2}}t_1^{-1}) = 0\,,\\ (T_0^\vee + it_2)(T_0^\vee + it_2^{-1}) = 0\,,\\ (T_1 + it_3)(T_1 + it_3^{-1}) = 0\,,\\ (T_1^\vee + it_4)(T_1^\vee + it_4^{-1}) = 0\,,\end{aligned} \tag{4.3}$$

with $t_j, j = 1,2,3,4$ parameters.

Sometimes, an alternative set of generators X, Y, T are also used, which are related to the original ones as follows:

$$X = (T_0^\vee T_0)^{-1}, \quad Y = T_0 T_1, \quad T = T_0\,. \tag{4.4}$$

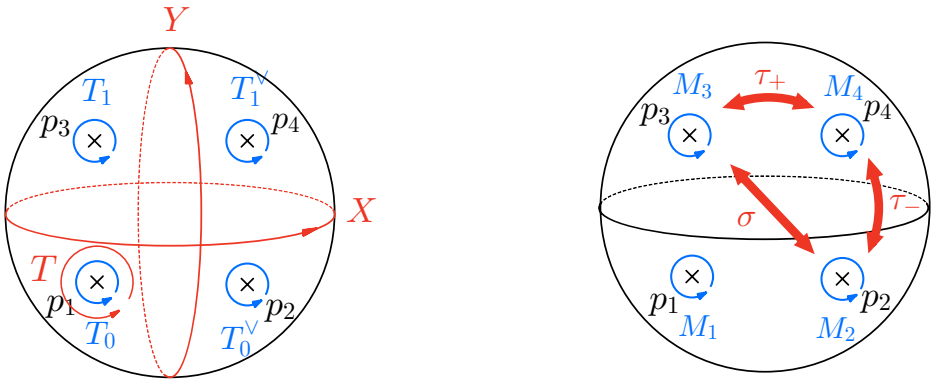

Figure 4-1 (Left) Two sets of generators of DAHA of type $C^\vee C_1$ presented by the fundamental group of a fourth-punctured sphere. (Right) Braid group action of B_3 on the generators of DAHA.

In terms of these new generators, we have the following expressions:

$$T_0 = T, \quad T_0^\vee = X^{-1}T^{-1}, \quad T_1 = T^{-1}Y, \quad T_1^\vee = q^{-\frac{1}{2}}Y^{-1}TX\ . \tag{4.5}$$

For instance, if we specialize the parameters to

$$(t_1, t_2, t_3, t_4) = (-iq^{-1/2}t, -i, -i, -i)\ , \tag{4.6}$$

the algebra reduces to the DAHA of type A_1, with the defining relations:

$$TXT = X^{-1}, \quad TY^{-1}T = Y, \quad (T - t^{-1})(T + t) = 0, \quad XYX^{-1}Y^{-1}T^2 = q^{-1}\ . \tag{4.7}$$

However, our focus is on a subalgebra of the DAHA, which we refer as the spherical DAHA, denoted by $S\ddot{H}_{q,t}$. The subalgebra can be constructed from the fact that the element

$$\mathbf{e} = \frac{iT_0 - q^{-\frac{1}{2}}t_1^{-1}}{q^{\frac{1}{2}}t_1 - q^{-\frac{1}{2}}t_1^{-1}} \tag{4.8}$$

is idempotent, satisfying $\mathbf{e}^2 = \mathbf{e}$ in $\ddot{H}_{q,t}$.[①] The spherical DAHA is then defined by the idempotent projection

$$S\ddot{H}_{q,t} = \mathbf{e}\ddot{H}_{q,t}\mathbf{e}\ . \tag{4.10}$$

The spherical DAHA $S\ddot{H}_{q,t}$ is generated by the following generators[78]

$$\begin{aligned} x &= \left(T_0^\vee T_0 + (T_0^\vee T_0)^{-1}\right)\mathbf{e}\ , \\ y &= \left(T_0\, T_1 + (T_0\, T_1)^{-1}\right)\mathbf{e}\ , \\ z &= \left(T_0 T_1^\vee + (T_0 T_1^\vee)^{-1}\right)\mathbf{e}\ , \end{aligned} \tag{4.11}$$

① Given the four Hecke relations, there are indeed four corresponding idempotent elements given by

$$(\mathbf{e}_1, \mathbf{e}_2, \mathbf{e}_3, \mathbf{e}_4) = \left(\frac{iT_0 - q^{-\frac{1}{2}}t_1^{-1}}{q^{\frac{1}{2}}t_1 - q^{-\frac{1}{2}}t_1^{-1}}, \frac{iT_0^\vee - t_2^{-1}}{t_2 - t_2^{-1}}, \frac{iT_1 - t_3^{-1}}{t_3 - t_3^{-1}}, \frac{iT_1^\vee - t_4^{-1}}{t_4 - t_4^{-1}}\right). \tag{4.9}$$

In this work, we select one of these idempotents to define the spherical subalgebra.

satisfing the following commutation relations

$$\begin{aligned}
[x,y]_q &= (q^{-1}-q)z + (q^{-\frac{1}{2}}-q^{\frac{1}{2}})\theta_3 \,, \\
[y,z]_q &= (q^{-1}-q)x + (q^{-\frac{1}{2}}-q^{\frac{1}{2}})\theta_1 \,, \\
[z,x]_q &= (q^{-1}-q)y + (q^{-\frac{1}{2}}-q^{\frac{1}{2}})\theta_2 \,,
\end{aligned} \tag{4.12}$$

where the q-commutator is defined by

$$[f,g]_q \equiv q^{-\frac{1}{2}}fg - q^{\frac{1}{2}}gf \,, \tag{4.13}$$

and using the notation $\overline{f} \equiv f + f^{-1}$, θ_i are expressed by

$$\begin{aligned}
\theta_1 &= \overline{t_1}\,\overline{t_2} + \overline{t_3}\,\overline{t_4} \,, \\
\theta_2 &= \overline{t_1}\,\overline{t_3} + \overline{t_2}\,\overline{t_4} \,, \\
\theta_3 &= \overline{t_1}\,\overline{t_4} + \overline{t_2}\,\overline{t_3} \,.
\end{aligned} \tag{4.14}$$

It can then be directly verified that there is a Casimir relation

$$-q^{-\frac{1}{2}}xyz + q^{-1}x^2 + qy^2 + q^{-1}z^2 + q^{-\frac{1}{2}}\theta_1 x + q^{\frac{1}{2}}\theta_2 y + q^{-\frac{1}{2}}\theta_3 z + \theta_4(q) = 0 \,, \tag{4.15}$$

where

$$\theta_4(q) = \overline{t_1}^2 + \overline{t_2}^2 + \overline{t_3}^2 + \overline{t_4}^2 + \overline{t_1}\,\overline{t_2}\,\overline{t_3}\,\overline{t_4} - q - q^{-1} - 2 \,. \tag{4.16}$$

In the "classical" limit $q = 1$, the spherical DAHA $\ddot{SH}_{q,t}$ becomes commutative and the Casimir relation (4.16) reduces to the equation of an affine cubic surface:

$$-xyz + x^2 + y^2 + z^2 + \theta_1 x + \theta_2 y + \theta_3 z + \theta_4 = 0 \,, \tag{4.17}$$

where

$$\theta_4 = \overline{t_1}^2 + \overline{t_2}^2 + \overline{t_3}^2 + \overline{t_4}^2 + \overline{t_1}\,\overline{t_2}\,\overline{t_3}\,\overline{t_4} - 4 \,. \tag{4.18}$$

This equation (4.17) is known to describe the moduli space of flat $\mathrm{SL}(2,\mathbb{C})$-connections on a four-punctured sphere[10]. Therefore, in the classical limit, $\ddot{SH}_{q,t}$ corresponds to the coordinate ring of the moduli space:

$$\ddot{SH}_{q,t} \xrightarrow[q\to 1]{} \mathcal{O}(\mathcal{M}_{\mathrm{flat}}(C_{0,4}, \mathrm{SL}(2,\mathbb{C}))) \,. \tag{4.19}$$

It is then naturally to view the spherical DAHA $\ddot{SH}_{q,t}$ as a q-deformation of the coordinate ring. Indeed, as is proven in[10], the deformation quantization of the coordinate ring is exactly the spherical DAHA $\ddot{SH}_{q,t}$.

4.1.1 Symmetries of DAHA algebra

In the later analysis, symmetries of the DAHA algebra play a central role. Therefore, let me summarize three symmetries that already appear from definition.

Weyl group $W(D_4)$: $\overline{t_j} \equiv t_j + t_j^{-1}$ can be naturally viewed as the Weyl character of the fundamental representation of an $\mathfrak{su}(2)$ algebra for each $j = 1, 2, 3, 4$. Therefore it is tempting to embed these $\mathfrak{su}(2)$ algebras into a larger Lie algebra and interpret all the parameters as characters of it. Indeed, this can be done by noticing that the parameters $\theta_1, \theta_2, \theta_3, \theta_4$ can be naturally interpreted as the module characters of the Lie algebra $\mathfrak{so}(8) = D_4$. More specifically, the correspondence is:

$$\theta_1 = \chi_{8_V}, \quad \theta_2 = \chi_{8_S}, \quad \theta_3 = \chi_{8_C}, \quad \theta_4 = \chi_{\text{adj}}, \tag{4.20}$$

which are the characters of the vector, spinor, conjugate spinor, and adjoint representations of $\mathfrak{so}(8)$, respectively.

An immediate consequence is that, since the characters are invariant under the Weyl group $W(D_4)$ of $\mathfrak{so}(8)$, the spherical DAHA should also be invariant under $W(D_4)$. Note that, the q-deformation simply adds θ_4 by a constant, thus preserves the Weyl symmetry.

Braid group B_3: There is an action of the braid group B_3[79–80], which geometrically permutes the relative positions of the four punctures on the sphere as in Figure 4-1. The braid group B_3 is generated by elements $\tau_\pm$, with the following relations:

$$\sigma = \tau_+ \tau_-^{-1} \tau_+ = \tau_- \tau_+^{-1} \tau_- \,. \tag{4.21}$$

Explicitly, the braid group acts on the DAHA by

$$\begin{aligned}
\tau_+ : (T_0, T_0^\vee, T_1, T_1^\vee) &\mapsto (T_0, T_0^\vee, T_1 T_1^\vee T_1^{-1}, T_1) \,, \\
(t_1, t_2, t_3, t_4) &\mapsto (t_1, t_2, t_4, t_3) \,, \\
\tau_- : (T_0, T_0^\vee, T_1, T_1^\vee) &\mapsto (T_0, T_0^{\vee -1} T_1^\vee T_0^\vee, T_1, T_0^\vee) \,, \\
(t_1, t_2, t_3, t_4) &\mapsto (t_1, t_4, t_3, t_2) \,, \\
\sigma : (T_0, T_0^\vee, T_1, T_1^\vee) &\mapsto (T_0, T_0^\vee, T_1 T_1^\vee T_0^\vee (T_1 T_1^\vee)^{-1}, T_1) \,, \\
(t_1, t_2, t_3, t_4) &\mapsto (t_1, t_3, t_2, t_4) \,.
\end{aligned} \tag{4.22}$$

Moreover, the spherical subalgebra $\ddot{SH}_{q,t}$ is invariant under this action:

$$\begin{aligned}
\tau_+ : (x, y, z, \theta_1, \theta_2, \theta_3, \theta_4) &\mapsto \left(x, q^{-\frac{1}{2}}(xy - q^{-\frac{1}{2}} z - \theta_3), y, \theta_1, \theta_3, \theta_2, \theta_4\right) \,, \\
\tau_- : (x, y, z, \theta_1, \theta_2, \theta_3, \theta_4) &\mapsto \left(q^{-\frac{1}{2}}(xy - q^{-\frac{1}{2}} z - \theta_3), y, x, \theta_3, \theta_2, \theta_1, \theta_4\right) \,, \\
\sigma : (x, y, z, \theta_1, \theta_2, \theta_3, \theta_4) &\mapsto \left(y, x, q^{-\frac{1}{2}}(xy - q^{-\frac{1}{2}} z - \theta_3), \theta_2, \theta_1, \theta_3, \theta_4\right) \,.
\end{aligned} \tag{4.23}$$

In particular, the Casimir relation (4.15) is invariant under the action of B_3. Under the limit $q \to 1$, these actions reduces to

$$\begin{aligned}
\tau_+ : \; & (x, y, z, \theta_1, \theta_2, \theta_3, \theta_4) \mapsto (x, xy - z - \theta_3, y, \theta_1, \theta_3, \theta_2, \theta_4) \,, \\
\tau_- : \; & (x, y, z, \theta_1, \theta_2, \theta_3, \theta_4) \mapsto (xy - z - \theta_3, y, x, \theta_3, \theta_2, \theta_1, \theta_4) \,, \\
\sigma : \; & (x, y, z, \theta_1, \theta_2, \theta_3, \theta_4) \mapsto (y, x, xy - z - \theta_3, \theta_2, \theta_1, \theta_3, \theta_4) \,.
\end{aligned} \tag{4.24}$$

Sign-flip group $\mathbb{Z}_2^{\times 2}$: Lastly, there is a sign-flip symmetry $\mathbb{Z}_2 \times \mathbb{Z}_2 = \mathbb{Z}_2^{\times 2}$ for the cubic surface, generated by ξ_1 and ξ_2:

$$\begin{aligned}
\xi_1 &: (x, y, z, \theta_1, \theta_2, \theta_3, \theta_4) \mapsto (-x, y, -z, -\theta_1, \theta_2, -\theta_3, \theta_4) \,, \\
\xi_2 &: (x, y, z, \theta_1, \theta_2, \theta_3, \theta_4) \mapsto (x, -y, -z, \theta_1, -\theta_2, -\theta_3, \theta_4) \,, \\
\xi_3 &: (x, y, z, \theta_1, \theta_2, \theta_3, \theta_4) \mapsto (-x, -y, z, -\theta_1, -\theta_2, \theta_3, \theta_4) \,,
\end{aligned} \tag{4.25}$$

with $\xi_3 = \xi_2 \circ \xi_1$.

The readers might notice that there is another evident symmetry, namely the cyclic permutation symmetry $\mathbb{Z}_3$ of the variables, generated by

$$s : (x, y, z, \theta_1, \theta_2, \theta_3, \theta_4) \mapsto (y, z, x, \theta_2, \theta_3, \theta_1, \theta_4) \,, \tag{4.26}$$

with $s^3 = \mathrm{id}$. And it can be directly verified using the commutation relation (4.12) that

$$\begin{aligned}
&- q^{-\frac{1}{2}} xyz + q^{-1}x^2 + qy^2 + q^{-1}z^2 + q^{-\frac{1}{2}}\theta_1 x + q^{\frac{1}{2}}\theta_2 y + q^{-\frac{1}{2}}\theta_3 z + \theta_4(q) \\
=&- q^{-\frac{1}{2}} yzx + q^{-1}y^2 + qz^2 + q^{-1}x^2 + q^{-\frac{1}{2}}\theta_2 y + q^{\frac{1}{2}}\theta_3 z + q^{-\frac{1}{2}}\theta_1 x + \theta_4(q) \,,
\end{aligned} \tag{4.27}$$

thus the Casimir relation is indeed invariant under this permutation symmetry. In fact, this group is a subgroup of the braid group B_3 by the embedding $s = \tau_+^{-1}\tau_-$.

4.1.2 Symmetry actions on the geometry

The symmetry action can be understood as the group of certain diffeomorphisms of the target space $\mathfrak{X}$ with different ramification parameters. Recall that the deformation parameters t are related to the (α, γ) parameters via $t_j = e^{-2\pi(\gamma_j + i\alpha_j)}$ (3.33). Here, we analyze the actions of the braid group B_3 and the sign-flip group $\mathbb{Z}_2 \times \mathbb{Z}_2$ at the level of homology classes. To achieve this, we must choose a preferred uplift of the group actions to the (α, γ) parameter space. To be explicit, we focus on the chamber $WXYZ$ defined in (3.74). Our goal is to analyze the action of the braid group B_3 as described in (4.24). A family of character varieties is parametrized by the ramification parameters (α, γ), and the generators of B_3 act as diffeomorphisms between the character varieties at different points in the parameter space. The explicit maps of the ramification parameters are given by:

$$\begin{aligned}
\tau_+ : \big(\alpha_1, \alpha_2, \alpha_3, \alpha_4\big) &\mapsto \big(\alpha_1, \alpha_2, \alpha_4, \alpha_3\big) \,, \\
\big(\gamma_1, \gamma_2, \gamma_3, \gamma_4\big) &\mapsto \big(\gamma_1, \gamma_2, \gamma_4, \gamma_3\big) \,, \\
\tau_- : \big(\alpha_1, \alpha_2, \alpha_3, \alpha_4\big) &\mapsto \big(\alpha_1, \alpha_4, \alpha_3, \alpha_2\big) \,, \\
\big(\gamma_1, \gamma_2, \gamma_3, \gamma_4\big) &\mapsto \big(\gamma_1, \gamma_4, \gamma_3, \gamma_2\big) \,, \\
\sigma : \big(\alpha_1, \alpha_2, \alpha_3, \alpha_4\big) &\mapsto \big(\alpha_1, \alpha_3, \alpha_2, \alpha_4\big) \,, \\
\big(\gamma_1, \gamma_2, \gamma_3, \gamma_4\big) &\mapsto \big(\gamma_1, \gamma_3, \gamma_2, \gamma_4\big) \,.
\end{aligned} \tag{4.28}$$

These parameter transformations induce corresponding diffeomorphisms of the character varieties, which we schematically write

$$\begin{aligned}
\tau_+ &: \mathfrak{X}(t_1, t_2, t_3, t_4) \to \mathfrak{X}(t_1, t_2, t_4, t_3) \,;\ (x, y, z) \mapsto (x, xy - z - \theta_3, y), \\
\tau_- &: \mathfrak{X}(t_1, t_2, t_3, t_4) \to \mathfrak{X}(t_1, t_4, t_3, t_2) \,;\ (x, y, z) \mapsto (xy - z - \theta_3, y, x), \\
\sigma &: \mathfrak{X}(t_1, t_2, t_3, t_4) \to \mathfrak{X}(t_1, t_3, t_2, t_4) \,;\ (x, y, z) \mapsto (y, x, xy - z - \theta_3).
\end{aligned} \tag{4.29}$$

Furthermore, computing the changes of the volumes using (3.80), we can determine the corresponding transformations of homology cycles:

$$\begin{aligned} \tau_+ &: [\mathbf{D}_3] \leftrightarrow [\mathbf{D}_4], \quad [\mathbf{D}_1] \text{ and } [\mathbf{D}_2] \text{ remain invariant}, \\ \tau_- &: [\mathbf{D}_2] \leftrightarrow [\mathbf{D}_4], \quad [\mathbf{D}_1] \text{ and } [\mathbf{D}_3] \text{ remain invariant}, \\ \sigma &: [\mathbf{D}_2] \leftrightarrow [\mathbf{D}_3], \quad [\mathbf{D}_1] \text{ and } [\mathbf{D}_4] \text{ remain invariant}. \end{aligned} \tag{4.30}$$

Next, we analyze the action of the sign-flip symmetry group $\mathbb{Z}_2^{\times 2}$, as defined in (4.25). This group can be understood as the group of diffeomorphisms between the character varieties at different points in the parameter space. Specifically, the diffeomorphisms ξ_1, ξ_2, and ξ_3 are written as

$$\begin{aligned} \xi_1 &: \mathfrak{X}(t_1,t_2,t_3,t_4) \to \mathfrak{X}(t_1,-t_2^{-1},t_3,-t_4^{-1}); \quad (x,y,z) \mapsto (-x,y,-z), \\ \xi_2 &: \mathfrak{X}(t_1,t_2,t_3,t_4) \to \mathfrak{X}(t_1,t_2,-t_3^{-1},-t_4^{-1}); \quad (x,y,z) \mapsto (x,-y,-z), \\ \xi_3 &: \mathfrak{X}(t_1,t_2,t_3,t_4) \to \mathfrak{X}(t_1,-t_2^{-1},-t_3^{-1},t_4); \quad (x,y,z) \mapsto (-x,-y,z). \end{aligned} \tag{4.31}$$

While we have so far considered the action at the level of the t_i-parameters, there is a natural way to lift this action to the ramification parameters (α_j, γ_j). This lifting is done by requiring the action to preserve the chamber structure. Explicitly, the action of $\mathbb{Z}_2^{\times 2}$ is given as follows:

$$\begin{aligned} \xi_1 &: (\alpha_1,\alpha_2,\alpha_3,\alpha_4) \mapsto (\alpha_1, \tfrac{1}{2}-\alpha_2, \alpha_3, \tfrac{1}{2}-\alpha_4), \\ &\quad (\gamma_1,\gamma_2,\gamma_3,\gamma_4) \mapsto (\gamma_1,-\gamma_2,\gamma_3,-\gamma_4), \\ \xi_2 &: (\alpha_1,\alpha_2,\alpha_3,\alpha_4) \mapsto (\alpha_1, \alpha_2, \tfrac{1}{2}-\alpha_3, \tfrac{1}{2}-\alpha_4), \\ &\quad (\gamma_1,\gamma_2,\gamma_3,\gamma_4) \mapsto (\gamma_1,\gamma_2,-\gamma_3,-\gamma_4), \\ \xi_3 &: (\alpha_1,\alpha_2,\alpha_3,\alpha_4) \mapsto (\alpha_1, \tfrac{1}{2}-\alpha_2, \tfrac{1}{2}-\alpha_3, \alpha_4), \\ &\quad (\gamma_1,\gamma_2,\gamma_3,\gamma_4) \mapsto (\gamma_1,-\gamma_2,-\gamma_3,\gamma_4). \end{aligned} \tag{4.32}$$

Therefore, the maps (4.31) provide diffeomorphisms between the character varieties at these two points. To understand the action of $\mathbb{Z}_2^{\times 2}$ on the homology classes, we compute the induced transformations using the volume formula. The action on the homology classes $[\mathbf{D}_i]$ is given by:

$$\begin{aligned} \xi_1^* &: [\mathbf{D}_1] \leftrightarrow [\mathbf{D}_3], \quad [\mathbf{D}_2] \leftrightarrow [\mathbf{D}_4], \\ \xi_2^* &: [\mathbf{D}_1] \leftrightarrow [\mathbf{D}_2], \quad [\mathbf{D}_3] \leftrightarrow [\mathbf{D}_4], \\ \xi_3^* &: [\mathbf{D}_1] \leftrightarrow [\mathbf{D}_4], \quad [\mathbf{D}_2] \leftrightarrow [\mathbf{D}_3]. \end{aligned} \tag{4.33}$$

By analyzing the combined action of the braid group B_3 and the sign-flip group $\mathbb{Z}_2^{\times 2}$ on the homology classes, we observe that they together generate the outer automorphism group of the affine D_4 Lie algebra.

4.1.3 A_1 limit of the DAHA

The spherical DAHA of type A_1, which is studied in great details in[6], admits generators x, y, z and parameters q, t, subject to the following relations:

$$\begin{aligned} [x,y]_q &= (q^{-1}-q)z\ , \\ [y,z]_q &= (q^{-1}-q)x\ , \\ [z,x]_q &= (q^{-1}-q)y\ , \\ -q^{-\frac{1}{2}}xyz + q^{-1}x^2 + qy^2 + q^{-1}z^2 &= q^{-1}t^2 + qt^{-2} + q + q^{-1}. \end{aligned} \tag{4.34}$$

Comparing this with (4.12), we observe that the A_1 limit is achieved by setting $\theta_j = 0$ for $j = 1, 2, 3$. From the definition of θ_j (4.14), there are two possible ways to take this limit:

$$\overline{t_k} = \overline{t_l} = \overline{t_m} = 0 \,, \tag{4.35}$$

or

$$\overline{t_j} = -\overline{t_k} = -\overline{t_l} = -\overline{t_m} \,, \tag{4.36}$$

for any permutation (j, k, l, m) of $(1, 2, 3, 4)$.

For the first condition (4.35), the corresponding solutions are given by

$$(t_j, t_k, t_l, t_m) = \left(\pm i \left(q^{-\frac{1}{2}} t \right)^{\pm 1}, \pm i, \pm i, \pm i \right) , \tag{4.37}$$

where the signs can be chosen freely. For the second condition (4.36), the solutions take the form

$$(t_j, t_k, t_l, t_m) = \left(t_*, -t_*^{\pm 1}, -t_*^{\pm 1}, -t_*^{\pm 1} \right) , \qquad t_* = \pm \left(\pm q^{-\frac{1}{2}} t \right)^{\pm \frac{1}{2}} , \tag{4.38}$$

where any choice of signs is allowed.

In the A_1 limit, the braid group action (4.23) reduces to the $\mathrm{PSL}(2, \mathbb{Z})$ action described in[6]. Although the sign-flip symmetry remains, the symmetry of the Weyl group $W(D_4)$ is lost in this limit.

4.2 Askey-Wilson polynomials as polynomial representations

The Macdonald q-symmetric polynomial[81] $P(X_1, \cdots, X_n; q, t) \in \mathbb{C}[X_1, \cdots, X_n]^{\mathfrak{S}_n}$ can be viewed as an element of the group algebra of the weight lattice of some root system R of rank n, invariant under the Weyl group action of R. Assume that the weight lattice is generated by fundamental weights $w_1, \cdots, w_n$, then the variables of the polynomials can be related to the weights by $X_i = e^{w_i}, i = 1, \cdots, n$. In this way, for each root system R, a family of orthonormal polynomials can indexed by the dominant weights, forming an orthonormal basis of $\mathbb{C}[X_1, \cdots, X_n]^{\mathfrak{S}_n}$ with respect to some properly defined inner product. They are parametrized by two complex parameters q, t, and in their special limits the Macdonald polynomials reduce to simpler polynomials. For example, when $q = t$, they become independent of q, and equals to the Weyl characters of R.

This construction is generalized by Macdonald to any admissible pair of affine root systems (R, S)[72,82], where R and S are finite roots systems in the same vector space, having the same Weyl group and S is reduced. The constructed polynomials are parametrized by parameters $q, t_1, \cdots, t_r$, where r is the number of Weyl orbits of R. An important tool to study these polynomials is the q-difference operators. Cherednik found out that[83–86], the q-differences can be constructed from the representation theory of affine Hecke algebras. In particular, the Macdonald polynomials associated with an admissible pair (R, S) can be studied from the representation theory of double affine Hecke algebra (DAHA)[87]. These constructions are further generalized to non-reduced affine root systems[77,88–91]. In this project, we focus on the case where the pair of root systems is $(C_1^\vee, C_1)$ (in short $C^\vee C_1$), which is associated with the Askey-Wilson polynomials[92], parametrized by (q, t_1, t_2, t_3, t_4).

4.2.1 Polynomial representation

As previously mentioned, the spherical DAHA serves as the underlying algebra governing q-difference operators acting on the Askey-Wilson polynomials. This connection is realized in the *polynomial representation* of $S\ddot{H}_{q,t}$[77,79–80], which acts on the space $\mathcal{P} \equiv \mathbb{C}_{q,t}[X, X^{-1}]^{\mathbb{Z}_2}$. Here, $\mathcal{P}$ represents the space of symmetric Laurent polynomials with coefficients in the ring $\mathbb{C}_{q,t}$ of rational functions in q and t, obtained via the localization (A.1). The representation is given by

$$\mathrm{pol} : S\ddot{H}_{q,t} \to \mathrm{End}(\mathcal{P}) , \tag{4.39}$$

and the actions of the generators are given by:

$$\begin{aligned}
&\mathrm{pol}(x) = X + X^{-1} , \\
&\mathrm{pol}(y) = A(X;t)(\varpi - 1) + A(X^{-1};t)(\varpi^{-1} - 1) - q^{\frac{1}{2}} t_1 t_3 - q^{-\frac{1}{2}} (t_1 t_3)^{-1} , \\
&\mathrm{pol}(z) = q^{\frac{1}{2}} \left[X A(X) \varpi + X^{-1} A(X^{-1}) \varpi^{-1} \right] \\
&\qquad - \frac{X + X^{-1}}{q^{\frac{1}{2}} + q^{-\frac{1}{2}}} \left[A(X) + A(X^{-1}) + q^{\frac{1}{2}} t_1 t_3 + q^{-\frac{1}{2}} t_1^{-1} t_3^{-1} \right] - \frac{\theta_3}{q^{\frac{1}{2}} + q^{-\frac{1}{2}}} .
\end{aligned} \tag{4.40}$$

Here, we define the function $A(X;t)$ as

$$A(X;t) = -\frac{(1 + q^{\frac{1}{2}} t_1 t_2 X)(1 + q^{\frac{1}{2}} t_1 X/t_2)(1 + q^{\frac{1}{2}} t_3 t_4 X)(1 + q^{\frac{1}{2}} t_3 X/t_4)}{q^{\frac{1}{2}} t_1 t_3 (1 - X^2)(1 - qX^2)} , \tag{4.41}$$

and ϖ is the q-shift operator, defined by:

$$\varpi \cdot f(X) = f(qX) . \tag{4.42}$$

A family of orthogonal symmetric polynomials of type $C^\vee C_1$, known as the Askey-Wilson polynomials, forms a basis for $\mathcal{P}$. These polynomials P_n ($n \in \mathbb{Z}_{\geq 0}$) can be expressed in terms of the basic hypergeometric series[92] as

$$P_n(X;q,t) := \frac{(qab, qac, qad; q)_n}{q^{\frac{n}{2}} a^n (abcdq^{n+1}; q)_n} {}_4\phi_3 \left(\left. \begin{matrix} q^{-n}, q^{n+1}abcd, q^{\frac{1}{2}} aX, q^{\frac{1}{2}} aX^{-1} \\ qab, qac, qad \end{matrix} \right| q; q \right) , \tag{4.43}$$

where

$$a = -t_1 t_2, \quad b = -\frac{t_1}{t_2}, \quad c = -t_3 t_4, \quad d = -\frac{t_3}{t_4}. \tag{4.44}$$

Note that ${}_4\phi_3$ is the basic hypergeometric series, which can be expressed as a series expansion at $z = 0$

$${}_4\phi_3 \left(\left. \begin{matrix} a_1, a_2, a_3, a_4 \\ b_1, b_2, b_3 \end{matrix} \right| q; z \right) = \sum_{k=0}^{\infty} \frac{(a_1, a_2, a_3, a_4; q)_k}{(b_1, b_2, b_3, q; q)_k} z^k. \tag{4.45}$$

Here, we use the notation

$$(a_1, a_2, \dots, a_m; q)_n = (a_1; q)_n (a_2; q)_n \dots (a_m; q)_n , \tag{4.46}$$

where we use the q-Pochhammer symbols

$$(a;q)_n = \prod_{k=0}^{n-1}(1-aq^k)\,. \tag{4.47}$$

Under the polynomial representation (4.40), the generators of $\ddot{SH}_{q,t}$ act on the Askey-Wilson polynomial as

$$\begin{aligned}
\mathrm{pol}(x)\cdot P_n(x;q,t) &= P_{n+1}(x;q,t) + B_n P_n(x;q,t) + C_n P_{n-1}(x;q,t)\ ,\\
\mathrm{pol}(y)\cdot P_n(x;q,t) &= \left(-q^{n+\frac{1}{2}}t_1t_3 - q^{-n-\frac{1}{2}}t_1^{-1}t_3^{-1}\right)P_n(x;q,t)\ ,\\
\mathrm{pol}(z)\cdot P_n(x;q,t) &= -q^{n+1}t_1t_3P_{n+1}(x;q,t) - q^{-n}t_1^{-1}t_3^{-1}C_nP_{n-1}(x;q,t)\\
&\quad + \left(B_n - q^{n+\frac{1}{2}}\frac{(t_1-t_3)(1-t_1t_3)(t_2-t_4)(1-t_2t_4)}{t_2t_4(1-t_1t_3q^n)(1-t_1t_3q^{n+1})}\right)P_n(x;q,t)\,,
\end{aligned} \tag{4.48}$$

where

$$\begin{aligned}
B_n &= \frac{-q^{n+\frac{1}{2}}}{t_2t_4(t_1^2t_3^2q^{2n}-1)(t_1^2t_3^2q^{2n+2}-1)}\Big(t_1(t_2^2+1)t_4\left\{1+t_3^2\left[1+q^{2n+1}t_1^2(t_3^2+1)-q^n(q+1)(t_1^2+1)\right]\right\}\\
&\qquad + t_2t_3(t_4^2+1)\left\{1+t_1^2\left[1+q^{2n+1}t_3^2(t_1^2+1)-q^n(q+1)(t_3^2+1)\right]\right\}\Big)\,,\\
C_n &= \frac{(q^n-1)(t_1^2q^n-1)(t_3^2q^n-1)(t_1^2t_3^2q^n-1)(t_1t_2t_3q^n-t_4)(t_1t_3q^n-t_2t_4)(t_1t_3t_4q^n-t_2)(t_1t_2t_3t_4q^n-1)}{t_2^2t_4^2(t_1^2t_3^2q^{2n}-1)^2(t_1^2t_3^2q^{2n-1}-1)(t_1^2t_3^2q^{2n+1}-1)}\,.
\end{aligned}$$

We can define the raising and lowering operators in $\ddot{SH}_{q,t}$ with respect to this basis[93] as

$$\begin{aligned}
R_n &= -q^{1-n}x - qt_1t_3z + E_n\,,\\
L_n &= -q^{n+2}x - \frac{q}{t_1t_3}z + D_n\,,
\end{aligned} \tag{4.49}$$

where

$$\begin{aligned}
D_n &= \frac{q^{3/2}t_1^{-1}t_3^{-1}\left(q^{-n}t_1^{-1}t_3^{-1}\theta_1-\theta_3\right)}{1-q^{-2n}t_1^{-2}t_3^{-2}}\,,\\
E_n &= \frac{q^{3/2}t_1t_3\left(q^{n+1}t_1t_3\theta_1-\theta_3\right)}{q^{2n+2}t_1^2t_3^2-1}\,.
\end{aligned}$$

Under the polynomial representation (4.39), these operators raise and lower the labels n of the Askey-Wilson polynomials as follows:

$$\mathrm{pol}(R_n)\cdot P_n(x;q,t) = q^{1-n}\left(t_1^2t_3^2q^{2n+1}-1\right)P_{n+1}(x;q,t)\,, \tag{4.50}$$

$$\begin{aligned}
\mathrm{pol}(L_n)\cdot P_n(x;q,t) &= -q^{1-n}\left(q^n-t_1^{-1}t_2t_3^{-1}t_4\right)\left(q^n-t_1^{-1}t_2t_3^{-1}t_4^{-1}\right)\left(q^n-t_1^{-1}t_2^{-1}t_3^{-1}t_4\right)\\
&\quad\times\left(q^n-t_1^{-1}t_2^{-1}t_3^{-1}t_4^{-1}\right)\frac{(q^n-1)(q^n-t_1^{-2})(q^n-t_3^{-2})(q^n-t_1^{-2}t_3^{-2})}{\left(q^{2n}-t_1^{-2}t_3^{-2}\right)^2\left(q^{2n-1}-t_1^{-2}t_3^{-2}\right)}P_{n-1}(x;q,t)\,.
\end{aligned} \tag{4.51}$$

As demonstrated above, the spherical DAHA $\ddot{SH}_{q,t}$ is invariant under the Weyl group $W(D_4)$. However, the polynomial representation is *not* invariant under $W(D_4)$. In fact, as we will see more explicitly, acting the Weyl group on the polynomial representation (4.40) yields eight distinct representations.

Furthermore, incorporating the action of the permutation group $\mathbb{Z}_3$, generated by (4.26), one can obtain 24 distinct representations in total from the polynomial representation. These symmetries enrich the structure of the representations, revealing a profound interplay between the representation theory of $\ddot{SH}_{q,t}$ and the root system of type D_4.

4.2.2 Finite-dimensional representations

A common way to construct a finite-dimensional representation is to find null vectors for the raising and lowering operators. The raising operators can never be null since the Askey-Wilson polynomial $P_{n+1}(x;q,t)$ always contains a factor $(t_1^2t_3^2q^{2n+1}-1)$ in the denominator that cancels the raising coefficient in (4.50). However, there are conditions where the lowering operator annihilates an Askey-Wilson polynomial, say $P_n(x;q,t)$, which becomes the lowest weight state of a sub-representation. In this way, a finite-dimensional $\ddot{SH}_{q,t}$-module appears as the quotient $\mathcal{P}/(P_n)$ of the polynomial representation by the ideal (P_n). It is worth noting that not all finite-dimensional representations can be obtained in this way.

Therefore, we can study finite-dimensional representations by imposing the condition $\mathrm{pol}(L_n)\cdot P_n = 0$. Namely, when the lowering coefficient (4.51) vanishes:

$$-q^{1-n}(q^n-t_1^{-1}t_2t_3^{-1}t_4)(q^n-t_1^{-1}t_2t_3^{-1}t_4^{-1})(q^n-t_1^{-1}t_2^{-1}t_3^{-1}t_4)$$
$$\times(q^n-t_1^{-1}t_2^{-1}t_3^{-1}t_4^{-1})\frac{(q^n-1)(q^n-t_1^{-2})(q^n-t_3^{-2})(q^n-t_1^{-2}t_3^{-2})}{(q^{2n}-t_1^{-2}t_3^{-2})^2(q^{2n-1}-t_1^{-2}t_3^{-2})}=0\,. \quad (4.52)$$

This amounts to the seven shortening conditions as follows

$$q^n=1,\ t_1^{-2},\ t_3^{-2},\ t_1^{-1}t_2t_3^{-1}t_4,\ t_1^{-1}t_2t_3^{-1}t_4^{-1},\ t_1^{-1}t_2^{-1}t_3^{-1}t_4,\ t_1^{-1}t_2^{-1}t_3^{-1}t_4^{-1}\,. \quad (4.53)$$

Note that the shortening condition $q^n = t_1^{-2}t_3^{-2}$ is ruled out because some lowering operator becomes ill-defined due to the vanishing of the denominator.

Taking into account the eight distinct representations obtained by the $W(D_4)$ action, the set of shortening conditions can be interpreted within the framework of the D_4 root system. The shortening conditions (4.53) can be identified with a subset of roots of type D_4. By using the Weyl group symmetry, all the shortening conditions for finite-dimensional representations obtained in this way can be neatly repackaged as

$$q^n = t_1^{-r_1}t_2^{-r_2}t_3^{-r_3}t_4^{-r_4} =: t^{-r}, \qquad r\in \mathsf{R}(D_4)\cup\{(0,0,0,0)\}\,. \quad (4.54)$$

(See Appendix A for the convention of the roots.) In the case where q is not a root of unity, a similar classification has been obtained for the finite-dimensional representation of the full DAHA $\ddot{H}_{q,t}$ in[94] by using the strict roots in the affine D_4 root system. We will return to the classification of finite-dimensional representations from the perspective of brane quantization in chapter 5.

Chapter 5

Algebra vs Geometry: Matching Branes and Representations

In this chapter, I will show the main result of this project: the explicit correspondence between A-branes and the representations of the $\dot{S\bar{H}}_{q,t}$. In the previous chapters, I have introduced the necessary informations on both the geometric side and the algebra side. Namely, on the geometric side, the characterizing properties of Lagrangian A-branes are the A-brane conditions and volume functions of the Lagrangian submanifolds supporting them. On the algebraic side, the characterizing properties of representations are the shortening conditions and dimensions of the representations. I will present the explicit matching between these properties on two sides. Moreover, since the full correspondence is at the level of category, I will also describe the explicit matching between morphisms on two sides.

5.1 Non-compact branes and infinite-dimensional representations

In this subsection, we study a brane for the polynomial representation (4.39). The polynomial representation, being infinite-dimensional, is naturally expected to correspond to a non-compact Lagrangian A-brane with infinite volume. Furthermore, we extend the polynomial representation from both the D_4 root system and a geometric perspective. Specifically, we relate the corresponding branes to the 24 lines in the target space $\mathfrak{X}$, further elucidating the structure of this correspondence.

To identify the A-brane associated with the polynomial representation in (4.48), we consider the classical limit $q \to 1$. In this limit, the lowering operator L_n becomes independent of n, so we denote $L^{(c)} = L_n|_{q\to 1}$. In the classical limit, certain operators act as scalar multiplications:

$$\begin{aligned} \mathrm{pol}(y) &= -t_1 t_3 - t_1^{-1} t_3^{-1}, \\ -\mathrm{pol}(L^{(c)}) = 0 &= \mathrm{pol}(x) + \frac{\mathrm{pol}(z)}{t_1 t_3} + t_1^{-1} t_2^{-1} + t_1^{-1} t_2 + t_3^{-1} t_4^{-1} + t_3^{-1} t_4. \end{aligned} \tag{5.1}$$

The second equation holds because the lowering operator becomes null in the classical limit $q \to 1$, as demonstrated in (4.51). Geometrically, this describes the support of the brane $\mathfrak{B}_{\mathbf{P}}$, for the polynomial representation:

$$\mathbf{P} = \{y = -t_1 t_3 - t_1^{-1} t_3^{-1}, z = -t_1 t_3 x - t_1 t_4^{-1} - t_1 t_4 - t_2^{-1} t_3 - t_2 t_3\} \tag{5.2}$$

The configuration specifies a holomorphic embedding of the complex plane $\mathbb{C}$ into the

cubic surface with respect to the complex structure J:[①]

$$\mathbf{P} : \mathbb{C} \hookrightarrow \mathfrak{X} \,. \tag{5.3}$$

Since the Dolbeault cohomology of a complex plane is trivial, $H_J^{2,0}(\mathbb{C}) = 0$, the pullback of the holomorphic 2-form, $\mathbf{P}^*\Omega_J$, must vanish. Consequently, $\mathbf{P}$ is Lagrangian with respect to the symplectic forms ω_I and ω_K. This establishes that $\mathfrak{B}_{\mathbf{P}}$ is an (A, B, A)-brane associated with the polynomial representation.

From the perspective of representation theory, we can construct new polynomial representations by applying the symmetries of $\ddot{SH}_{q,t}$ to (4.40). The supports of these branes can thus be found as the images of $\mathbf{P}$ in (5.2) under the symmetry actions. This approach provides additional examples of the correspondence between non-compact (A, B, A)-branes and polynomial representations.

Weyl group $W(D_4)$ and $\mathbb{Z}_3$ actions on the line

We begin by applying the Weyl group action $W(D_4)$ and the cyclic group $\mathbb{Z}_3$ (see (4.26)) to $\mathbf{P}$. Since both group actions act linearly on the coordinates (x, y, z), they map the line $\mathbf{P}$ to other lines. As a result, 24 distinct lines can be generated from $\mathbf{P}$, as detailed in Appendix B.

A notable feature of these lines is that they all lie in planes where one of the coordinates x, y, or z remains constant. Thus, the slope of each line can be described by a single complex number. To formalize this, we define the slope as follows: if x is constant along the line, the slope is given by $\frac{dy}{dz}$; if y is constant, the slope is $\frac{dz}{dx}$; and if z is constant, the slope is $\frac{dx}{dy}$.

Furthermore, we denote these slopes by $\mathbb{S}_x$, $\mathbb{S}_y$, and $\mathbb{S}_z$, corresponding to lines in planes where x, y, or z is constant, respectively. Interestingly, these sets have a natural interpretation in terms of SO(8) representation theory:

$$\begin{aligned} \mathbb{S}_x &= \{-t^w \mid w \in \mathsf{P}(\mathbf{8}_V)\}, \\ \mathbb{S}_y &= \{-t^w \mid w \in \mathsf{P}(\mathbf{8}_S)\}, \\ \mathbb{S}_z &= \{-t^w \mid w \in \mathsf{P}(\mathbf{8}_C)\}, \end{aligned} \tag{5.4}$$

where $t^w \equiv t_1^{w_1} t_2^{w_2} t_3^{w_3} t_4^{w_4}$, and $\mathsf{P}(\mathbf{8}_V)$, $\mathsf{P}(\mathbf{8}_S)$, and $\mathsf{P}(\mathbf{8}_C)$ are the weights of the SO(8) vector, spinor, and cospinor representations, respectively. These weights correspond to the shortest weights in the D_4 weight lattice (see (A.10) for the conventions used).

Consequently, the 24 non-zero roots of the D_4 root system are organized into three distinct sets, each in one-to-one correspondence with the weights of the SO(8) vector, spinor, and cospinor representations. Furthermore, a similar argument based on the pullback of Ω_J confirms that the branes corresponding to these 24 lines are (A, B, A)-branes in the cubic surface.

The remaining question is whether all lines of type (A, B, A) have been identified in the target space. A classical result in algebraic geometry establishes that a smooth *projective* cubic variety contains exactly 27 lines[95]. Among them, three lines lie at infinity $xyz = 0$ and intersect each other to form a triangle. (For a modern and elementary derivation of the result, see[96]Section 7.) To focus on the lines in the *affine* cubic surface, we exclude these three lines at infinity. This exclusion leaves precisely 24 lines in the

[①] To clarify, in the case of a projective cubic surface, a line corresponds to a holomorphic embedding of $\mathbb{CP}^1$. However, in the affine cubic surface, rather than the projective one, a line specifies a holomorphic embedding of $\mathbb{C}$.

affine cubic surface, which are precisely the ones obtained via the symmetry actions described above.

As a result, the lines and their corresponding infinite-dimensional representations can be labeled using the shortest weights $w \in \mathsf{P}(D_4)$. We denote the lines as $\mathbf{P}_w$ and the polynomial representations as $\mathcal{P}^w$. In addition, the raising and lowering operators in the representation $\mathcal{P}^w$ are denoted as R_n^w and L_n^w, respectively, while the associated Askey-Wilson polynomials are denoted by P_n^w.

Using this convention, the polynomial representation discussed in §4.2 is written as $\mathcal{P}^{w=(1,0,1,0)}$, and the line described in (5.1) is labeled as $\mathbf{P}_{(1,0,1,0)}$, corresponding to its slope $-t_1t_3$. However, for simplicity, we often omit the explicit weight $w = (1,0,1,0)$ when referring to the polynomial representation in §4.2, unless it is necessary for clarity.

Truncation criterion for finite-dimensional representations The relation between lines and the shortest weights provides a useful criterion to determine whether a finite-dimensional representation, as given in (4.54), can be obtained by truncating an infinite-dimensional representation supported on a line.

Recall that finite-dimensional representations obtained by truncating the infinite-dimensional representation $\mathcal{P}^{(1,0,1,0)}$ with weight $w = (1,0,1,0)$ are classified by the conditions in (4.53). These representations correspond to six roots of the D_4 root system, explicitly given by

$$\big\{(2,0,0,0),(0,0,2,0),(1,1,1,1),(1,1,1,-1),(1,-1,1,1),(1,-1,1,-1)\big\} \subset \mathsf{R}(D_4). \tag{5.5}$$

A direct calculation shows that these are the only roots that meet the condition $\langle r, w\rangle > 0$. Since the actions of the Weyl group preserve the inner product, applying these actions to both the weight w and the identified roots guarantees that the result holds for any other weight w'. Therefore, we obtain the following claim:

Claim 5.1 *The finite-dimensional representation, labeled by a root $r \in \mathsf{R}(D_4)$, can be obtained by truncating the polynomial representation $\mathcal{P}^w$ if and only if $\langle r, w\rangle > 0$, where $\langle\cdot,\cdot\rangle$ is the standard Euclidean inner product.*

Braid group action on the line

Next, we apply the action of the braid group B_3 to $\mathbf{P}_w$ in order to identify additional (A,B,A)-branes. As discussed in §4.1.2, the parameters of the cubic surface can change under the braid group action, and therefore, the braid group action is *not*, in general, a symplectomorphism from the surface to itself. However, as shown below, the braid group action determines an algebraic equation that specifies the support of a non-compact (A,B,A)-brane. Thus, we can consistently regard such (A,B,A)-branes as objects in the same target space $\mathfrak{X}$.

Let us first consider the braid group action on $\mathbf{P}_{(1,0,1,0)}$. We denote the image of the line $\mathbf{P}_{(1,0,1,0)}$ after applying τ_+^n for some $n \in \mathbb{Z}$ as

$$\tau_+^n(\mathbf{P}_{(1,0,1,0)}) = \big\{(x,y,z) \in \mathbb{C}^3 | y = f_n(x), z = g_n(x)\big\}, \tag{5.6}$$

where $f_n(x)$ and $g_n(x)$ are functions parametrized by t_j. The initial conditions are

$$\begin{aligned} f_0 &= -t_1t_3 - t_1^{-1}t_3^{-1}, \\ g_0 &= -t_1t_3x - t_1t_4^{-1} - t_1t_4 - t_2^{-1}t_3 - t_2t_3, \end{aligned} \tag{5.7}$$

as specified in (5.2). A straightforward calculation shows that the restriction of the holomorphic symplectic form Ω_J to the variety $\tau_+^n(\mathbf{P}_{(1,0,1,0)})$ vanishes. Thus, the action of the braid group generates additional (A, B, A)-branes.

To obtain a generic expression for the family of polynomials $f_n(x)$ and $g_n(x)$, we define an operator $\hat{\zeta}$ by

$$\hat{\zeta} : f(x; t_1, t_2, t_3, t_4) \mapsto f(x; t_1, t_2, t_4, t_3), \tag{5.8}$$

where f is any function of x parametrized by t_j, and $\hat{\zeta}^2 = \mathrm{id}$. Then, using (4.24), the recursive relations for f_n and g_n are given by

$$\begin{aligned} f_{n+1}(x) &= x\hat{\zeta}(f_n)(x) - \hat{\zeta}(g_n)(x) - \hat{\zeta}(\theta_3), \\ g_{n+1}(x) &= \hat{\zeta}(f_n)(x). \end{aligned} \tag{5.9}$$

Eliminating f_n, we find

$$\hat{\zeta}^{n+1}(g_{n+1})(x) = x\hat{\zeta}^n(g_n)(x) - \hat{\zeta}^{n-1}(g_{n-1})(x) - \hat{\zeta}^{n+1}(\theta_3). \tag{5.10}$$

This recursion relation can be solved by constructing the generating function for $\hat{\zeta}^n(g_n)$:

$$G(x, u) = \sum_{n=0}^{\infty} \hat{\zeta}^n(g_n)u^n, \tag{5.11}$$

where u is a formal variable. Using standard techniques for solving recursion relations, we find

$$G(x, u) = \frac{\theta_3 u^2 + \theta_2 u + (1 - u^2)(uf_0 - g_0)}{(u^2 - 1)(u^2 - ux + 1)}, \tag{5.12}$$

with f_0, g_0 given by (5.7). with f_0 and g_0 given in (5.7). Expanding in powers of u, one can obtain $\hat{\zeta}^n(g_n)$, and hence g_n, for any $n \in \mathbb{Z}_{\geq 0}$. For example, the first few g_n are

$$\begin{aligned} g_1 &= \hat{\zeta}(g_0)x - \hat{\zeta}(f_0) - \theta_3, \\ g_2 &= g_0x^2 - (f_0 + \theta_2)x - \theta_3, \\ g_3 &= \hat{\zeta}(g_0)x^3 - (\hat{\zeta}(f_0) + \theta_3)x^2 - (2\hat{\zeta}(g_0) + \theta_2)x + \hat{\zeta}(f_0), \\ g_4 &= g_0x^4 - (f_0 + \theta_2)x^3 - (3g_0 + \theta_3)x^2 + (2f_0 + \theta_2)x + g_0. \end{aligned} \tag{5.13}$$

The corresponding expressions for f_n can be derived using the second equation in (5.9). By applying the Weyl group and the $\mathbb{Z}_3$ permutation symmetries, the loci of the A-branes can be determined starting from $\mathbf{P}_w$ for any weight w.

As a remark, in the limit (4.6) of the DAHA of type A_1, the generating function simplifies even more. In this limit, the action of $\hat{\zeta}$ becomes trivial, and the generating function reduces to

$$G(x, u) = -\frac{(u - x)t^2 + u}{t(u^2 - ux + 1)}. \tag{5.14}$$

Moreover, by taking the additional limit $t \to i$, the generating function further simplifies to:

$$G(x, u) = ixG_C(x, u), \tag{5.15}$$

where $G_C(x, u) = \frac{1}{u^2 - ux + 1}$ is the generating function for the Chebyshev polynomials of the second kind, as mentioned in[6].

5.2 Compact branes and finite-dimensional representations

In this subsection, we present evidence for the claim of the derived equivalence between the category of compact A-branes and the category of finite-dimensional representations of $\ddot{SH}_{q,t}$. This equivalence involves matching both objects and morphisms.

To match objects, we establish a correspondence between compact Lagrangian A-branes and finite-dimensional representations of $\ddot{SH}_{q,t}$ by comparing the shortening conditions described in (4.54) with the existence conditions for A-branes (referred to as A-brane conditions) derived from the dimension formula (3.29).

To illustrate this correspondence, we consider a case study that covers all possible "generic" configurations of Hitchin fibration, as classified in Table 3-3. We begin by considering the case where $\hbar$ is real, with the symplectic form given by $\omega_{\mathfrak{X}} = \frac{\omega_K}{\hbar}$. Since Hitchin fibration (3.44) is completely integrable, each fiber is Lagrangian of type (B, A, A). Consequently, every component of a Hitchin fiber is Lagrangian with respect to $\omega_{\mathfrak{X}}$ for any value of γ. For all configurations of Hitchin fibration, we show that the shortening conditions in (4.54) have a precise geometric interpretation, corresponding to A-branes supported on the components of a Hitchin fiber.

We then turn to matching morphisms. Specifically, two distinct A-branes supported on components of a singular fiber exhibit non-trivial morphisms when they intersect at a singular fiber, forming bound states. Our analysis identifies these bound states of compact A-branes and their corresponding $\ddot{SH}_{q,t}$-modules using an extension. This provides additional evidence for the equivalence of morphism structures as described in (2.35).

Lastly, we generalize our analysis to the case where $\hbar$ is arbitrary. In this broader context, although a Hitchin fiber is no longer Lagrangian with respect to $\omega_{\mathfrak{X}}$, cycles suspended between singular fibers can become Lagrangian under appropriate choices of (α, γ). The corresponding matching of objects and morphisms in this setting is carried out analogously.

5.2.1 Generic fibers of the Hitchin fibration

We begin by considering the case where $\hbar$ is real. In this case, a generic fiber $\mathbf{F}$ is Lagrangian with respect to $\mathrm{Im}\Omega = \frac{\omega_K}{\hbar}$, and thus $\mathbf{F}$ can serve as the support of an A-brane $\mathfrak{B}_{\mathbf{F}}$. Thus, we consider a brane $\mathfrak{B}_{\mathbf{F}}$ supported on a generic fiber and the corresponding representation $\mathcal{F}$. The story is parallel to[6].

Object Matching Combining the dimension formula (3.29) and the volume formula for a generic fiber (3.66), we have

$$m := \dim \mathrm{Hom}(\mathfrak{B}_{\mathbf{F}}, \mathfrak{B}_{\mathrm{cc}}) = \int_{\mathbf{F}} \frac{\omega_I}{2\pi\hbar} = \frac{1}{\hbar}. \tag{5.16}$$

Consequently, the A-brane $\mathfrak{B}_{\mathbf{F}}$ can exist if and only if $\frac{1}{\hbar} = m \in \mathbb{Z}_{>0}$. Physically, this condition can be interpreted as the Bohr-Sommerfeld quantization condition. More specifically, if one interprets $(\mathbf{F}, \omega_I)$ as a symplectic manifold representing a phase system in classical mechanics, the dimension formula (5.16) implies that the volume of the symplectic manifold $\mathbf{F}$, measured in units of $\hbar$, determines the dimension of the

quantum Hilbert space. Consequently, to ensure the existence of a well-defined Hilbert space, the volume of the symplectic manifold must be quantized.

By $q = e^{2\pi i\hbar}$, the dimension formula implies $q^m = 1$, which is precisely the shortening condition (4.54) with $r = (0,0,0,0)$. Under this shortening condition, we obtain the finite-dimensional $\ddot{SH}_{q,t}$-module

$$\mathcal{F}_m = \mathcal{P}/(P_m)\,, \tag{5.17}$$

where

$$\begin{aligned} P_m(X, q = e^{\frac{2\pi i}{m}}, t) &= X^m + X^{-m} + F_m(t), \\ F_m(t) &= \frac{(t_3^m t_4^m + t_3^m/t_4^m)(t_1^{2m}-1) + (t_1^m t_2^m + t_1^m/t_2^m)(t_3^{2m}-1)}{(t_1 t_3)^{2m}-1}. \end{aligned} \tag{5.18}$$

In fact, such an analysis can be performed for the other polynomial representations $\mathcal{P}^w$, where the corresponding $\ddot{SH}_{q,t}$-modules can be constructed in a similar way

$$\mathcal{F}_m^w = \mathcal{P}^w/(P_m^w)\,. \tag{5.19}$$

As a remark, for the generic choice of t, the $\ddot{SH}_{q,t}$-modules $\mathcal{F}_m^w$ are *not* isomorphic to each other, as each representation $\mathcal{F}_m^w$ uses different raising/lowering operators.

As a further generalization, (5.18) can be viewed as a special case of

$$Q_m(X, x_m) := X^m + X^{-m} - x_m - x_m^{-1}, \tag{5.20}$$

where $x_m \in \mathbb{C}^\times$ is a complex parameter possibly depending on t. When q is an m-th root of unity, the action of $\ddot{SH}_{q,t}$ under the polynomial representation (4.40) commutes with Q_m for any x_m, since the q-shift operator ϖ, defined in (4.42), acts trivially on Q_m. The ideal generated by Q_m in $\mathcal{P}$ becomes a submodule so that a family of finite-dimensional representations labeled by x_m can be constructed as

$$\mathcal{F}_m^{(x_m)} = \mathcal{P}/(Q_m(X, x_m))\,. \tag{5.21}$$

As $Q_m(X, x_m)$ is of degree m, $\mathcal{F}_m^{(x_m)}$ is indeed m-dimensional, which matches the analysis of the A-brane condition (5.16).

This family of finite-dimensional modules $\mathcal{F}_m^{(x_m)}$ corresponds to a family of branes $\mathfrak{B}_{\mathbf{F}}^{(x_m,+)}$ supported on generic Hitchin fibers. Since a generic Hitchin fiber $\mathbf{F}$ is topologically a two-torus, an A-brane $\mathfrak{B}_{\mathbf{F}}$ carries holonomies along one-cycles, $\pi_1(\mathbf{F}) \cong \mathbb{Z}\oplus\mathbb{Z}$, associated with a flat Spin^c-bundle on $\mathbf{F}$ (3.26).

We expect that the parameter x_m encodes information about both the brane's position in the x coordinate and the holonomy along the $(1,0)$-cycle of $\mathfrak{B}_{\mathbf{F}}^{(x_m,+)}$, as discussed in Appendix C and Section 2.6.1 of[6]. Furthermore, the flat Spin^c-bundle has trivial holonomy and a Ramond spin structure along the other $(0,1)$-cycle.

For the DAHA of type A_1, there exists a family of polynomial representations that encode the position of the corresponding A-brane $\mathfrak{B}_{\mathbf{P}}$ in the y coordinate. This leads to the construction of a two-parameter family of finite-dimensional modules $\mathcal{F}_m^{(x_m,y_m)}$. However, for the DAHA of type $C^\vee C_1$,the method for incorporating the y_m parameter into the polynomial representation (4.39) is unknown to us.

5.2.2 At global nilpotent cone of type I_0^*

In the following sections, we will establish the more intricate and intriguing correspondence between A-branes supported on components of singular fibers and finite-dimensional $\ddot{SH}_{q,t}$-modules. As we continue to assume that $\hbar$ is real, here we begin with the I_0^* singular fiber that appears when $\beta_j = 0 = \gamma_j$, as considered in §3.2.4. As illustrated in Figure 3-5, the irreducible components of the I_0^* singular fiber consist of both the moduli space $\mathbf{V}$ of SU(2)-bundles on $C_{0,4}$ and the exceptional divisors $\mathbf{D}_j$ ($j = 1, 2, 3, 4$).

Object Matching We first establish the correspondence between objects by comparing the A-brane conditions for the irreducible components in the I_0^* singular fiber with the shortening conditions of $\ddot{SH}_{q,t}$, as classified in (4.54).

We start with the brane $\mathfrak{B}_{\mathbf{V}}$ supported on the irreducible component $\mathbf{V}$. By combining the dimension formula (3.29) with the volume formula for $\mathfrak{B}_{\mathbf{V}}$ given in (3.75), we find that the dimension of the corresponding representation is:

$$k := \dim \mathrm{Hom}(\mathfrak{B}_{\mathbf{V}}, \mathfrak{B}_{\mathrm{cc}}) = \int_{\mathbf{V}} \frac{F+B}{2\pi} = \int_{\mathbf{V}} \frac{\omega_I}{2\pi\hbar} = \frac{2\alpha_1}{\hbar}. \tag{5.22}$$

The A-brane $\mathfrak{B}_{\mathbf{V}}$ can exist if and only if k is a positive integer. Using (3.33) and noting that $q = e^{2\pi i\hbar}$, this requirement translates to the condition:

$$q^k = t_1^{-2}\,, \tag{5.23}$$

which corresponds to the shortening condition (4.54), with the D_4 root $r = (2, 0, 0, 0)$. When the shortening condition is satisfied, the corresponding k-dimensional representation, denoted by $\mathcal{V}_k$, can be explicitly constructed as the quotient:

$$\mathcal{V}_k = \mathcal{P}/(P_k). \tag{5.24}$$

Using the same approach, one can identify an $\ddot{SH}_{q,t}$-module $\mathcal{D}^{(j)}_{\ell_j}$ corresponding to a brane $\mathfrak{B}_{\mathbf{D}_j}$ supported on each exceptional divisor $\mathbf{D}_j$. The dimension of the morphism space is given by:

$$\ell_j := \dim \mathrm{Hom}(\mathfrak{B}_{\mathbf{D}_j}, \mathfrak{B}_{\mathrm{cc}}) = \int_{\mathbf{D}_j} \frac{F+B}{2\pi} = \int_{\mathbf{D}_j} \frac{\omega_I}{2\pi\hbar} = \frac{\mathrm{vol}(\mathbf{D}_j)}{\hbar}. \tag{5.25}$$

The results are summarized in Table 5-1, based on the volume formulas provided in (3.75). However, these representations *cannot* be constructed as quotients of a single polynomial representation $\mathcal{P}^w$. Instead, one must apply Claim 5.1 to determine a compatible polynomial representation for each case.

For example, as shown in Table 5-1, the A-brane condition for $\mathbf{D}_1$ leads to the shortening condition $q^{\ell_1} = t^{-r}$, with $r = (-1, -1, -1, -1)$. This condition does not align with the shortening conditions (4.53) associated with the polynomial representation $\mathcal{P}^{(1,0,1,0)}$. However, since $\langle r, w\rangle > 0$ for $w = (-1, 0, -1, 0)$, Claim 5.1 ensures that the $\ddot{SH}_{q,t}$-module $\mathcal{D}^{(1)}_{\ell_1}$ can be constructed as the quotient module:

$$\mathcal{D}^{(1)}_{\ell_1} := \mathcal{P}^{(-1,0,-1,0)}/(P^{(-1,0,-1,0)}_{\ell_1}). \tag{5.26}$$

finite-dim rep	shortening condition	A-brane	A-brane condition
$\mathcal{F}_m^{(x_m)}$	$q^m = 1$	$\mathfrak{B}_{\mathbf{F}}^{(x_m)}$	$m = \frac{1}{\hbar}$
$\mathcal{V}_k$	$q^k = t_1^{-2}$	$\mathfrak{B}_{\mathbf{V}}$	$k = \frac{2\alpha_1}{\hbar}$
$\mathcal{D}_{\ell_1}^{(1)}$	$q^{\ell_1} = t_1 t_2 t_3 t_4$	$\mathfrak{B}_{\mathbf{D}_1}$	$\ell_1 = \frac{1}{\hbar} - \frac{\alpha_1+\alpha_2+\alpha_3+\alpha_4}{\hbar}$
$\mathcal{D}_{\ell_2}^{(2)}$	$q^{\ell_2} = t_1 t_2 t_3^{-1} t_4^{-1}$	$\mathfrak{B}_{\mathbf{D}_2}$	$\ell_2 = \frac{-\alpha_1-\alpha_2+\alpha_3+\alpha_4}{\hbar}$
$\mathcal{D}_{\ell_3}^{(3)}$	$q^{\ell_3} = t_1 t_2^{-1} t_3 t_4^{-1}$	$\mathfrak{B}_{\mathbf{D}_3}$	$\ell_3 = \frac{-\alpha_1+\alpha_2-\alpha_3+\alpha_4}{\hbar}$
$\mathcal{D}_{\ell_4}^{(4)}$	$q^{\ell_4} = t_1 t_2^{-1} t_3^{-1} t_4$	$\mathfrak{B}_{\mathbf{D}_4}$	$\ell_4 = \frac{-\alpha_1+\alpha_2+\alpha_3-\alpha_4}{\hbar}$

Table 5-1 A summary of finite-dimensional $\ddot{SH}_{q,t}$-modules with their shortening conditions and the corresponding A-brane configurations at the I_0^* singular fiber, under the assumption $|q| = 1$.

Under the braid group action, the homology cycles transform as described in (4.30). From the perspective of representation theory, the corresponding $\ddot{SH}_{q,t}$-modules are exchanged as follows:

$$\begin{aligned} \tau_+ &: \mathcal{D}_{\ell_3}^{(3)} \leftrightarrow \mathcal{D}_{\ell_4}^{(4)} \quad \text{and} \quad \mathcal{D}_{\ell_1}^{(1)}, \mathcal{D}_{\ell_2}^{(2)} \quad \text{are invariant,} \\ \tau_- &: \mathcal{D}_{\ell_2}^{(2)} \leftrightarrow \mathcal{D}_{\ell_4}^{(4)} \quad \text{and} \quad \mathcal{D}_{\ell_1}^{(1)}, \mathcal{D}_{\ell_3}^{(3)} \quad \text{are invariant,} \\ \sigma &: \mathcal{D}_{\ell_2}^{(2)} \leftrightarrow \mathcal{D}_{\ell_3}^{(3)} \quad \text{and} \quad \mathcal{D}_{\ell_1}^{(1)}, \mathcal{D}_{\ell_4}^{(4)} \quad \text{are invariant.} \end{aligned} \tag{5.27}$$

In particular, both $\mathcal{V}_k$ and $\mathcal{D}_{\ell_1}^{(1)}$ are invariant under the entire braid group action. This phenomenon has been observed in[6], where the braid group action reduces to the $\mathrm{PSL}(2,\mathbb{Z})$ action in the case of DAHA of type A_1. This action leads to the relationship of the DAHA modules with the modular tensor categories[97–98].

Beyond a single irreducible component of the I_0^* singular fiber, one can consider a brane supported on a union of several components, denoted by $\mathbf{N}_r$, which is Lagrangian with respect to $\omega_{\mathfrak{X}} = \omega_K/\hbar$. The homology class of $\mathbf{N}_r$ is represented with the standard basis by

$$[\mathbf{N}_r] = a_0[\mathbf{D}_1] + a_1[\mathbf{D}_2] + a_2[\mathbf{D}_3] + a_3[\mathbf{D}_4] + a_4[\mathbf{V}], \tag{5.28}$$

where $a = (a_0, a_1, a_2, a_3, a_4)$ and the subscript r are related by

$$r = -a_0\theta + \sum_{i=1}^{4} a_i e^i\,, \qquad (a_i = \{0,1,2\})\,. \tag{5.29}$$

Here, e^i are the simple roots, and θ is the highest root in the D_4 root system (3.76). Then, it is straightforward from (3.63) to show that $r \in \mathsf{R}(D_4)$ if and only if a cycle $\mathbf{N}_r$ has a self-intersection number minus two: $[\mathbf{N}_r]\cdot[\mathbf{N}_r] = -2$. Using the same approach, we determine the A-brane condition for $\mathbf{N}_r$. Applying the dimension formula (3.29) and the volume formula (3.77), the A-brane condition is given by

$$m := \dim \mathrm{Hom}(\mathfrak{B}_{\mathbf{N}_r}, \mathfrak{B}_{\mathrm{cc}}) = \int_{\mathbf{N}_r} \frac{F+B}{2\pi} = \int_{\mathbf{N}_r} \frac{\omega_I}{2\pi\hbar} = \frac{a_0 + \left(\sum_{i=1}^4 a_i e^i - a_0\theta\right)\cdot\alpha}{\hbar}. \tag{5.30}$$

The corresponding shortening condition takes the form

$$q^m = t^{-r}, \tag{5.31}$$

where $t^r = t_1^{r_1} t_2^{r_2} t_3^{r_3} t_4^{r_4}$. Thus, we write the corresponding $S\ddot{H}_{q,t}$-module

$$\mathcal{N}_m^{r,w} = \mathcal{P}^w / (P_m^w) \,, \tag{5.32}$$

where $\langle r, w \rangle > 0$ due to Claim 5.1. As a result, if we consider all the cycles with self-intersection number minus two, all 24 roots in the D_4 root system $\mathsf{R}(D_4)$ are exhausted. In this way, the A-brane conditions in (5.30) recover all the shortening conditions classified in (4.54).

If the self-intersection number of a cycle $\mathbf{N}_r$ is *not* minus two, the condition (5.31) does not fit into the shortening conditions for polynomial representations. For example, in the case of the A-brane $\mathfrak{B}_{\mathbf{N}_r}$ with $a = (0, 2, 0, 0, 0)$, the condition $q^m = t^{-2e^1}$ does not align with any shortening condition for polynomial representations because $2e^1$ is not an element of the D_4 root system.[①] This suggests that the existence of an A-brane requires the self-intersection number of its supporting cycle to be precisely minus two.

Morphism Matching Let us consider the morphisms in the two categories. In the category of A-branes, a morphism between two A-branes becomes non-trivial when they intersect, forming a bound state[99–100]. In this section, we will examine the bound states of A-branes and identify the corresponding morphisms in the $S\ddot{H}_{q,t}$-module category. As we will demonstrate, there is a clear correspondence between the morphisms in the A-brane category and those in the representation category.

Let $\mathfrak{B}_{\mathbf{N}_r}$ and $\mathfrak{B}_{\mathbf{N}_{r'}}$ be A-branes supported on components of the I_0^* singular fiber. The A-brane conditions are given by:

$$m = \dim \mathrm{Hom}(\mathfrak{B}_{\mathbf{N}_r}, \mathfrak{B}_{\mathrm{cc}}), \quad m' = \dim \mathrm{Hom}(\mathfrak{B}_{\mathbf{N}_{r'}}, \mathfrak{B}_{\mathrm{cc}}). \tag{5.33}$$

As in (5.32), we denote the corresponding $S\ddot{H}_{q,t}$-modules by $\mathcal{N}_m^{r,w}$ and $\mathcal{N}_{m'}^{r',w'}$ where the shortening conditions are given by $q^m = t^{-r}$ and $q^{m'} = t^{-r'}$, respectively.

Claim 5.2 *If $\mathfrak{B}_{\mathbf{N}_r}$ and $\mathfrak{B}_{\mathbf{N}_{r'}}$ intersect at a point q, then the morphism space is one-dimensional*

$$\mathrm{Hom}(\mathfrak{B}_{\mathbf{N}_r}, \mathfrak{B}_{\mathbf{N}_{r'}}) = \mathbb{C}\langle q \rangle \,. \tag{5.34}$$

Then, the roots $r, r' \in \mathsf{R}(D_4)$ satisfy $\langle r, r' \rangle = -2$. Moreover, there exists a weight w such that $\langle w, r \rangle > 0$, $\langle s_r(w), r' \rangle > 0$. In this setting, there exists a short exact sequence of finite-dimensional $S\ddot{H}_{q,t}$-modules

$$0 \longrightarrow \mathcal{N}_{m'}^{r', s_r(w)} \longrightarrow \mathcal{N}_{m+m'}^{r+r', w} \longrightarrow \mathcal{N}_m^{r,w} \longrightarrow 0 \,. \tag{5.35}$$

This exact sequence is uniquely determined up to isomorphism, independent of the choice of w. Thus, $\mathrm{Ext}^1(\mathcal{N}_m^{r,w}, \mathcal{N}_{m'}^{r', s_r(w)})$ is one-dimensional.

Proof *From (5.28) and (5.29), it is straightforward to show that the intersection number $[\mathbf{N}_r] \cdot [\mathbf{N}_{r'}] = 1$ implies $\langle r, r' \rangle = -2$. This indicates that the root sublattice generated by r and r' forms an A_2 root lattice. Consequently, there always exists a weight w, as illustrated in Figure 5-1, such that*

$$\langle w, r \rangle > 0 \,, \qquad \langle s_r(w), r' \rangle > 0 \,, \tag{5.36}$$

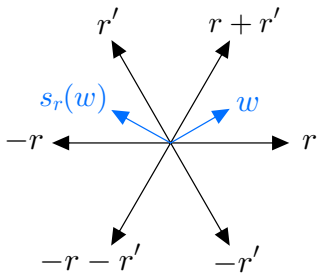

Figure 5-1 The roots r and r' generate an A_2 root lattice, and there always exists a weight w such that (5.36) holds.

where s_r denotes the Weyl reflection (3.101) with respect to r.

As shown in (5.32), when $q^m = t^{-r}$, the $S\ddot{H}_{q,t}$-module $\mathcal{N}_m^{r,w}$ is obtained from the polynomial representation $\mathcal{P}^w$ with $\langle r, w\rangle > 0$. This leads to a short exact sequence

$$0 \longrightarrow \operatorname{Ker}\pi \longrightarrow \mathcal{P}^w \xrightarrow{\pi} \mathcal{N}_m^{r,w} \longrightarrow 0\,. \tag{5.37}$$

Under the condition $q^m = t^{-r}$ and $\langle r, w\rangle > 0$, the direction calculation using (4.50) and (4.51) shows that the raising and lowering operators for $\mathcal{P}^w$ and $\mathcal{P}^{s_r(w)}$ satisfy the following relations

$$\begin{aligned} R_n^w &= q^{-m} R_{n-m}^{s_r(w)}\,, \\ L_n^w &= q^m L_{n-m}^{s_r(w)}\,, \end{aligned} \tag{5.38}$$

for any $n \geq m$. Consequently, the raising and lowering operators in $\operatorname{Ker}\pi$ coincide with those in the polynomial representation $\mathcal{P}^{s_r(w)}$ up to scalar multiplication. This establishes an isomorphism of $S\ddot{H}_{q,t}$-representations $\operatorname{Ker}\pi \cong \mathcal{P}^{s_r(w)}$, and the exact sequence (5.37) can be rewritten as

$$0 \longrightarrow \mathcal{P}^{s_r(w)} \xrightarrow{i} \mathcal{P}^w \xrightarrow{\pi} \mathcal{N}_m^{r,w} \longrightarrow 0,\,, \tag{5.39}$$

which represents an element in $\operatorname{Ext}^1(\mathcal{N}_m^{r,w}, \mathcal{P}^{s_r(w)})$. From the perspective of the A model, it can be verified that the line $\mathbf{P}_{s_r(w)}$ intersects the A-brane $\mathbf{N}_r$ under the conditions $q^m = t^{-r}$ and $\langle r, w\rangle > 0$.

Since $\langle s_r(w), r'\rangle > 0$, the $S\ddot{H}_{q,t}$-module $\mathcal{N}_{m'}^{r',s_r(w)}$ can be constructed as the quotient

$$\mathcal{N}_{m'}^{r',s_r(w)} := \mathcal{P}^{s_r(w)}/(P_{m'}^{s_r(w)})\,, \tag{5.40}$$

when $q^{m'} = t^{-r'}$. The simultaneous conditions $q^m = t^{-r}$ and $q^{m'} = t^{-r'}$ imply $q^{m+m'} = t^{-r-r'}$. Since $s_r(r') = r + r'$, it follows that $\langle r + r', w\rangle = \langle r', s_r(w)\rangle > 0$. By Claim 5.1, another $S\ddot{H}_{q,t}$-module can be constructed as

$$\mathcal{N}_{m+m'}^{r+r',w} = \mathcal{P}^w/(P_{m+m'}^w), \tag{5.41}$$

which gives rise to the short exact sequence

$$0 \longrightarrow \mathcal{N}_{m'}^{r',s_r(w)} \xrightarrow{i_*} \mathcal{N}_{m+m'}^{r+r',w} \xrightarrow{\pi_*} \mathcal{N}_m^{r,w} \longrightarrow 0. \tag{5.42}$$

① Here, we assume that m is odd. Otherwise, it reduces to $q^{m/2} = t^{-e^1}$, which implies that the corresponding representation is simply a direct sum $\mathcal{D}_{m/2}^{(2)} \oplus \mathcal{D}_{m/2}^{(2)}$.

For a graphical representation, see Figure 5-2.

There are always three such weights w_1, w_2, w_3 that give rise to the short exact sequence (5.42), each corresponding to one of the eight-dimensional representations 8_V, 8_S, and 8_C. However, it can be shown using Schur's lemma that the short exact sequences associated with these three different weights are isomorphic. In fact, the character of the finite-dimensional module $\mathcal{N}_m^{r,w_1}$ can be explicitly computed from (4.48) as

$$\begin{aligned}
\mathrm{Tr}_{\mathcal{N}_m^{r,w_1}}(\mathrm{pol}(x)) &= -\frac{q^{m/2}-q^{-m/2}}{q^{1/2}-q^{-1/2}}\left(q^{m/2}t^{w_1}+q^{-m/2}t^{-w_1}\right),\\
\mathrm{Tr}_{\mathcal{N}_m^{r,w_1}}(\mathrm{pol}(y)) &= -\frac{q^{m/2}-q^{-m/2}}{q^{1/2}-q^{-1/2}}\left(q^{m/2}t^{w_2}+q^{-m/2}t^{-w_2}\right),\\
\mathrm{Tr}_{\mathcal{N}_m^{r,w_1}}(\mathrm{pol}(z)) &= -\frac{q^{m/2}-q^{-m/2}}{q^{1/2}-q^{-1/2}}\left(q^{m/2}t^{w_3}+q^{-m/2}t^{-w_3}\right),
\end{aligned} \tag{5.43}$$

under the shortening condition $q^m = t^{-r}$. Recalling that 8_V, 8_S, and 8_C are exchanged under the triality transformation (4.26), the above expression is manifestly symmetric under the triality action on w_1, w_2, and w_3. By Schur's lemma, this symmetry leads to an isomorphism between the short exact sequences for $i \neq j$:

$$\begin{array}{ccccccccc}
0 & \longrightarrow & \mathcal{N}_{m'}^{r',s_r(w_i)} & \longrightarrow & \mathcal{N}_{m+m'}^{r+r',w_i} & \longrightarrow & \mathcal{N}_m^{r,w_i} & \longrightarrow & 0\\
 & & \wr\downarrow & & \wr\downarrow & & \wr\downarrow & & \\
0 & \longrightarrow & \mathcal{N}_{m'}^{r',s_r(w_j)} & \longrightarrow & \mathcal{N}_{m+m'}^{r+r',w_j} & \longrightarrow & \mathcal{N}_m^{r,w_j} & \longrightarrow & 0
\end{array} \tag{5.44}$$

Consequently, $\mathrm{Ext}^1(\mathcal{N}_m^{r,w}, \mathcal{N}_{m'}^{r',s_r(w)})$ is one-dimensional. This completes the proof. ∎

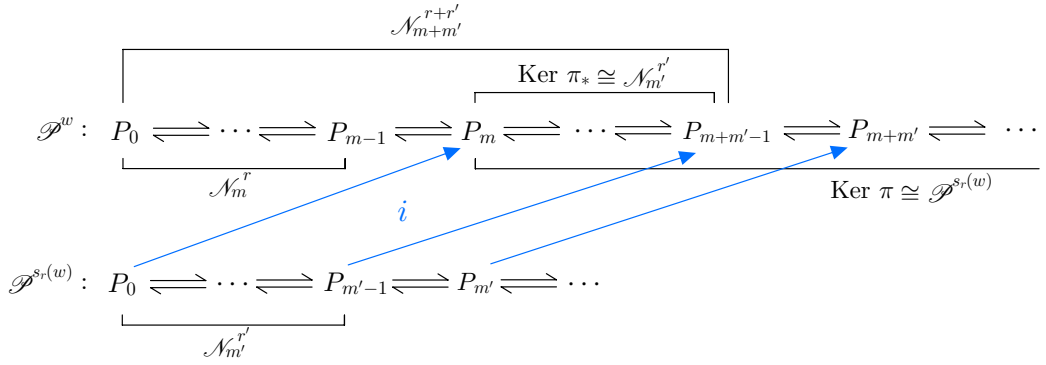

Figure 5-2 The polynomial representation $\mathcal{P}^w$ can be understood as the extension of $\mathcal{N}_m^{r,w}$ by $\mathcal{P}^{s_r(w)}$ under the condition $q^m = t^{-r}$, as in (5.39). Imposing the condition $q^{m'} = t^{-r'}$ further, $\mathcal{N}_{m+m'}^{r+r',w}$ is constructed as the extension of $\mathcal{N}_m^{r,w}$ by $\mathcal{N}_{m'}^{r',s_r(w)}$ as in (5.42).

Example: As an explicit example, let us consider the morphism space $\mathrm{Hom}^*(\mathfrak{B}_{\mathbf{V}}, \mathfrak{B}_{\mathbf{D}_1})$. Since $\mathbf{D}_1$ and $\mathbf{V}$ intersect at a single point q_1 (see Figure 3-5), the geometric perspective predicts that the morphism space is one-dimensional:

$$\mathrm{Hom}^1\left(\mathfrak{B}_{\mathbf{V}}, \mathfrak{B}_{\mathbf{D}_1}\right) \cong \mathbb{C}\left\langle q_1 \right\rangle . \tag{5.45}$$

The A-brane $\mathfrak{B}_{\mathbf{N}_r}$, representing their bound state, is supported on $\mathbf{N}_r = \mathbf{V} \cup \mathbf{D}_1$, with the corresponding root given by:

$$r = -\theta + e_4 = (1, -1, -1, -1). \tag{5.46}$$

The A-brane condition for $\mathfrak{B}_{\mathbf{N}_r}$ is evaluated as:

$$m = \dim \mathrm{Hom}(\mathfrak{B}_{\mathbf{N}_r}, \mathfrak{B}_{\mathrm{cc}}) = \int_{\mathbf{N}_r} \frac{F+B}{2\pi} = \frac{1}{\hbar} - \frac{-\alpha_1 + \alpha_2 + \alpha_3 + \alpha_4}{\hbar}, \tag{5.47}$$

which translates to the shortening condition $q^m = t_1^{-1} t_2 t_3 t_4$.

In the following discussion, we will explain how to construct the corresponding morphism space $\mathrm{Ext}^1(\mathcal{V}_k, \mathcal{D}_\ell^{(1)})$ as an $\ddot{SH}_{q,t}$-module. The roots that correspond to $\mathbf{V}$ and $\mathbf{D}_1$ are $r = (2,0,0,0)$ and $r' = (-1,-1,-1,-1)$, respectively. There are three weights that satisfy the condition (5.36):

$$\begin{aligned}
&\mathbf{8}_V \ni w_1 = (1,-1,0,0)\,, \quad s_r(w_1) = (-1,-1,0,0)\,,\\
&\mathbf{8}_S \ni w_2 = (1,0,-1,0)\,, \quad s_r(w_2) = (-1,0,-1,0)\,,\\
&\mathbf{8}_C \ni w_3 = (1,0,0,-1)\,, \quad s_r(w_3) = (-1,0,0,-1)\,.
\end{aligned} \tag{5.48}$$

It follows from the proof using Schur's lemma that finite-dimensional $\ddot{SH}_{q,t}$-modules associated to these weights are all isomorphic. Therefore, it suffices to focus on the second choice $w := w_2$.

Consider the polynomial representation $\mathcal{P}^w$ where the action of lowering operators L_m^w contains a factor $(q^m - t_1^{-2})(q^m - t_1^{-1}t_2t_3t_4)$, which can be verified from (4.51). Suppose that we impose the two shortening conditions simultaneously

$$q^k = t_1^{-2}\,, \quad \text{and} \quad q^{k+\ell} = t_1^{-1}t_2t_3t_4\,, \tag{5.49}$$

where the first condition is for $\mathcal{V}_k$ (see Table 5-1). Then, we obtain the following short exact sequence from $\mathcal{P}^w$:

$$0 \longrightarrow \mathrm{Ker}\,\pi_* \longrightarrow \mathcal{N}_{k+\ell}^{r,w} \xrightarrow{\pi_*} \mathcal{V}_k \longrightarrow 0\,. \tag{5.50}$$

Since (5.49) implies $q^\ell = t_1t_2t_3t_4$ that is for $\mathcal{D}_\ell^{(1)}$, it is easy to see that $\mathcal{D}_\ell^{(1)} \cong \mathrm{Ker}\,\pi$ by (5.38), and as a result, we obtain the short exact sequence

$$0 \longrightarrow \mathcal{D}_\ell^{(1)} \longrightarrow \mathcal{N}_{k+\ell}^{r,w} \longrightarrow \mathcal{V}_k \longrightarrow 0\,. \tag{5.51}$$

This represents a non-trivial element in $\mathrm{Ext}^1(\mathcal{V}_k, \mathcal{D}_\ell^{(1)})$.

If we switch the role of w and $s_r(w)$, we can construct a short exact sequence in the opposite direction, representing an element in $\mathrm{Ext}^1(\mathcal{D}_\ell^{(1)}, \mathcal{V}_k)$:

$$0 \longrightarrow \mathcal{V}_k \longrightarrow \mathcal{N}_{k+\ell}^{r,s_r(w)} \xrightarrow{\pi} \mathcal{D}_\ell^{(1)} \longrightarrow 0\,. \tag{5.52}$$

This is indeed the Poincaré dual of (5.51) in the representation category.

In this way, one can construct bound states of compact A-branes and their corresponding $\ddot{SH}_{q,t}$-modules. Let us consider two more illustrative examples. For the first

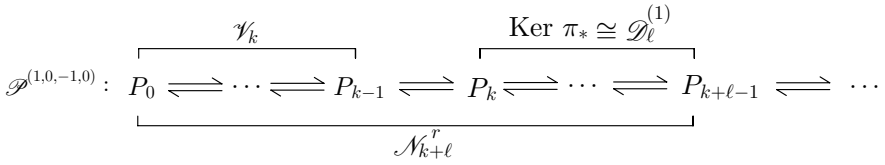

Figure 5-3 The finite-dimensional module $\mathcal{N}_k^{r,w}$ is shown as an extension of $\mathcal{V}_k$ by $\mathcal{D}_\ell^{(1)}$ through the short exact sequence (5.51).The weights $w = (1,0,-1,0)$ are omitted from the superscripts of the polynomials for simplicity. Note that $\mathcal{D}_\ell^{(1)}$ is not obtained as a quotient of $\mathcal{P}^w$ but rather from $\mathcal{P}^{s_r(w)}$, where $s_r(w) = (-1,0,-1,0)$.

example, consider an A-brane $\mathfrak{B}_{\mathbf{N}_r}$ supported on the union of cycles $\mathbf{N}_r = \mathbf{D}_1 \cup \mathbf{D}_2 \cup \mathbf{D}_3 \cup \mathbf{V}$, which corresponds to the root

$$r = (-1,-1,-1,1). \tag{5.53}$$

Imposing the shortening conditions for $\mathcal{D}_{\ell_j}^{(j)}$ and $\mathcal{V}_k$ simultaneously (see Table 5-1), we obtain:

$$q^m = t_1 t_2 t_3 t_4^{-1}, \tag{5.54}$$

where $m = k + \ell_1 + \ell_2 + \ell_3$. This result is consistent with the A-brane condition

$$m = \dim \mathrm{Hom}(\mathfrak{B}_{\mathbf{N}_r}, \mathfrak{B}_{\mathrm{cc}}) = \frac{1}{\hbar} - \frac{\alpha_1+\alpha_2+\alpha_3-\alpha_4}{\hbar}. \tag{5.55}$$

To identify the corresponding $\ddot{SH}_{q,t}$-module explicitly, we choose $w = (-1,0,-1,0)$ and consider the polynomial representation $\mathcal{P}^w$ under the simultaneous shortening conditions. Following a similar argument as before, we find that there exists a short exact sequence

$$0 \to \bigoplus_{j=1,2,3} \mathcal{D}_{\ell_j}^{(j)} \to \mathcal{N}_m^{r,w} \to \mathcal{V}_k \to 0\,. \tag{5.56}$$

The module $\mathcal{N}_m^{r,w}$ can be understood as a diagonal element in the representation category, $q_1+q_2+q_3 \in \mathrm{Hom}^*(\mathfrak{B}_{\mathbf{V}}, \bigoplus_{j=1,2,3} \mathfrak{B}_{\mathbf{D}_j})$. Thus, we can express the corresponding A-brane as:

$$\mathfrak{B}_{\mathbf{N}_r} \in \mathrm{Hom}^*\left(\mathfrak{B}_{\mathbf{V}}, \bigoplus_{j=1,2,3} \mathfrak{B}_{\mathbf{D}_j}\right). \tag{5.57}$$

In the limit of the DAHA of type A_1, this module corresponds to the finite-dimensional representation newly discovered in[6]§2.7,2. While this representation cannot be constructed as a quotient of the polynomial representation of the DAHA of type A_1, the correspondence with the A-brane predicts its existence. For the DAHA of type $C^\vee C_1$, however, this module can be obtained as a quotient of the polynomial representation by leveraging the $W(D_4)$ Weyl group and the $\mathbb{Z}_3$ cyclic symmetry of the algebra.

As the second example, consider the A-brane supported on the entire global nilpotent cone $\mathbf{N}_r := h^{-1}(0) = \mathbf{V} \cup \bigcup_{j=1}^4 \mathbf{D}_j$ (see Figure 3-5), which corresponds to the root

$$r = (-2,0,0,0). \tag{5.58}$$

The dimension formula for the corresponding A-brane $\mathfrak{B}_{\mathbf{N}_r}$ can be evaluated as

$$m = \dim \mathrm{Hom}(\mathfrak{B}_{\mathbf{N}_r}, \mathfrak{B}_{\mathrm{cc}}) = \int_{\mathbf{N}_r} \frac{F+B}{2\pi} = \frac{1}{\hbar} - \frac{2\alpha_1}{\hbar}. \tag{5.59}$$

This yields the shortening condition $q^m = t_1^2$. If we further assume the existence of $\mathfrak{B}_{\mathbf{V}}$, which implies $q^k = t_1^{-2}$, then q must be a $(m+k)$-root of unity. As discussed in §5.2.1, this condition aligns with the A-brane condition for $\mathfrak{B}_{\mathbf{F}}$ supported on a generic Hitchin fiber. The representation associated with the nilpotent cone $\mathbf{N}_r$ can then be constructed as the quotient module

$$\mathcal{N}_m^r := \mathcal{F}_{m+k}/\mathcal{V}_k. \tag{5.60}$$

By construction, this quotient module fits into the following short exact sequence

$$0 \longrightarrow \mathcal{V}_k \longrightarrow \mathcal{F}_{m+k} \longrightarrow \mathcal{N}_m^r \longrightarrow 0\,. \tag{5.61}$$

If we impose additional shortening conditions appropriately, a similar analysis yields the short exact sequence:

$$0 \longrightarrow \bigoplus_{j=1}^4 \mathcal{D}_{\ell_j}^{(j)} \longrightarrow \mathcal{N}_a \longrightarrow \mathcal{V}_k \longrightarrow 0\,, \tag{5.62}$$

which represents an element in $\mathrm{Ext}^1(\mathcal{V}_k, \bigoplus_{j=1}^4 \mathcal{D}_{\ell_j}^{(j)})$.

As a consistency check, consider the limit of the DAHA of type A_1 specified by (4.6). Under this specification, we recover all the A-brane conditions discussed in[6].

5.2.3 At other singular fibers

At a singular fiber of type I_4

In the previous subsection, we provided a detailed analysis of the correspondence between compact A-branes and finite-dimensional $\ddot{SH}_{q,t}$-modules in the case where $\beta_j = \gamma_j = 0$ and $\hbar$ is real. We now turn to the analysis of other fibration configurations listed in Table 3-3. To proceed, we keep $\hbar$ to be real and adjust the ramification parameter γ to realize the I_4 singular fiber, as illustrated in §3.2.5. In this case, a generic fiber remains Lagrangian. Therefore, all the irreducible components of the I_4 singular fiber are also Lagrangian. To be concrete, we focus on the specific case where $(\gamma_1, \gamma_2, \gamma_3, \gamma_4) = (\gamma_1, 0, \gamma_1, 0)$.

Object Matching We apply the same technique as in the previous cases to match the A-branes and finite-dimensional $\ddot{SH}_{q,t}$-modules, by comparing the shortening conditions and A-brane conditions. The compact A-branes $\mathfrak{B}_{\mathbf{F}}$ and $\mathfrak{B}_{\mathbf{U}_i}$ $(i = 1, 2, 3, 4)$ can exist when q is a root of unity and specific t are chosen. In this case, the homology classes and the volumes of the irreducible components have been analyzed in (3.84). The A-brane condition is thus specified by

$$d_i := \dim \mathrm{Hom}(\mathfrak{B}_{\mathbf{U}_i}, \mathfrak{B}_{\mathrm{cc}}) = \int_{\mathbf{U}_i} \frac{F+B}{2\pi} = \frac{\mathrm{vol}_I(\mathbf{U}_i)}{\hbar}, \qquad (i = 1, 2, 3, 4) \tag{5.63}$$

from which one could read off the corresponding shortening conditions. The finite-dimensional representation $\mathcal{U}_{d_i}^{(i)}$ can be constructed by a quotient of an appropriate polynomial representation $\mathcal{P}^w$. The correspondence between irreducible components and finite-dimensional representations is summarized in Table 5-2.

finite-dim rep	shortening condition	A-brane	A-brane condition
$\mathcal{U}_{d_1}^{(1)}$	$q^{d_1} = t_1^{-1}t_2t_3t_4$	$\mathfrak{B}_{\mathbf{U}_1}$	$d_1 = \frac{1}{\hbar} - \frac{-\alpha_1+\alpha_2+\alpha_3+\alpha_4}{\hbar}$
$\mathcal{U}_{d_2}^{(2)}$	$q^{d_2} = t_1t_2t_3^{-1}t_4^{-1}$	$\mathfrak{B}_{\mathbf{U}_2}$	$d_2 = \frac{-\alpha_1-\alpha_2+\alpha_3+\alpha_4}{\hbar}$
$\mathcal{U}_{d_3}^{(3)}$	$q^{d_3} = t_1^{-1}t_2^{-1}t_3t_4^{-1}$	$\mathfrak{B}_{\mathbf{U}_3}$	$d_3 = \frac{\alpha_1+\alpha_2-\alpha_3+\alpha_4}{\hbar}$
$\mathcal{U}_{d_4}^{(4)}$	$q^{d_4} = t_1t_2^{-1}t_3^{-1}t_4$	$\mathfrak{B}_{\mathbf{U}_4}$	$d_4 = \frac{-\alpha_1+\alpha_2+\alpha_3-\alpha_4}{\hbar}$

Table 5-2 A summary of finite-dimensional $\bar{SH}_{q,t}$-modules with their shortening conditions and the corresponding A-brane configurations at the I_4 singular fiber, under the assumption $|q| = 1$.

Morphism Matching From Figure 3.2.5, the fiber of type I_4 consists of four $\mathbb{CP}^1$ joining like a necklace, or the affine $\dot{A}_3$ Dynkin diagram. Therefore, the morphism of the A-branes $\mathfrak{B}_{\mathbf{U}_i}$ and $\mathfrak{B}_{\mathbf{U}_{i+1}}$ is

$$\mathrm{Hom}^*\left(\mathfrak{B}_{\mathbf{U}_i}, \mathfrak{B}_{\mathbf{U}_{i+1}}\right) := CF^*\left(\mathfrak{B}_{\mathbf{U}_i}, \mathfrak{B}_{\mathbf{U}_{i+1}}\right) \cong \mathbb{C}\langle p_i\rangle\,, \qquad (i = 1,2,3,4). \tag{5.64}$$

where we denote $\mathbf{U}_5 := \mathbf{U}_1$ and p_i as the intersection point between $\mathbf{U}_i$ and $\mathbf{U}_{i+1}$.

From the perspective of representation theory, the morphism space can be directly constructed from the analysis above, as the cycles $\mathbf{U}_i$ and $\mathbf{U}_{i+1}$ intersect at a single point. Specifically, let $\mathcal{U}_{d_i+d_{i+1}}^{(i,i+1)}$ denote the finite-dimensional representation corresponding to A-brane supported on the cycle $\mathbf{U}_i \cup \mathbf{U}_{i+1}$. Using the method described in the I_0^* singular fiber, the following short exact sequence can be constructed in the representation theory side:

$$0 \to \mathcal{U}_{d_i}^{(i)} \to \mathcal{U}_{d_i+d_{i+1}}^{(i,i+1)} \to \mathcal{U}_{d_{i+1}}^{(i+1)} \to 0 \quad , \qquad (i = 1,2,3,4) \tag{5.65}$$

which yields an element in $\mathrm{Ext}^1(\mathcal{U}_{d_{i+1}}^{(i+1)}, \mathcal{U}_{d_i}^{(i)})$. Thus, we establish the matching of the morphism space in the case of the I_4 singular fiber.

At a singular fiber of type I_3

We adjust the ramification parameters to realize the I_3 singular fiber. Since a generic fiber is Lagrangian, all irreducible components of the I_3 singular fiber are also Lagrangian. For clarity, we focus on the specific case where $(\gamma_1, \gamma_2, \gamma_3, \gamma_4) = (\gamma_1, 0, \gamma_3, \gamma_1+\gamma_3)$.

Object Matching We apply the same technique as in the previous cases to match the A-branes and finite-dimensional representations, by comparing the shortening conditions and A-brane conditions. With the volumes of the irreducible components $\mathbf{U}_i$ evaluated in (3.88), the A-brane condition writes:

$$d_i := \dim \mathrm{Hom}(\mathfrak{B}_{\mathbf{U}_i}, \mathfrak{B}_{\mathrm{cc}}) = \int_{\mathbf{U}_i} \frac{F+B}{2\pi} = \frac{\mathrm{vol}_I(\mathbf{U}_i)}{\hbar} \quad i = 1,2,3 \tag{5.66}$$

We can extract the shortening condition. The finite-dimensional representation $\mathcal{U}_{d_i}^{(i)}$ is constructed as a quotient of $\mathcal{P}^w$ by $(P_{d_i}^w)$, where w is an appropriate element in $W(D_4)$. The correspondence between the irreducible components and the finite-dimensional representations is summarized in Table 5-3.

finite-dim rep	shortening condition	A-brane	A-brane condition
$\mathcal{U}_{d_1}^{(1)}$	$q^{d_1} = t_2^2$	$\mathfrak{B}_{\mathbf{U}_1}$	$d_1 = \frac{1}{\hbar} - \frac{2\alpha_2}{\hbar}$
$\mathcal{U}_{d_2}^{(2)}$	$q^{d_2} = t_1^{-1}t_2^{-1}t_3^{-1}t_4$	$\mathfrak{B}_{\mathbf{U}_2}$	$d_2 = \frac{\alpha_1+\alpha_2+\alpha_3-\alpha_4}{\hbar}$
$\mathcal{U}_{d_3}^{(3)}$	$q^{d_3} = t_1t_2^{-1}t_3t_4^{-1}$	$\mathfrak{B}_{\mathbf{U}_3}$	$d_3 = \frac{-\alpha_1+\alpha_2-\alpha_3+\alpha_4}{\hbar}$

Table 5-3 A summary of finite-dimensional $\bar{S}\bar{H}_{q,t}$-modules with their shortening conditions and the corresponding A-brane configurations at the I_3 singular fiber, under the assumption $|q| = 1$.

Morphism Matching The analysis is the same as in an I_4 fiber:

$$\mathrm{Hom}^*\left(\mathfrak{B}_{\mathbf{U}_i}, \mathfrak{B}_{\mathbf{U}_{i+1}}\right) := CF^*\left(\mathfrak{B}_{\mathbf{U}_i}, \mathfrak{B}_{\mathbf{U}_{i+1}}\right) \cong \mathbb{C}\left\langle p_i\right\rangle, i = 1, 2, 3 \tag{5.67}$$

where we denote $\mathbf{U}_4 := \mathbf{U}_1$ and p_i as the intersection point between $\mathbf{U}_i$ and $\mathbf{U}_{i+1}$.

From the viewpoint of representation theory, the morphism space can be constructed directly based on the analysis above, given that the cycles $\mathbf{U}_i$ and $\mathbf{U}_{i+1}$ intersect at a single point. More precisely, the corresponding $\bar{\bar{S}}\bar{\bar{H}}_{q,t}$-module can be expressed in terms of the short exact sequence

$$0 \to \mathcal{U}_{d_i}^{(i)} \to \mathcal{U}_{d_i+d_{i+1}}^{(i,i+1)} \to \mathcal{U}_{d_{i+1}}^{(i+1)} \to 0\,, \tag{5.68}$$

which yields an element in $\mathrm{Ext}^1(\mathcal{U}_{d_{i+1}}^{(i+1)}, \mathcal{U}_{d_i}^{(i)})$. Hence, we conclude the matching of the morphism space in the case of I_3 singular fiber.

At a singular fiber of type I_2

We adjust the ramification parameters to realize the I_2 singular fiber. Since a generic fiber is Lagrangian, all irreducible components of the I_2 singular fiber are also Lagrangian. For clarity, we focus on the specific case where $(\gamma_1, \gamma_2, \gamma_3, \gamma_4) = (\gamma_1, 0, \gamma_3, \gamma_4)$.

Object Matching The volumes of the irreducible components have been previously analyzed in (3.93), with associated A-brane condition:

$$d_i := \dim \mathrm{Hom}(\mathfrak{B}_{\mathbf{U}_i}, \mathfrak{B}_{\mathrm{cc}}) = \int_{\mathbf{U}_i} \frac{F+B}{2\pi} = \frac{\mathrm{vol}_I(\mathbf{U}_i)}{\hbar}, i = 1, 2 \tag{5.69}$$

From this, we can extract the shortening conditions. The finite-dimensional representation $\mathcal{U}_{d_i}^{(i)}$ is constructed by quotienting $\mathcal{P}^w$ over $P_{d_i}^w$. The correspondence between the irreducible components and the finite-dimensional representations is summarized in Table 5-3.

Morphism Matching The I_2 case differs from the analysis above, as two irreducible components $\mathbf{U}_1$ and $\mathbf{U}_2$ intersect at two points, denoted as p_1, p_2. In this case, the morphism of the A-branes $\mathfrak{B}_{\mathbf{U}_1}$ and $\mathfrak{B}_{\mathbf{U}_2}$ is

$$\mathrm{Hom}^*\left(\mathfrak{B}_{\mathbf{U}_1}, \mathfrak{B}_{\mathbf{U}_2}\right) := CF^*\left(\mathfrak{B}_{\mathbf{U}_1}, \mathfrak{B}_{\mathbf{U}_2}\right) \cong \mathbb{C}\left\langle p_1\right\rangle \oplus \mathbb{C}\left\langle p_2\right\rangle. \tag{5.70}$$

finite-dim rep	shortening condition	A-brane	A-brane condition
$\mathcal{U}_{d_1}^{(1)}$	$q^{d_1} = t_2^2$	$\mathfrak{B}_{\mathbf{U}_1}$	$d_1 = \frac{1}{\hbar} - \frac{2\alpha_2}{\hbar}$
$\mathcal{U}_{d_2}^{(2)}$	$q^{d_2} = t_2^{-2}$	$\mathfrak{B}_{\mathbf{U}_2}$	$d_2 = \frac{2\alpha_2}{\hbar}$

Table 5-4 A summary of finite-dimensional $\bar{SH}_{q,t}$-modules with their shortening conditions and the corresponding A-brane configurations at the I_2 singular fiber, under the assumption $|q| = 1$.

From the viewpoint of representation theory, the morphism space is expected to be two-dimensional. In this case, applying a similar technique as before, a short exact sequence is obtained from the polynomial representation $\mathcal{P}^w$ with $w = (0, 1, 0, 1)$

$$0 \longrightarrow \mathcal{U}_{d_1}^{(1)} \longrightarrow \mathcal{F}_{d_1+d_2}^{(0,1,0,1)} \longrightarrow \mathcal{U}_{d_2}^{(2)} \longrightarrow 0\,, \tag{5.71}$$

which yields an element in $\mathrm{Ext}^1(\mathcal{U}_{d_2}^{(2)}, \mathcal{U}_{d_1}^{(1)})$.

However, as the morphism space is two-dimensional, from the representation theory side, there must be another morphism that one can find. To identify the corresponding module, we consider the quotients of the polynomial representation with a different weight $w = (0, 1, 0, -1)$

$$0 \longrightarrow \mathcal{U}_{d_1}^{(1)} \longrightarrow \mathcal{F}_{d_1+d_2}^{(0,1,0,-1)} \longrightarrow \mathcal{U}_{d_2}^{(2)} \longrightarrow 0\,, \tag{5.72}$$

which yields another element in $\mathrm{Ext}^1(\mathcal{U}_{d_2}^{(2)}, \mathcal{U}_{d_1}^{(1)})$. As the raising/lowering operators in $\mathcal{F}_{d_1+d_2}^{(0,1,0,1)}$ and $\mathcal{F}_{d_1+d_2}^{(0,1,0,-1)}$ are different, they provide two distinct generators for $\mathrm{Ext}^1(\mathcal{U}_{d_2}^{(2)}, \mathcal{U}_{d_1}^{(1)})$. Therefore, we conclude the matching of the morphism space in the case of I_2 singular fiber.

5.2.4 Generic $\hbar$ parameter

Until now, we have assumed that $\hbar$ is real. However, the analysis of finite-dimensional representations in (4.53) does not rely on this assumption. Let us now explore the scenario where $\hbar = |\hbar| e^{i\theta}$ is complex rather than real. In this case, the symplectic form $\omega_{\mathfrak{X}} = \mathrm{Im}\Omega$ of the A-model is no longer proportional to ω_K but instead becomes a linear combination of ω_I and ω_K. As a result, for generic values of $\hbar$, a Hitchin fiber is no longer Lagrangian with respect to $\omega_{\mathfrak{X}}$.

As shown in (3.57), the second integral homology group of the target space $\mathfrak{X}$ is isomorphic to the affine D_4 root lattice. The standard generators $[\mathbf{D}_j]$ $(j = 1, 2, 3, 4)$ and $[\mathbf{V}]$ correspond to the simple roots e^ℓ $(\ell = 0, \ldots, 4)$ of the affine D_4 root system, as shown in (3.78). For simplicity, we denote the homology classes by their corresponding roots in the following paragraphs. Using (3.80), their volumes with respect to Ω can be written as

$$\int_{e^\ell} \frac{\Omega}{2\pi} = \frac{e^\ell \cdot (\alpha - i\gamma)}{\hbar}\,, \qquad (\ell = 0, \ldots, 4). \tag{5.73}$$

Therefore, a necessary condition for the homology class e^ℓ to be represented by a Lagrangian submanifold with respect to $\omega_{\mathfrak{X}}$ is

$$\mathrm{Im}\frac{e^\ell \cdot (\alpha - i\gamma)}{\hbar} = 0\,. \tag{5.74}$$

In fact, comparison with the representations of $\ddot{SH}_{q,t}$ indicates that it is also sufficient although a rigorous derivation is unknown to us. In other words, for any homology class e^ℓ satisfying this condition, there exists a corresponding Lagrangian submanifold with respect to $\omega_{\mathcal{X}}$. Based on this assumption, the correspondence between compact A-branes and $\ddot{SH}_{q,t}$-modules for generic $\hbar$ is summarized in Table 5-5. In addition to these branes, we can consider bound states of the branes to exhaust all finite-dimensional $\ddot{SH}_{q,t}$-modules. The procedure is analogous, so that we omit the details to keep the discussion concise and focused.

finite-dim rep	shortening condition	A-brane	A-brane condition
$\mathcal{D}^{(1)}_{\ell_1}$	$q^{\ell_1} = t_1t_2t_3t_4$	$\mathfrak{B}_{\mathbf{D}_1}$	$\ell_1 = \frac{1}{\hbar} - \frac{\theta\cdot(\alpha - i\gamma)}{\hbar}$
$\mathcal{D}^{(2)}_{\ell_2}$	$q^{\ell_2} = t_1t_2t_3^{-1}t_4^{-1}$	$\mathfrak{B}_{\mathbf{D}_2}$	$\ell_2 = \frac{e^1\cdot(\alpha - i\gamma)}{\hbar}$
$\mathcal{D}^{(3)}_{\ell_3}$	$q^{\ell_3} = t_1t_2^{-1}t_3t_4^{-1}$	$\mathfrak{B}_{\mathbf{D}_3}$	$\ell_3 = \frac{e^2\cdot(\alpha - i\gamma)}{\hbar}$
$\mathcal{D}^{(4)}_{\ell_4}$	$q^{\ell_4} = t_1t_2^{-1}t_3^{-1}t_4$	$\mathfrak{B}_{\mathbf{D}_4}$	$\ell_4 = \frac{e^3\cdot(\alpha - i\gamma)}{\hbar}$
$\mathcal{V}_k$	$q^k = t_1^{-2}$	$\mathfrak{B}_{\mathbf{V}}$	$k = \frac{e^4\cdot(\alpha - i\gamma)}{\hbar}$

Table 5-5 A summary of finite-dimensional representations of $\ddot{SH}_{q,t}$ with corresponding shortening and A-brane conditions at I_0^* singular fiber.

As a special case, consider the scenario where $\hbar$ is purely imaginary ($i\hbar \in \mathbb{R}_{>0}$) so that the symplectic form becomes $\omega_{\mathcal{X}} = \omega_I/|\hbar|$. As described in (3.98), the suspended cycles $\mathbf{W}_{ij}$ serve as generators of the second homology group, corresponding to the simple roots e^ℓ ($\ell = 1, 2, 3, 4$), when the ramification parameters γ_j are generic, and the Hitchin fibration has $6I_1$.

A particularly interesting limit occurs when $\alpha_j = 0$ and γ_j lie within the chamber specified by (3.97). In this case, the volumes of the suspended cycles with respect to Ω are given by (3.99):

$$\int_{e^\ell} \frac{\Omega}{2\pi} = -\frac{ie^\ell \cdot \gamma}{\hbar} \in \mathbb{R}, \qquad (\ell = 1, 2, 3, 4). \tag{5.75}$$

Then, applying the above assumption, there exist four compact branes of type (A, A, B) suspended between the I_1 singular fibers. The correspondence between these A-branes and $\ddot{SH}_{q,t}$-modules is summarized in Table 5-6.

finite-dim rep	shortening condition	A-brane	A-brane condition
$\mathcal{W}^{(13)}_{d_1}$	$q^{d_1} = t_1^{-2}$	$\mathfrak{B}_{\mathbf{W}_{13}}$	$d_1 = \frac{2\gamma_1}{\lvert\hbar\rvert}$
$\mathcal{W}^{(12)}_{d_2}$	$q^{d_2} = t_1t_2t_3^{-1}t_4^{-1}$	$\mathfrak{B}_{\mathbf{W}_{12}}$	$d_2 = \frac{-\gamma_1-\gamma_2+\gamma_3+\gamma_4}{\lvert\hbar\rvert}$
$\mathcal{W}^{(34)}_{d_3}$	$q^{d_3} = t_1t_2^{-1}t_3t_4^{-1}$	$\mathfrak{B}_{\mathbf{W}_{34}}$	$d_3 = \frac{-\gamma_1+\gamma_2-\gamma_3+\gamma_4}{\lvert\hbar\rvert}$
$\mathcal{W}^{(56)}_{d_4}$	$q^{d_4} = t_1t_2^{-1}t_3^{-1}t_4$	$\mathfrak{B}_{\mathbf{W}_{56}}$	$d_4 = \frac{-\gamma_1+\gamma_2+\gamma_3-\gamma_4}{\lvert\hbar\rvert}$

Table 5-6 A summary of finite-dimensional representation of $\ddot{SH}_{q,t}$ with corresponding shortening and A-brane conditions under $\alpha_j = 0$ limit.

Chapter 6
Conclusion

In this paper, the brane quantization framework is applied to the Hitchin fibration of gauge group $SU(2)$. The Lagrangian A-branes in this space are identified for various types of parameters. The polynomial representations of DAHA algebra of type $C^\vee C_1$ are classified. The important role played by the affine Weyl group of type D_4 is revealed. Finally, the explicit correspondence between the representations of DAHA of type $C^\vee C_1$ and the Lagrangian A-branes is established.

In the future, we can continue to apply this construction to more interesting target space, to give more verifications of the scheme of brane quantization, and provide more examples of the interplay between geometry and algebra.

Appendix A
Notations

The conventions and notations largely follow those in[6].

- Sans-serif symbols: Single sans-serif symbols are used to denote lattices or free $\mathbb{Z}$-modules (e.g., Q and P for the root and weight lattices, respectively). Words in sans-serif type (e.g., A-Brane) refer to categories.
- Calligraphic letters: Symbols such as $\mathcal{M}$ or $\mathcal{B}$ are reserved for objects that are moduli spaces or closely related to them.
- Boldface symbols: Boldface symbols are used for two-cycles of the target space, often representing the support of A-branes (e.g., $\mathbf{F}$ for a generic fiber of the Hitchin fibration).
- Gothic letters: Capital gothic symbols (e.g., $\mathfrak{X}$ for the target space) denote objects equipped with the structure required by the topological A-model. For example, $\mathfrak{B}$ represents an A-brane associated with specific data, while $\mathfrak{B}_{\mathbf{F}}$ denotes a brane supported on a generic fiber $\mathbf{F}$ of the Hitchin fibration.
- Script letters: Script letters are used for modules over the algebra $\mathcal{O}^q(\mathfrak{X})$, with the specific algebra being clear from the context. For consistency, the same symbol is used for a brane and its corresponding representation. For instance, a representation $\mathcal{F}$ of the spherical DAHA $\ddot{SH}_{q,t}$ is identified with an A-brane $\mathfrak{B}_{\mathbf{F}}$ under the equivalence (2.35) between the two categories.

Let $\mathbb{C}[q^{\pm\frac{1}{2}}, t^{\pm}] := \mathbb{C}[q^{\pm\frac{1}{2}}, t_1^{\pm}, t_2^{\pm}, t_3^{\pm}, t_4^{\pm}]$ be the ring of Laurent polynomials in the formal parameters $q^{1/2}$ and $t = (t_1, t_2, t_3, t_4)$, and consider a multiplicative system M in $\mathbb{C}[q^{\pm\frac{1}{2}}, t^{\pm}]$ generated by elements of the form $(q^{\ell/2}t_1t_3 - q^{-\ell/2}t_1^{-1}t_3^{-1})$ for any non-negative integer $\ell \in \mathbb{Z}_{\geq 0}$. We define the coefficient ring $\mathbb{C}_{q,t}$ to be the localization (or formal "fraction") of the ring $\mathbb{C}[q^{\pm\frac{1}{2}}, t^{\pm}]$ at M:

$$\mathbb{C}_{q,t} = M^{-1}\mathbb{C}[q^{\pm\frac{1}{2}}, t^{\pm}]. \tag{A.1}$$

The standard notation of DAHA of $C^\vee C_1$ used in[10] is given by

$$\begin{aligned} \left(T_0 - t_1\right)\left(T_0 + t_1^{-1}\right) &= 0, \\ \left(T_0^\vee - t_2\right)\left(T_0^\vee + t_2^{-1}\right) &= 0, \\ \left(T_1 - t_3\right)\left(T_1 + t_3^{-1}\right) &= 0, \\ \left(T_1^\vee - t_4\right)\left(T_1^\vee + t_4^{-1}\right) &= 0, \end{aligned} \tag{A.2}$$

and

$$T_1^\vee T_1 T_0 T_0^\vee = q^{-\frac{1}{2}}. \tag{A.3}$$

To match with the geometry side, we make the following change of variables to obtain our definition on DAHA (4.1):

$$\begin{aligned}(T_0, T_0^\vee, T_1, T_1^\vee) &\to (T_1, T_1^\vee, T_0, T_0^\vee)\\ (t_1, t_2, t_3, t_4) &\to (-it_3, -it_4, -q^{\frac{1}{2}} it_1, -it_2)\,.\end{aligned} \tag{A.4}$$

Root system and weight lattice

In this paper, we establish notation for the root system and weight lattice of type D_4. For the discussion of the root system, we assume an orthogonal basis in $\mathbb{R}^4$ equipped with the standard Euclidean inner product, allowing us to express the roots accordingly. The standard convention for the D_4 root system and weight systems is as follows, with a tilde ($\sim$) placed above the notation to distinguish it from our chosen notation. The D_4 root system consists of 24 non-zero roots and 4 zero roots, among whom the non-zero roots are expressed as:

$$\tilde{\mathsf{R}}(D_4) = \{\pm\epsilon^i \pm \epsilon^j \mid i, j \in \{1,2,3,4\}, i > j\}, \tag{A.5}$$

where the basis vectors ϵ^i are defined as:

$$\epsilon^1 = (1,0,0,0), \quad \epsilon^2 = (0,1,0,0), \quad \epsilon^3 = (0,0,1,0), \quad \epsilon^4 = (0,0,0,1). \tag{A.6}$$

To match the geometry of the cubic surface, we adopt a slightly unconventional presentation of the D_4 root system:

$$\mathsf{R}(D_4) = \left\{(\pm1,\pm1,\pm1,\pm1), (\pm2,0,0,0), (0,\pm2,0,0), (0,0,\pm2,0), (0,0,0,\pm2)\right\}. \tag{A.7}$$

Two conventions differ by change of bases, specified by

$$r = A\tilde{r}\,, \qquad A = \begin{pmatrix} 1 & 1 & 0 & 0\\ 1 & -1 & 0 & 0\\ 0 & 0 & 1 & 1\\ 0 & 0 & 1 & -1 \end{pmatrix}, \quad \tilde{r} \in \tilde{\mathsf{R}}(D_4) \tag{A.8}$$

As a result, the norm of vectors in $\mathsf{R}(D_4)$ in our notation is normalized to 2 instead of $\sqrt{2}$. We take the set of simple roots for D_4 root system as

$$\{e^1, e^2, e^3, e^4\} = \{(-1,-1,1,1), (-1,1,-1,1), (-1,1,1,-1), (2,0,0,0)\}\,, \tag{A.9}$$

Then, the highest root is expressed by $\theta = e^1 + e^2 + e^3 + 2e^4 = (1,1,1,1)$, as drawn in Figure 3-10. For the affine D_4 root system, we use δ to denote the imaginary root. The extra simple root in affine D_4 root system is given by $e^0 = \delta - \theta$.

Under this convention, the weights of inside $\mathbf{8}_V, \mathbf{8}_S, \mathbf{8}_C$ are as follows, which we denote as $\mathsf{P}(\mathbf{8}_V), \mathsf{P}(\mathbf{8}_S)$ and $\mathsf{P}(\mathbf{8}_C)$.

$$\begin{aligned}\mathsf{P}(\mathbf{8}_V) &= \{(\pm1,\pm1,0,0), (0,0,\pm1,\pm1)\}\\ \mathsf{P}(\mathbf{8}_S) &= \{(\pm1,0,\pm1,0), (0,\pm1,0,\pm1)\}\\ \mathsf{P}(\mathbf{8}_C) &= \{(\pm1,0,0,\pm1), (0,\pm1,\pm1,0)\}\end{aligned} \tag{A.10}$$

Here all the weights have the multiplicity one. Throughout the paper, we adopt the following notation:

$$\overline{t_j} \equiv t_j + t_j^{-1}\,. \tag{A.11}$$

Then, the characters can be expressed as

$$\begin{aligned}
\chi_{\mathbf{8}_V} &= \sum_{w\in \mathsf{P}(\mathbf{8}_V)} t^w = \bar{t}_1\bar{t}_2 + \bar{t}_3\bar{t}_4 = \theta_1 \\
\chi_{\mathbf{8}_S} &= \sum_{w\in \mathsf{P}(\mathbf{8}_S)} t^w = \bar{t}_1\bar{t}_3 + \bar{t}_2\bar{t}_4 = \theta_2 \\
\chi_{\mathbf{8}_C} &= \sum_{w\in \mathsf{P}(\mathbf{8}_C)} t^w = \bar{t}_1\bar{t}_4 + \bar{t}_2\bar{t}_3 = \theta_3 \\
\chi_{\mathrm{adj}} &= \sum_{r\in \mathsf{R}(D_4)\cup\{(0,0,0,0)\}^{\times 4}} t^r = -4 + \bar{t}_1^{-2} + \bar{t}_2^{-2} + \bar{t}_3^{-2} + \bar{t}_4^{-2} + \bar{t}_1\,\bar{t}_2\,\bar{t}_3\,\bar{t}_4 = \theta_4
\end{aligned} \tag{A.12}$$

where $t^w = t_1^{w_1}t_2^{w_2}t_3^{w_3}t_4^{w_4}$, $\{(0,0,0,0)\}^{\times 4}$ means four copies of the zero root coming from the Cartan subalgebra. In the last formula, we apply the identity $t_1^2 + t_1^{-2} = \bar{t}_1^{-2} - 2$.

Infinite/finite-dimensional representations

In §5.1, we demonstrated that there are 24 line-like (A, B, A)-branes, whose support corresponds to the 24 lines in the cubic surface. These lines, characterized by their slopes, can be labeled by the 24 shortest weights in the D_4 weight lattice $\mathsf{P}(D_4)$. Accordingly, we label the infinite-dimensional representation associated with the shortest weight w as $\mathcal{P}^w$.

In this context, we denote the raising and lowering operators in the representation $\mathcal{P}^w$ as R_n^w and L_n^w, respectively, where the corresponding Askey-Wilson polynomials are denoted as P_n^w. In this notation, the polynomial representation discussed in §4.2.1 is denoted as $\mathcal{P}^{w=(1,0,1,0)}$, with the raising and lowering operators in equation (4.49) labeled as $R_n^{(1,0,1,0)}$ and $L_n^{(1,0,1,0)}$, respectively. However, for brevity, we often omit the explicit weight $w = (1, 0, 1, 0)$ when referring to the polynomial representation in §4.2.1, unless explicit clarification is needed.

Appendix B

24 lines in affine cubic surface

We have mentioned in §5.1 that there are, in total, 24 lines in the affine cubic surface. We can use the symmetry action of $\ddot{SH}_{q,t}$ in §4.1.1 to identify the positions of these lines. In §5.1, we denote the slopes of the lines located on the plane where x,y or z is constant as $\mathbb{S}_x, \mathbb{S}_y, \mathbb{S}_z$ respectively. Moreover, the slopes of the lines $\mathbb{S}_x, \mathbb{S}_y, \mathbb{S}_z$ are in one-to-one correspondence with the weights in the $SO(8)$ vector, spinor, and cospinor representations $\mathsf{P}(\mathbf{8}_V), \mathsf{P}(\mathbf{8}_S), \mathsf{P}(\mathbf{8}_C)$ respectively.

$$\begin{aligned}\mathbb{S}_x &= \{-t^w \mid w \in \mathsf{P}(\mathbf{8}_V)\},\\ \mathbb{S}_y &= \{-t^w \mid w \in \mathsf{P}(\mathbf{8}_S)\},\\ \mathbb{S}_z &= \{-t^w \mid w \in \mathsf{P}(\mathbf{8}_C)\},\end{aligned} \tag{B.1}$$

where $t^w = t_1^{w_1}t_2^{w_2}t_3^{w_3}t_4^{w_4}$. Therefore, we could label the 24 lines with the weight in the $\mathbf{P}_w$, whose slope is $-t^w$. As mentioned in §5.1, the 24 lines serve as the support of (A, B, A)-brane inside the Hitchin moduli space.

Eight lines on the plane where x is constant are denoted by $\mathbf{P}_w$, where $w \in \mathsf{P}(\mathbf{8}_V)$.

$$\begin{aligned}\mathbf{P}_{(-1,-1,0,0)} &= \left\{x = -t_1t_2 - t_1^{-1}t_2^{-1}, y = -t_1^{-1}t_2^{-1}z - t_1^{-1}t_3 - t_1^{-1}t_3^{-1} - t_2^{-1}t_4 - t_2^{-1}t_4^{-1}\right\},\\ \mathbf{P}_{(1,1,0,0)} &= \left\{x = -t_1t_2 - t_1^{-1}t_2^{-1}, y = -t_1t_2z - t_1t_3 - t_1t_3^{-1} - t_2t_4 - t_2t_4^{-1}\right\},\\ \mathbf{P}_{(1,-1,0,0)} &= \left\{x = -t_1^{-1}t_2 - t_1t_2^{-1}, y = -t_1t_2^{-1}z - t_1t_3 - t_1t_3^{-1} - t_2^{-1}t_4 - t_2^{-1}t_4^{-1}\right\},\\ \mathbf{P}_{(-1,1,0,0)} &= \left\{x = -t_1^{-1}t_2 - t_1t_2^{-1}, y = -t_1^{-1}t_2z - t_2t_4 - t_2t_4^{-1} - t_1^{-1}t_3 - t_1^{-1}t_3^{-1}\right\},\\ \mathbf{P}_{(0,0,-1,-1)} &= \left\{x = -t_3t_4 - t_3^{-1}t_4^{-1}, y = -t_3^{-1}t_4^{-1}z - t_1t_3^{-1} - t_1^{-1}t_3^{-1} - t_2t_4^{-1} - t_2^{-1}t_4^{-1}\right\},\\ \mathbf{P}_{(0,0,1,1)} &= \left\{x = -t_3t_4 - t_3^{-1}t_4^{-1}, y = -t_3t_4z - t_1t_3 - t_1^{-1}t_3 - t_2t_4 - t_2^{-1}t_4\right\},\\ \mathbf{P}_{(0,0,1,-1)} &= \left\{x = -t_3^{-1}t_4 - t_3t_4^{-1}, y = -t_3t_4^{-1}z - t_1t_3 - t_1^{-1}t_3 - t_2^{-1}t_4^{-1} - t_2t_4^{-1}\right\},\\ \mathbf{P}_{(0,0,-1,1)} &= \left\{x = -t_3^{-1}t_4 - t_3t_4^{-1}, y = -t_3^{-1}t_4z - t_1t_3^{-1} - t_1^{-1}t_3^{-1} - t_2t_4 - t_2^{-1}t_4\right\}.\end{aligned} \tag{B.2}$$

Eight lines on the plane where y is constant are denoted by $\mathbf{P}_w$, where $w \in \mathsf{P}(\mathbf{8}_S)$.

$$\begin{aligned}\mathbf{P}_{(1,0,1,0)} &= \left\{y = -t_1t_3 - t_1^{-1}t_3^{-1}, z = -t_1t_3x - t_1t_4 - t_1t_4^{-1} - t_2t_3 - t_2^{-1}t_3\right\},\\ \mathbf{P}_{(-1,0,-1,0)} &= \left\{y = -t_1t_3 - t_1^{-1}t_3^{-1}, z = -t_1^{-1}t_3^{-1}x - t_1^{-1}t_4 - t_1^{-1}t_4^{-1} - t_2t_3^{-1} - t_2^{-1}t_3^{-1}\right\},\\ \mathbf{P}_{(-1,0,1,0)} &= \left\{y = -t_1^{-1}t_3 - t_1t_3^{-1}, z = -t_1^{-1}t_3x - t_2t_3 - t_2^{-1}t_3 - t_1^{-1}t_4 - t_1^{-1}t_4^{-1}\right\},\\ \mathbf{P}_{(1,0,-1,0)} &= \left\{y = -t_1^{-1}t_3 - t_1t_3^{-1}, z = -t_1t_3^{-1}x - t_1t_4 - t_1t_4^{-1} - t_2t_3^{-1} - t_2^{-1}t_3^{-1}\right\},\\ \mathbf{P}_{(0,1,0,1)} &= \left\{y = -t_2t_4 - t_2^{-1}t_4^{-1}, z = -t_2t_4x - t_2t_3 - t_2t_3^{-1} - t_1t_4 - t_1^{-1}t_4\right\},\\ \mathbf{P}_{(0,-1,0,-1)} &= \left\{y = -t_2t_4 - t_2^{-1}t_4^{-1}, z = -t_2^{-1}t_4^{-1}x - t_2^{-1}t_3 - t_2^{-1}t_3^{-1} - t_1t_4^{-1} - t_1^{-1}t_4^{-1}\right\},\\ \mathbf{P}_{(0,-1,0,1)} &= \left\{y = -t_2^{-1}t_4 - t_2t_4^{-1}, z = -t_2^{-1}t_4x - t_2^{-1}t_3 - t_1t_4 - t_1^{-1}t_4 - t_2^{-1}t_3^{-1}\right\},\\ \mathbf{P}_{(0,1,0,-1)} &= \left\{y = -t_2^{-1}t_4 - t_2t_4^{-1}, z = -t_2t_4^{-1}x - t_1t_4^{-1} - t_2t_3 - t_2t_3^{-1} - t_1^{-1}t_4^{-1}\right\}.\end{aligned} \tag{B.3}$$

Eight lines on the plane where z is constant are denoted by $\mathbf{P}_w$, where $w \in \mathsf{P}(\mathbf{8}_C)$.

$$\begin{aligned}
\mathbf{P}_{(-1,0,0,-1)} &= \left\{z = -t_1t_4 - t_1^{-1}t_4^{-1}, x = -t_1^{-1}t_4^{-1}y - t_1^{-1}t_2 - t_1^{-1}t_2^{-1} - t_3t_4^{-1} - t_3^{-1}t_4^{-1}\right\},\\
\mathbf{P}_{(1,0,0,1)} &= \left\{z = -t_1t_4 - t_1^{-1}t_4^{-1}, x = -t_1t_4y - t_1t_2 - t_1t_2^{-1} - t_3t_4 - t_3^{-1}t_4\right\},\\
\mathbf{P}_{(1,0,0,-1)} &= \left\{z = -t_1^{-1}t_4 - t_1t_4^{-1}, x = -t_1t_4^{-1}y - t_1t_2 - t_1t_2^{-1} - t_3t_4^{-1} - t_3^{-1}t_4^{-1}\right\},\\
\mathbf{P}_{(-1,0,0,1)} &= \left\{z = -t_1^{-1}t_4 - t_1t_4^{-1}, x = -t_1^{-1}t_4y - t_1^{-1}t_2 - t_1^{-1}t_2^{-1} - t_3t_4 - t_3^{-1}t_4\right\},\\
\mathbf{P}_{(0,-1,-1,0)} &= \left\{z = -t_2t_3 - t_2^{-1}t_3^{-1}, x = -t_2^{-1}t_3^{-1}y - t_1t_2^{-1} - t_1^{-1}t_2^{-1} - t_3^{-1}t_4 - t_3^{-1}t_4^{-1}\right\},\\
\mathbf{P}_{(0,1,1,0)} &= \left\{z = -t_2t_3 - t_2^{-1}t_3^{-1}, x = -t_2t_3y - t_1t_2 - t_1^{-1}t_2 - t_3t_4 - t_3t_4^{-1}\right\}\\
\mathbf{P}_{(0,1,-1,0)} &= \left\{z = -t_2^{-1}t_3 - t_2t_3^{-1}, x = -t_2t_3^{-1}y - t_1t_2 - t_1^{-1}t_2 - t_3^{-1}t_4 - t_3^{-1}t_4^{-1}\right\},\\
\mathbf{P}_{(0,-1,1,0)} &= \left\{z = -t_2^{-1}t_3 - t_2t_3^{-1}, x = -t_2^{-1}t_3y - t_1t_2^{-1} - t_1^{-1}t_2^{-1} - t_3t_4 - t_3t_4^{-1}\right\}
\end{aligned} \tag{B.4}$$

Appendix C

Chamber structures

In this Appendix, we provide a detailed analysis of the chamber structure for the volumes of the irreducible components in the global nilpotent cone, as discussed in §3.2.4. Thanks to the periodicity of the parameters $\alpha_j \to \alpha_j + 1$ and the Weyl group symmetry $\alpha_j \to -\alpha_j$ of the cubic equation, we can restrict the parameter space to the 4-dimensional unit cube:

$$\mathsf{Cube} = \left\{ (\alpha_1, \alpha_2, \alpha_3, \alpha_4) \mid \alpha_j \in \left[0, \frac{1}{2}\right] \right\} \subset \mathbb{R}^4. \tag{C.1}$$

The walls described in (3.68) divide Cube into 24 distinct chambers. Singularities of all types, as classified in Table 3-2, appear on these walls and at their intersection points. The configurations of $\mathbf{V}$ and $\mathbf{D}_j$ corresponding to different singularities are illustrated in Figure 3-6.

Within each chamber, the volumes of $\mathbf{V}$ and $\mathbf{D}_j$ are linear functions of the parameters α_j. As we move from one chamber to another, crossing a wall, the volume functions exhibit a wall-crossing phenomenon.

We can slice the cube Cube along a fixed value of α_1, resulting in a 3-dimensional sub-cube, as shown in Figure 3-9:

1. Each of the eight vertices of this 3-cube, which corresponds to an edge of Cube, lies entirely in a single chamber (including its boundary). These vertices correspond either to $A_1^{\oplus 3}$ singularities (shown in blue) or A_3 singularities (shown in red).
2. Each line segment in Figure 3-9 represents either an $A_1^{\oplus 2}$ singularity (in blue or black) or an A_2 singularity (in red).
3. Each wall in Figure 3-9 corresponds to an A_1 singularity, where either $\mathbf{V}$ or some $\mathbf{D}_j$ shrinks to a point. The positions of these walls are summarized in Table C-1 and are explicitly illustrated in Figure C-2.

At special values of α_1, $A_1^{\oplus 4}$ or D_4 singularities may appear, as shown in Figure C-1.

At the origin, where $\alpha_j = 0$ for all $j = 1, 2, 3, 4$, the cubic surface exhibits a D_4 singularity. At this point, $\mathbf{V}$ and three of the $\mathbf{D}_j$'s vanish, as shown in the bottom-right

A_1 singularities	Positions of A_1 walls
$\mathrm{vol}_I(\mathbf{D_1}) = 0$	$BCHLIF$, BCQ, CHR, HLV, LIS, IFT, FBP
$\mathrm{vol}_I(\mathbf{D_2}) = 0$	$CDEIJG$, CDR, DEO, EIS, IJT, JGU, GCQ
$\mathrm{vol}_I(\mathbf{D_3}) = 0$	$ABGKLE$, ABP, BGQ, GKU, KLV, LES, EAO
$\mathrm{vol}_I(\mathbf{D_4}) = 0$	$ADHKJF$, ADO, DHR, HKV, KJU, JFT, FAP
$\mathrm{vol}_I(\mathbf{V}) = 0$	$ABCD, AEIF, BFJG, CGKH, DELH, IJKL, ADE, BCG, IJF, HKL$

Table C-1 Positions of A_1 walls in Figure 3-9 when either $\mathbf{V}$ or one of $\mathbf{D}_j$ shrinks to a point.

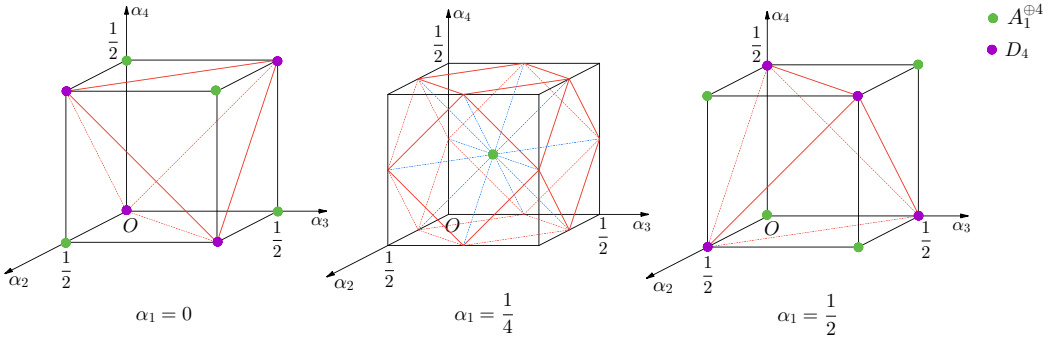

Figure C-1 3-cube cross sections of Cube at $\alpha_1 = 0, \frac{1}{4}, \frac{1}{2}$. The $A_1^{\oplus 4}$ and D_4 singularities are marked out, which show up only for these special values of α_1.

Chambers	vertices contained	$\mathrm{vol}_I(\mathbf{D}_j)$	$\mathrm{vol}_I(\mathbf{V})$
$OADE$	$(0,0,0)$	$(1-2\alpha_1, 2\alpha_2, 2\alpha_3, 2\alpha_4)$	$\alpha_1-\alpha_2-\alpha_3-\alpha_4$
$PABF$	$(1,0,0)$	$(1-2\alpha_2, 2\alpha_1, 2\alpha_4, 2\alpha_3)$	$-\alpha_1+\alpha_2-\alpha_3-\alpha_4$
$RCDH$	$(0,1,0)$	$(1-2\alpha_3, 2\alpha_4, 2\alpha_1, 2\alpha_2)$	$-\alpha_1-\alpha_2+\alpha_3-\alpha_4$
$SEIL$	$(0,0,1)$	$(1-2\alpha_4, 2\alpha_3, 2\alpha_2, 2\alpha_1)$	$-\alpha_1-\alpha_2-\alpha_3+\alpha_4$
$QBCG$	$(1,1,0)$	$(2\alpha_4, 1-2\alpha_3, 1-2\alpha_2, 2\alpha_1)$	$-\frac{1}{2}-\alpha_1+\alpha_2+\alpha_3-\alpha_4$
$TFIJ$	$(1,0,1)$	$(2\alpha_3, 1-2\alpha_4, 2\alpha_1, 1-2\alpha_2)$	$-\frac{1}{2}-\alpha_1+\alpha_2-\alpha_3+\alpha_4$
$VHKL$	$(0,1,1)$	$(2\alpha_2, 2\alpha_1, 1-2\alpha_4, 1-2\alpha_3)$	$-\frac{1}{2}-\alpha_1-\alpha_2+\alpha_3+\alpha_4$
$UGJK$	$(1,1,1)$	$(2\alpha_1, 1-2\alpha_2, 1-2\alpha_3, 1-2\alpha_4)$	$-1-\alpha_1+\alpha_2+\alpha_3+\alpha_4$

Table C-2 Volume functions at 8 chambers containing the 3-cube vertices. The first column lists the chambers in Figure 3-9. The second column lists the 3-cube vertices contained in each chamber.

case of Figure 3-6. In Cube, the origin lies at the boundary of 12 chambers simultaneously, four of which contain the α_j-axes. The chamber that contains the α_1-axis is the tetrahedral chamber $OADE$ in the 3-cube shown in Figure 3-9.

We label the four $\mathbf{D}_j$'s as $j = 1, 2, 3, 4$, and in this chamber, the volumes are given by:

$$\mathrm{vol}_I(\mathbf{D}_j) = \left(1-2\alpha_1, 2\alpha_2, 2\alpha_3, 2\alpha_4\right), \quad \mathrm{vol}_I(\mathbf{V}) = \alpha_1-\alpha_2-\alpha_3-\alpha_4. \tag{C.2}$$

In this convention, the volume functions for the 8 chambers $OADE$, $PABF$, $RCDH$, $SEIL$, $QBCG$, $TFIJ$, $VHKL$, and $UGJK$ in the 3-cube are listed in Table C-2.

There are 16 additional chambers, which we call the internal chambers. The volume functions for these chambers are uniformly expressed as

$$\begin{aligned}\mathrm{vol}_I(\mathbf{D}_j) = \Big(&\left|-1+\alpha_1+\alpha_2+\alpha_3+\alpha_4\right|, \left|\alpha_1+\alpha_2-\alpha_3-\alpha_4\right|, \\ &\left|\alpha_1-\alpha_2+\alpha_3-\alpha_4\right|, \left|\alpha_1-\alpha_2-\alpha_3+\alpha_4\right| \Big), \\ \mathrm{vol}_I(\mathbf{V}) = \frac{1}{2}&\left(1-\sum_{j=1}^{4}\mathrm{vol}_I(\mathbf{D}_j)\right).\end{aligned} \tag{C.3}$$

In these 16 chambers, the expressions in the absolute values in (C.3) take different combinations of signs. Since there are four parameters α_j, there are $2^4 = 16$ possible sign combinations, each corresponding to one of the 16 chambers. The specific sign combinations and the corresponding volumes of $\mathbf{V}$ are explicitly listed in Table C-3.

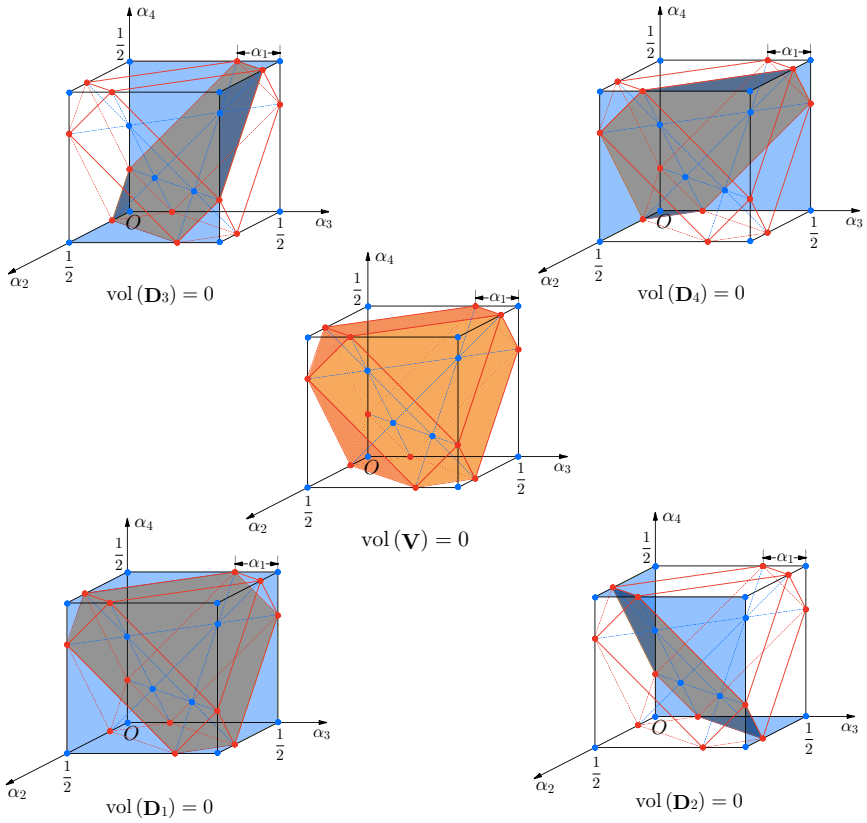

Figure C-2 A_1 singularities can show up in 5 cases where either $\mathbf{V}$ or one $\mathbf{D}_j$ shrinks to a point. They correspond to the planes inside the 3-cube in Figure 3-9 as summarized in Table C-1.

Chambers	signs	$\mathrm{vol}_I(\mathbf{V})$	Chambers	signs	$\mathrm{vol}_I(\mathbf{V})$
$WXYZ-$	$(---\!-)$	$2\alpha_1$	$WXYZ+$	$(+++\!+)$	$1-2\alpha_1$
$WDEXHL$	$(--++)$	$2\alpha_2$	$ZBGYFJ$	$(++--)$	$1-2\alpha_2$
$WAEYFI$	$(-+-\!+)$	$2\alpha_3$	$ZCGXHK$	$(+-+\!-)$	$1-2\alpha_3$
$WADZBC$	$(-++\!-)$	$2\alpha_4$	$XKLYJI$	$(+--\!+)$	$1-2\alpha_4$
$XYZKJG$	$(+---)$	$1+\alpha_1-\alpha_2-\alpha_3-\alpha_4$	$WADE$	$(-+++)$	$-\alpha_1+\alpha_2+\alpha_3+\alpha_4$
$WYZAFB$	$(-+--)$	$\alpha_1-\alpha_2+\alpha_3+\alpha_4$	$XHKL$	$(+-++)$	$1-\alpha_1+\alpha_2-\alpha_3-\alpha_4$
$WXZDHC$	$(--+-)$	$\alpha_1+\alpha_2-\alpha_3+\alpha_4$	$YFIJ$	$(++-\!+)$	$1-\alpha_1-\alpha_2+\alpha_3-\alpha_4$
$WXYELI$	$(---\!+)$	$\alpha_1+\alpha_2+\alpha_3-\alpha_4$	$ZBCG$	$(+++\!-)$	$1-\alpha_1-\alpha_2-\alpha_3+\alpha_4$

Table C-3 Volume functions at 16 internal chambers. The first and fourth columns list the chambers in Figure 3-9. In particular $WXYZ-$ and $WXYZ+$ are the center chambers when $\alpha_1 < \frac{1}{4}$ and $\alpha_1 > \frac{1}{4}$ respectively. The second and fifth columns list the signs of the expressions in the absolute values in (C.3).

There are two conditions, given by (4.37) and (4.38), under which we reach the A_1 limit of the DAHA. The loci of these points in Cube are shown in Figure C-3.

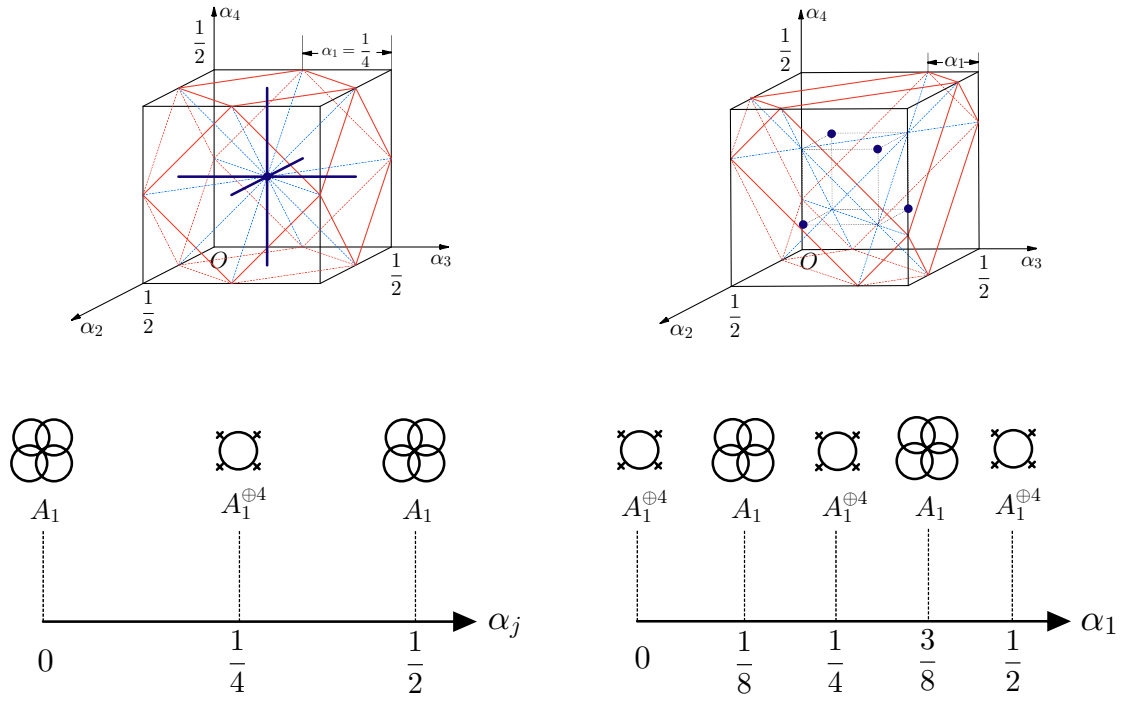

Figure C-3 There are four lines satisfying the first A_1 limit condition (4.37) in Cube, along whom three of α_j equal $\frac{1}{2}$ and the remaining α is the direction this line extends along. Three of these lines are visible in the 3-cube when $\alpha_1 = \frac{1}{4}$, as drawn in dark blue in the top left figure. The remaining line is the trajectory of the center point $(\alpha_1, \frac{1}{4}, \frac{1}{4}, \frac{1}{4})$ propagating along α_1 direction in Cube. There are again four lines satisfying the second A_1 limit condition (4.38). Along three of these lines, three of α_j equals α_1 and the remaining one $\frac{1}{2} - \alpha_1$. Along the remaining line, all α_j equal $\frac{1}{2} - \alpha_1$ except α_1 itself. They are drawn on the top right, and there are four distinct points whose trajectories along α_1 are these lines. The du Val singularities along each of the 8 lines are drawn out in the bottom figures.

Appendix D

Winding cycles and Argyres-Douglas surface

In this Appendix, we provide a detailed analysis of the monodromies associated with singular fibers and demonstrate the existence of 2-cycles that wind around these fibers. Furthermore, we pinpoint the locations of Argyres-Douglas points, which arise from the collisions of singular fibers containing mutually non-local degrees of freedom. As a result, we reveal that the Argyres-Douglas surfaces introduce a non-trivial monodromy to the γ space. This insight explains why the winding cycles are homologous to the straight ones.

D.1 Winding cycles

As discussed in §3.2.3, in addition to the 2-cycles depicted in Figure 3-17 (referred to as *straight cycles* in the following), there exist additional cycles that wind around singular fibers.

To demonstrate their existence, we begin by examining how the monodromies evolve when two I_1 fibers rotate around each other. Consider two singular fibers labeled 1 and 2, with monodromies M_1 and M_2, as shown in Figure D-1. After successive rotations of π,

$$\begin{aligned} M_1 &\xrightarrow{\pi} M_2 M_1 M_2^{-1} \xrightarrow{\pi} (M_1M_2)M_1(M_1M_2)^{-1} \xrightarrow{\pi} (M_2M_1M_2)M_1(M_2M_1M_2)^{-1} \to \cdots, \\ M_2 &\xrightarrow{\pi} M_2 M_2 M_2^{-1} \xrightarrow{\pi} (M_1M_2)M_2(M_1M_2)^{-1} \xrightarrow{\pi} (M_2M_1M_2)M_2(M_2M_1M_2)^{-1} \to \cdots. \end{aligned} \tag{D.1}$$

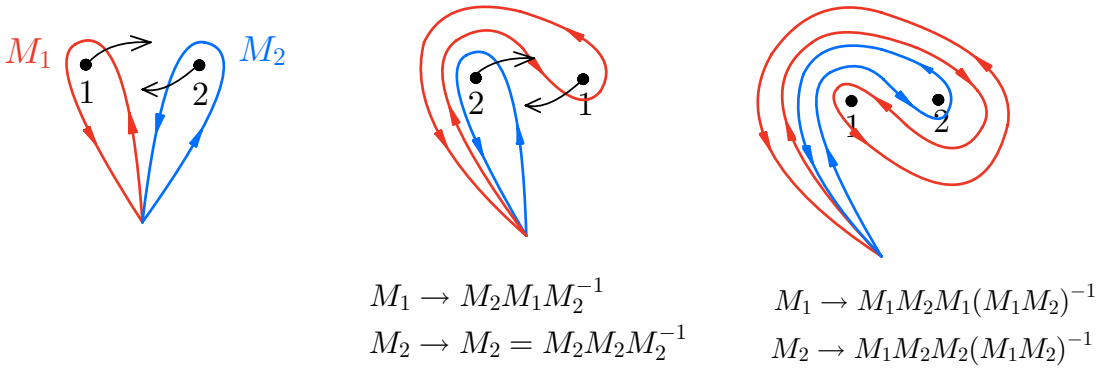

Figure D-1 Rotate two singular fibers with monodromies M_1 and M_2 respectively. Every π rotation conjugates both monodromies and M_i. When $M_1 = M_2$, monodromies are unchanged and when $M_1 = M_q, M_2 = M_d$, monodromies behave as (D.2).

When $M_1 = M_2$ equals M_q or M_d defined above (3.50), the monodromies are unaltered under any rotation. However, this invariance does not hold when $M_1 = M_q$ and $M_2 = M_d$. A straightforward calculation shows that the resulting monodromies evolve as follows:

$$\begin{aligned} M_q &\xrightarrow{3\pi} M_d \xrightarrow{3\pi} M_q, \\ M_d &\xrightarrow{3\pi} M_q \xrightarrow{3\pi} M_d. \end{aligned} \tag{D.2}$$

This demonstrates that after a 3π rotation, the monodromy matrices of the two fibers are exchanged. Following another 3π rotation, their monodromy matrices return to their original values.

Let us now examine the implications of this property for the second homology. Recall that a suspended cycle is constructed as the result of a deformation process between two singular fibers of the same type, i.e., fibers with identical monodromy matrices, in a fixed frame.

Consider two singular fibers located at p_i and p_j, and assume their monodromy matrices are identical. In this case, there exists a straight suspended cycle, denoted $\mathbf{W}$, connecting these two fibers. Now, suppose there is an additional singular fiber at p_k nearby. If the monodromy matrix around p_k equals those around p_i and p_j, the deformation process between p_i and p_j can wind around p_k an arbitrary number $n \in \mathbb{Z}$ of times, since rotations involving p_k do not alter the monodromies. Consequently, we can construct a cycle suspended between p_i and p_j that winds around p_k for n times. Extending this idea, we can construct cycles suspended between any pair of the three singular fibers while winding around the third. However, these winding cycles can always be decomposed into straight cycles suspended between the fibers.

On the other hand, if the monodromy matrix around p_k is distinct from those around p_i and p_j, the 6π periodicity described in (D.2) implies that the deformation process between p_i and p_j can wind around p_k an additional $3n$ times, where $n \in \mathbb{Z}$. This results in the construction of a new cycle, $\mathbf{W}'$, suspended between p_i and p_j and winding p_k $3n$ times more than $\mathbf{W}$, as illustrated by the red cycle in Figure D-2. Similarly, by the 3π exchange in (D.2), we can construct another cycle, $\mathbf{W}''$, suspended between p_j and p_k, shown as the blue cycle in Figure D-2.

Unlike the previous case, these winding cycles cannot be directly decomposed into straight cycles. However, as we will demonstrate later, these cycles are homologous to the straight cycles by going around the Argyres-Douglas surfaces in the parameter space.

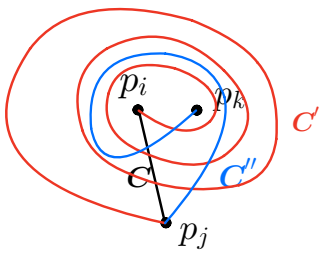

Figure D-2 For every cycle suspended between p_i and p_j, if there is a nearby singular fiber p_k of a distinct type, it is possible to construct cycles suspended between p_i and p_j that wind around p_k $3n$ times for any $n \in \mathbb{Z}$. For instance, one such cycle is $\mathbf{W}'$, where $n = -1$. Additionally, there exists another cycle, $\mathbf{W}''$, suspended between p_j and p_k, which winds around p_i .

D.2 Argyres-Douglas types of singular fibers

When two I_1 fibers of distinct types, i.e., with distinct monodromies, collide into a single fiber, no new fiber cycle is generated, as there is no straight suspended cycle between them. We refer to this type of collision as the Argyres-Douglas (AD) collision. This terminology reflects the fact that distinct types of I_1 fibers correspond to mutually non-local massless degrees of freedom, and their collision leads to the Argyres-Douglas SCFT discovered in[68–69].

This phenomenon can be verified by analyzing the Weierstrass form of the Seiberg-Witten curve at the collision points, which takes the form

$$y^2 = (x - x_0(\tau))^3, \tag{D.3}$$

for some τ-dependent x_0.

The Kodaira type of the resulting AD singular fiber can be determined by computing the product of the monodromy matrices associated with the colliding fibers. Choosing the frame as described in §3.2.3, let the monodromy matrices around the two I_1 fibers be M_q and M_d, respectively. The monodromy of the resulting singular fiber is given by[①]

$$M_d \cdot M_q = \begin{pmatrix} -1 & 3 \\ -1 & 2 \end{pmatrix} \sim \begin{pmatrix} 1 & 1 \\ -1 & 0 \end{pmatrix}, \tag{D.4}$$

which is the monodromy matrix associated with fibers of Kodaira type II. Geometrically, the M_q fibers are tori with $(0,1)$-cycles shrinking to a point, while M_d fibers are tori with $(1,-2)$-cycles shrinking to a point. The collision of an M_q fiber and an M_d fiber is shown at the bottom of Figure 3-3.

Physically, the resulting AD singular fiber corresponds to the (A_1, A_2) Argyres-Douglas theory, as both a quark and a dyon become massless simultaneously. A similar analysis can be carried out for other collisions, such as when an I_2 or I_3 fiber collides with a dyon I_1 fiber. These collisions result in singular fibers of Kodaira types III and IV, respectively, corresponding to the (A_1, A_3) and (A_1, D_4) Argyres-Douglas theories. The possibilities of AD-type collisions are summarized as the red arrows in Figure 3-4. As noted in[68], there are no higher-level Argyres-Douglas theories in the Coulomb branch moduli space of SU(2) $N_f = 4$ SQCD.

The conditions for the appearance of AD-type singular fibers are more complicated than those for the usual I_k-type or I_0^*-type fibers. In addition to tuning the mass parameters, the complex coupling τ must also be carefully adjusted. These conditions can be determined by solving (D.3) directly. The generic Seiberg-Witten curve is given by (3.7). By equating (D.3) with this generic form and eliminating x_0, one can derive two complex equations involving the u parameter.

$$\begin{aligned} 9B\tilde{u}^2 + 12A(\gamma_1^2+\gamma_2^2+\gamma_3^2+\gamma_4^2)\tilde{u} + 16B^2(\gamma_1^4+\gamma_2^4+\gamma_3^4+\gamma_4^4) \\ + 16C(-\vartheta_3^4, \vartheta_4^4)(\gamma_1^2\gamma_2^2+\gamma_3^2\gamma_4^2) + 16C(\vartheta_2^4, -\vartheta_3^4)(\gamma_1^2\gamma_3^2+\gamma_2^2\gamma_4^2) \\ + 16C(\vartheta_4^4, \vartheta_2^4)(\gamma_1^2\gamma_4^2+\gamma_2^2\gamma_3^2) = 0, \end{aligned}$$

① The singular type of the resulting fiber is independent of the order of the matrix product.

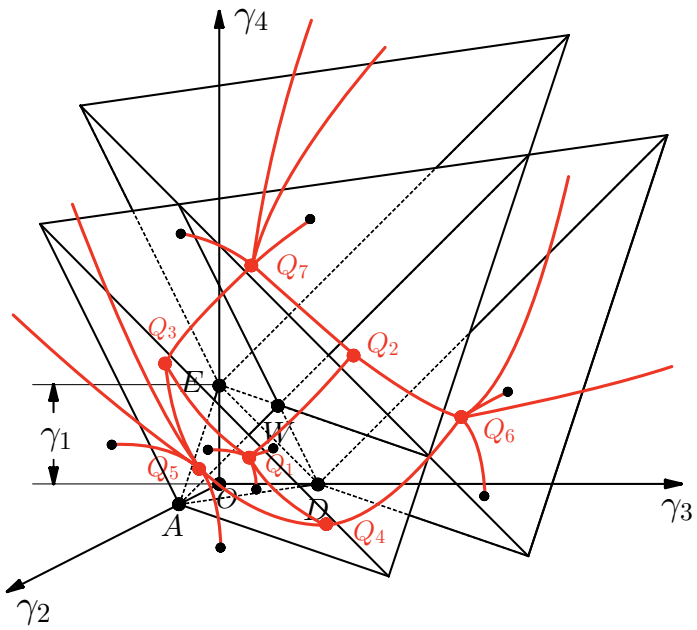

Figure D-3 The structure of the γ-space is visualized by taking a section along a fixed value of γ_1. By the black lines, we draw the walls in γ-space where normal collisions occur, such as ΔADE and ΔWDE, as determined by the conditions in Table 3-3. The red curves correspond to Argyres-Douglas (AD) surfaces, which are codimension-2 surfaces defined by solving equation (D.5). Points along these red curves correspond to (A_1, A_2) AD theories, while the vertex points labeled Q_1 to Q_7 represent (A_1, A_3) AD theories. The numerical visualization of these AD surfaces is shown in Figure D-4.

$$
\begin{aligned}
27A\tilde{u}^3 - 144\Big(&AB(\gamma_1^4+\gamma_2^4+\gamma_3^4+\gamma_4^4) + D(-\vartheta_3^4,\vartheta_4^4)(\gamma_1^2\gamma_2^2+\gamma_3^2\gamma_4^2)\\
&+ D(\vartheta_2^4,-\vartheta_3^4)(\gamma_1^2\gamma_3^2+\gamma_2^2\gamma_4^2) + D(\vartheta_4^4,\vartheta_2^4)(\gamma_1^2\gamma_4^2+\gamma_2^2\gamma_3^2)\Big)\tilde{u}\\
&+ 64A^2\left(\gamma_1^6+\gamma_2^6+\gamma_3^6+\gamma_4^6\right) - 512B^3\left(\gamma_1^2+\gamma_2^2+\gamma_3^2+\gamma_4^2\right)^3\\
&- 192F\left(\gamma_1^2\gamma_2^2\left(\gamma_3^2+\gamma_4^2\right)+\gamma_3^2\gamma_4^2\left(\gamma_1^2+\gamma_2^2\right)\right)\\
&+ 192E(-\vartheta_3^4,\vartheta_4^4)\left(\gamma_1^2\gamma_2^2\left(\gamma_1^2+\gamma_2^2\right)+\gamma_3^2\gamma_4^2\left(\gamma_3^2+\gamma_4^2\right)\right)\\
&+ 192E(\vartheta_2^4,-\vartheta_3^4)\left(\gamma_1^2\gamma_3^2\left(\gamma_1^2+\gamma_3^2\right)+\gamma_2^2\gamma_4^2\left(\gamma_2^2+\gamma_4^2\right)\right)\\
&+ 192E(\vartheta_4^4,\vartheta_2^4)\left(\gamma_1^2\gamma_4^2\left(\gamma_1^2+\gamma_4^2\right)+\gamma_2^2\gamma_3^2\left(\gamma_2^2+\gamma_3^2\right)\right) = 0,
\end{aligned}
\tag{D.5}
$$

with

$$
\begin{aligned}
\tilde{u} &= u - \frac{2}{3}\vartheta_2^4(\gamma_1^2+\gamma_2^2+\gamma_3^2+\gamma_4^2),\\
A &= \left[(-\vartheta_3^4)-\vartheta_4^4\right]\left[\vartheta_2^4-(-\vartheta_3^4)\right]\left[\vartheta_2^4-\vartheta_4^4\right],\\
B &= \vartheta_2^8-\vartheta_2^4\vartheta_3^4+\vartheta_3^8,\\
C(a,b) &= 2a^4+31a^3b+60a^2b^2+31ab^3+2b^4,\\
D(a,b) &= (a-b)(4a^4-13a^3b-36a^2b^2-13ab^3+4b^4),\\
E(a,b) &= (a-b)^2(4a^4-7a^3b-21a^2b^2-7ab^3+4b^4),\\
F &= -8\vartheta_2^{24}+24\vartheta_3^4\vartheta_2^{20}+249\vartheta_3^8\vartheta_2^{16}-538\vartheta_3^{12}\vartheta_2^{12}\\
&\quad+249\vartheta_3^{16}\vartheta_2^8+24\vartheta_3^{20}\vartheta_2^4-8\vartheta_3^{24},
\end{aligned}
\tag{D.6}
$$

where a and b are arbitrary expressions, and $\vartheta_i = \vartheta_i(\tau)$ are Jacobi theta functions given by (3.6). By eliminating the u parameter, one can obtain a single complex equation,

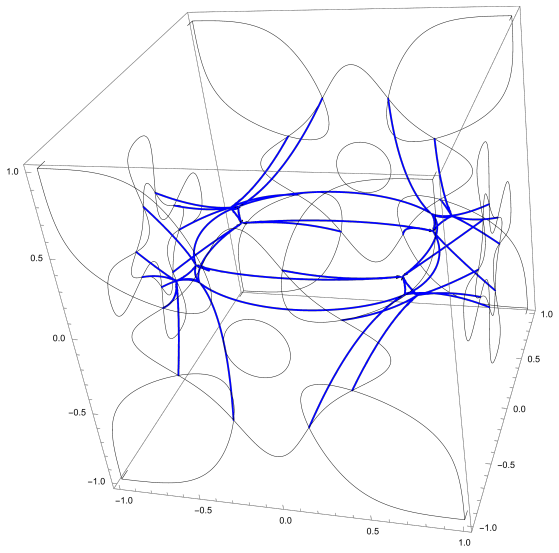

Figure D-4 The Argyres-Douglas surfaces, as plotted by Mathematica, correspond to the case where $q = 0.001i$ and $\gamma_1 = \frac{1}{2}$.

which corresponds to two real equations that constrain γ_j. These equations involve theta functions of τ as their coefficients. Therefore, the loci where AD-type fibers appear form codimension-2 surfaces in the γ space, which vary with τ. We refer to these surfaces as the Argyres-Douglas surfaces, as illustrated in Figure D-3 and numerically plotted in D-4.

In addition to the codimension-2 Argyres-Douglas surfaces, there are codimension-1 walls determined by normal collisions, similar to those in Figure 3-9. The conditions for these normal collisions are precisely the conditions for the appearance of I_k-type or I_0^*-type singular fibers, as listed in Table 3-3. These conditions define the codimension-1 walls in the γ space, as illustrated in Figure D-3.

However, unlike the walls in Figure 3-9, there is no periodicity for the γ parameters. As a result, the wall-crossings form the Weyl group $W(D_4)$ of the usual D_4 algebra, rather than the affine one.

Similar to the I_0^* case, the Picard-Lefschetz transformation occurs when passing through a normal collision wall. For example, starting with a length assignment on the left side of Figure 3-17, if we tune $\gamma_1 - \gamma_2 - \gamma_3 - \gamma_4$ from positive to negative, all the cycles will change according to the PL transformation rule described in (3.72). As a result, the length assignment will transform to the configuration shown on the right side of Figure 3-17.

In each chamber, there are three components of Argyres-Douglas (AD) surfaces where (A_1, A_2) AD theories appear. These three surfaces intersect simultaneously at one of the walls of the chamber, such as the Q_1 point on the ADE wall, where the (A_1, A_3) AD theory appears. By tuning the τ parameter appropriately, the intersection points Q_i can situate at the intersection of two walls, leading to the appearance of the (A_1, D_4) AD theory.

Monodromies around Argyres-Douglas surfaces

Finally, we observe an interesting phenomenon: the Argyres-Douglas (AD) surfaces endow the γ space with non-trivial monodromies. When the parameter point lies on an

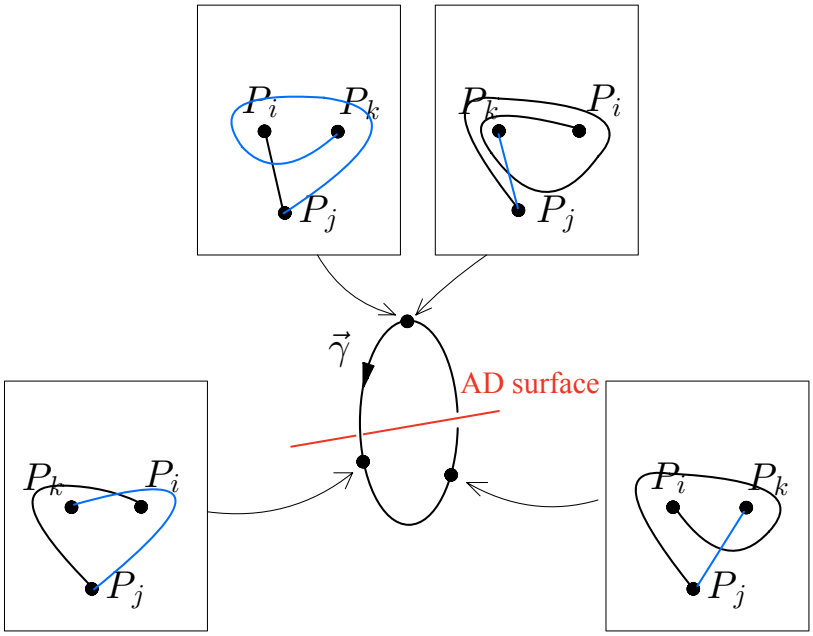

Figure D-5 In the γ space, monodromy around AD-surface colliding p_i and p_k will produce a 3π rotation between p_i and p_k. Therefore, the straight cycle between p_i and p_j will wind around p_k, while the winding cycle between p_j and p_k will be straightened.

AD surface, two I_1 fibers of different types collide. If the parameter point is slightly displaced from the AD surface and goes around a loop linking this AD surface, it is observed that the two I_1 fibers will rotate 3π times around each other, as shown in Figure D-5. This results in a continuous exchange of the types and positions of the two fibers.

An immediate consequence is that we can rotate the fibers p_i and p_k in Figure D-2 by going two rounds around an AD surface in the γ space. This allows the cycle $\mathbf{W}'$ to be continuously deformed into $\mathbf{W}$. In this way, every winding cycle can be deformed into, and thus be homologous to, a straight cycle as shown in Figure 3-17.

Bibliography

[1] SOURIAU J M. Quantification géométrique. Applications[J/OL]. Annales De L Institut Henri Poincare-physique Theorique, 1967, 6: 311–341. https://api.semanticscholar.org/CorpusID:125989107.

[2] SOURIAU J M. Structure des systèmes dynamiques : maîtrises de mathématiques[C/OL]//. 1970. https://api.semanticscholar.org/CorpusID:117064099.

[3] BAYEN F, FLATO M, FRONSDAL C, et al. Deformation Theory and Quantization. 1. Deformations of Symplectic Structures[J]. Annals Phys., 1978, 111: 61. DOI: 10.1016/0003-4916(78)90224-5.

[4] KONTSEVICH M. Deformation quantization of Poisson manifolds[J]. Letters in Mathematical Physics, 2003, 66(3): 157–216. arXiv: q-alg/9709040. DOI: 10.1023/B:MATH.0000027508.00421.bf.

[5] GUKOV S, WITTEN E. Branes and Quantization[J]. Adv. Theor. Math. Phys., 2009, 13: 1. arXiv: 0809.0305 [hep-th]. DOI: 10.4310/ATMP.2009.v13.n5.a5.

[6] GUKOV S, KOROTEEV P, NAWATA S, et al. Branes and DAHA Representations[J]. SpringerBriefs in Mathematical Physics, 2023. arXiv: 2206.03565 [hep-th].

[7] SEIBERG N, WITTEN E. Electric-magnetic duality, monopole condensation, and confinement in N=2 supersymmetric Yang-Mills theory[J]. Nucl. Phys. B, 1994, 426: 19–52. arXiv: hep-th/9407087. DOI: 10.1016/0550-3213(94)90124-4.

[8] SEIBERG N, WITTEN E. Monopoles, duality and chiral symmetry breaking in N=2 supersymmetric QCD[J]. Nucl. Phys., 1994, B431: 484–550. arXiv: hep-th/9408099. DOI: 10.1016/0550-3213(94)90214-3.

[9] HITCHIN N. The self-duality equations on a Riemann surface[J]. Proc. London Math. Soc., 1987, 55(1): 59–126. DOI: 10.1112/plms/s3-55.1.59.

[10] OBLOMKOV A. Double affine Hecke algebras of rank 1 and affine cubic surfaces[J]. International Mathematics Research Notices, 2004, 2004(18): 877–912. arXiv: math/0306393 [math.RT]. DOI: 10.1155/S10737928041330072.

[11] KOSTANT B. Line bundles and the prequantized Schrödinger equation[R]. 1972.

[12] BATES S, WEINSTEIN A. Lectures on the geometry of quantization[M]. 1997.

[13] DEREZIŃSKI J, GÉRARD C. Mathematics of Quantization and Quantum Fields[M]. Oxford University Press, 2013. DOI: 10.1017/9781009290876.

[14] CAROSSO A. Geometric Quantization[J]. 2018. arXiv: 1801.02307 [math-ph].

[15] NAIR V P. Elements of Geometric Quantization and Applications to Fields and Fluids[J]. 2016. arXiv: 1606.06407 [hep-th].

[16] KOSTANT B. Quantization and unitary representations[C/OL]//. 1970. https://api.semanticscholar.org/CorpusID:115918831.

[17] WITTEN E. Topological Sigma Models[J]. Commun. Math. Phys., 1988, 118: 411. DOI: 10.1007/BF01466725.

[18] VONK M. A Mini-course on topological strings[J]. 2005. arXiv: hep-th/0504147.

[19] WITTEN E. Topological Quantum Field Theory[J]. Commun.Math.Phys., 1988, 117: 353. DOI: 10.1007/BF01223371.

[20] HORI K, KATZ S, KLEMM A, et al. Mirror symmetry[J]. 2003.

[21] KAPUSTIN A, WITTEN E. Electric-Magnetic Duality And The Geometric Langlands Program[J]. Communications in Number Theory and Physics, 2007, 1: 1–236. arXiv: 0604151 [hep-th]. DOI: 10.4310/CNTP.2007.v1.n1.a1.

[22] ALDI M, ZASLOW E. Coisotropic branes, noncommutativity, and the mirror correspondence[J]. Journal of High Energy Physics, 2005, 2005(06): 019.

[23] DONAGI R, WITTEN E. Supersymmetric Yang-Mills theory and integrable systems[J]. Nucl.Phys., 1996, B460: 299–334. eprint: hep-th/9510101 (hep-th). DOI: 10.1016/0550-3213(95)00609-5.

[24] GORSKY A, KRICHEVER I, MARSHAKOV A, et al. Integrability and Seiberg-Witten exact solution[J]. Phys.Lett., 1995, B355: 466–474. arXiv: hep-th/9505035 [hep-th]. DOI: 10.1016/0370-2693(95)00723-X.

[25] WITTEN E. Solutions of four-dimensional field theories via M-theory[J]. Nucl.Phys., 1997, B500: 3–42. arXiv: hep-th/9703166 [hep-th]. DOI: 10.1016/S0550-3213(97)00416-1.

[26] GUKOV S, WITTEN E. Gauge Theory, Ramification, And The Geometric Langlands Program[J]. Current Developments in Mathematics, 2008, 2006: 35–180. eprint: hep-th/0612073 (hep-th).

[27] GAIOTTO D. N=2 dualities[J]. JHEP, 2012, 08: 034. arXiv: 0904.2715 [hep-th]. DOI: 10.1007/JHEP08(2012)034.

[28] GAIOTTO D, MOORE G W, NEITZKE A. Wall-crossing, Hitchin Systems, and the WKB Approximation[J]. Advances in Mathematics, 2013, 234: 239–403. arXiv: 0907.3987 [hep-th].

[29] GAIOTTO D, MOORE G W, NEITZKE A. Framed BPS States[J]. Adv. Theor. Math. Phys., 2013, 17(2): 241–397. arXiv: 1006.0146 [hep-th]. DOI: 10.4310/ATMP.2013.v17.n2.a1.

[30] SIMPSON C T. Harmonic bundles on noncompact curves[J]. Journal of the American Mathematical Society, 1990, 3(3): 713–770.

[31] NEKRASOV N A. Seiberg-Witten prepotential from instanton counting[J]. Adv.Theor.Math.Phys., 2004, 7: 831–864. arXiv: hep-th/0206161 [hep-th].

[32] ALDAY L F, GAIOTTO D, TACHIKAWA Y. Liouville Correlation Functions from Four-dimensional Gauge Theories[J]. Lett. Math. Phys., 2010, 91: 167–197. arXiv: 0906.3219 [hep-th]. DOI: 10.1007/s11005-010-0369-5.

[33] YOSHIDA Y. Quantized Coulomb branch of 4d $\mathcal{N} = 2$ $Sp(N)$ gauge theory and spherical DAHA of $(C_N^\vee, C_N)$-type[J].

[34] TACHIKAWA Y. Magnetic discrete gauge field in the confining vacua and the supersymmetric index[J]. JHEP, 2015, 03: 035. arXiv: 1412.2830 [hep-th]. DOI: 10.1007/JHEP03(2015)035.

[35] MIKHAILOV A. BPS states and minimal surfaces[J]. Nucl. Phys. B, 1998, 533: 243–274. arXiv: hep-th/9708068. DOI: 10.1016/S0550-3213(98)00524-0.

[36] ALDAY L F, GAIOTTO D, GUKOV S, et al. Loop and surface operators in N=2 gauge theory and Liouville modular geometry[J]. JHEP, 2010, 1001: 113. arXiv: 0909.0945 [hep-th]. DOI: 10.1007/JHEP01(2010)113.

[37] DRUKKER N, GOMIS J, OKUDA T, et al. Gauge Theory Loop Operators and Liouville Theory[J]. JHEP, 2010, 1002: 057. arXiv: 0909.1105 [hep-th].

[38] DONALDSON S K. Twisted harmonic maps and the self-duality equations [J/OL]. Proceedings of The London Mathematical Society, 1987, 55: 127–131. https://api.semanticscholar.org/CorpusID:119814357.

[39] CORLETTE K. Flat G-bundles with canonical metrics[J/OL]. Journal of Differential Geometry, 1988, 28(3): 361–382. https://doi.org/10.4310/jdg/1214442469. DOI: 10.4310/jdg/1214442469.

[40] BERSHADSKY M, JOHANSEN A, SADOV V, et al. Topological reduction of 4-d SYM to 2-d sigma models[J]. Nucl. Phys. B, 1995, 448: 166–186. arXiv: hep-th/9501096. DOI: 10.1016/0550-3213(95)00242-K.

[41] HARVEY J A, MOORE G W, STROMINGER A. Reducing S duality to T duality[J]. Phys. Rev. D, 1995, 52: 7161–7167. arXiv: hep-th/9501022. DOI: 10.1103/PhysRevD.52.7161.

[42] KAPUSTIN A, ORLOV D. Remarks on A branes, mirror symmetry, and the Fukaya category[J]. J. Geom. Phys., 2003, 48: 84. arXiv: hep-th/0109098. DOI: 10.1016/S0393-0440(03)00026-3.

[43] NEKRASOV N, WITTEN E. The Omega Deformation, Branes, Integrability, and Liouville Theory[J]. JHEP, 2010, 09: 092. arXiv: 1002.0888 [hep-th]. DOI: 10.1007/JHEP09(2010)092.

[44] GOLDMAN W M. Trace coordinates on Fricke spaces of some simple hyperbolic surfaces[C]//Handbook of Teichmüller Theory, Volume II. 2009: 611–684. arXiv: 0901.1404 [math.GT].

[45] ITO Y, OKUDA T, TAKI M. Line operators on $S^1 \times R^3$ and quantization of the Hitchin moduli space[J]. JHEP, 2012, 04: 010. arXiv: 1111.4221 [hep-th]. DOI: 10.1007/JHEP04(2012)010.

[46] YAGI J. Ω-deformation and quantization[J]. JHEP, 2014, 08: 112. arXiv: 1405.6714 [hep-th]. DOI: 10.1007/JHEP08(2014)112.

[47] BULLIMORE M, DIMOFTE T, GAIOTTO D, et al. Boundaries, Mirror Symmetry, and Symplectic Duality in 3d $\mathcal{N} = 4$ Gauge Theory[J]. JHEP, 2016, 10: 108. arXiv: 1603.08382 [hep-th]. DOI: 10.1007/JHEP10(2016)108.

[48] DEDUSHENKO M, FAN Y, PUFU S S, et al. Coulomb Branch Quantization and Abelianized Monopole Bubbling[J]. JHEP, 2019, 10: 179. arXiv: 1812.08788 [hep-th]. DOI: 10.1007/JHEP10(2019)179.

[49] OKUDA T, YOSHIDA Y. SUSY localization for Coulomb branch operators in omega-deformed 3d N=4 gauge theories[J]. 2019. arXiv: 1910.01802 [hep-th].

[50] CIRAFICI M. A note on discrete dynamical systems in theories of class S[J]. JHEP, 2021, 05: 224. arXiv: 2011.12887 [hep-th]. DOI: 10.1007/JHEP05(2021)224.

[51] TURAEV V G. Skein quantization of Poisson algebras of loops on surfaces[J]. Annales scientifiques de l'Ecole normale supérieure, 1991, 24(6): 635–704.

[52] PRZYTYCKI J H. Skein modules of 3-manifolds[J]. Bull. Polish Acad. Sci., 1991, 39: 91–100. arXiv: math/0611797 [math.GT].

[53] BULLOCK D. Rings of $\mathrm{SL}(2,\mathbb{C})$ characters and the Kauffman bracket skein module[J]. Commentarii Mathematici Helvetici, 1997, 72(4): 521–542. arXiv: q-alg/9604014 [math.QA].

[54] PRZYTYCKI J, SIKORA A S. On Skein Algebras And $\mathrm{SL}_2(\mathbb{C})$ Character Varieties[J]. Topology, 2000, 39.1: 115–148. arXiv: q-alg/9705011.

[55] BULLOCK D, PRZYTYCKI J. Multiplicative structure of Kauffman bracket skein module quantizations[J]. Proceedings of the American Mathematical Society, 2000, 128(3): 923–931. arXiv: math/9902117 [math.QA].

[56] BEREST Y, SAMUELSON P. Double affine Hecke algebras and generalized Jones polynomials[J]. Compositio Mathematica, 2016, 152(7): 1333–1384. arXiv: 1402.6032 [math.QA].

[57] BEREST Y, SAMUELSON P. Affine cubic surfaces and character varieties of knots[J]. Journal of Algebra, 2018, 500: 644–690. arXiv: 1610 . 08947 [math.GT].

[58] HIKAMI K. DAHA and skein algebra of surfaces: double-torus knots[J]. Lett. Math. Phys., 2019, 109(10): 2305–2358. arXiv: 1901 . 02743 [math-ph]. DOI: 10.1007/s11005-019-01189-5.

[59] ALLEGRETTI D G L, SHAN P. Skein algebras and quantized Coulomb branches[J]. 2024. arXiv: 2401.06737 [math.RT].

[60] VOGT H. Sur les invariants, fondamentaux des équations différentielles linéaires du second ordre[J]. Annales Scientifiques de l'École Normale Supérieure. 3rd ser. 1889, 6: Suppl. 3–72.

[61] FRICKE R, KLEIN F. Vorlesungen über die Theorie der automorphen Funktionen. I[M]. Leipzig: Druck und Verlag von B. G. Teubner, 1897.

[62] JIMBO M. Monodromy problem and the boundary condition for some Painlevé equations[J]. Publ. Res. Inst. Math. Sci., 1982, 18(3): 1137–1161.

[63] IWASAKI K. A modular group action on cubic surfaces and the monodromy of the Painlevé VI equation[J]. Proc. Japan Acad. Ser. A Math. Sci., 2002, 78(7): 131–135. DOI: 10.3792/pjaa.78.131.

[64] IWASAKI K. Finite branch solutions to Painlevé VI around a fixed singular point[J]. Advances in Mathematics, 2007, 217: 1889–1934. arXiv: 0704.0679 [math.AG].

[65] KODAIRA K. On the structure of compact complex analytic surfaces, I[J]. American Journal of Mathematics, 1964, 86(4): 751–798.

[66] KODAIRA K. On the structure of compact complex analytic surfaces, II[J]. American Journal of Mathematics, 1966, 88(3): 682–721.

[67] NÉRON A. Modèles minimaux des variétés abéliennes sur les corps locaux et globaux[J]. Publications Mathématiques de l'IHÉS, 1964, 21: 5–128.

[68] ARGYRES P C, DOUGLAS M R. New phenomena in SU(3) supersymmetric gauge theory[J]. Nucl. Phys., 1995, B448: 93–126. arXiv: hep-th/9505062. DOI: 10.1016/0550-3213(95)00281-V.

[69] ARGYRES P C, PLESSER M R, SEIBERG N, et al. New N=2 Superconformal Field Theories in Four Dimensions[J]. Nucl. Phys., 1996, B461: 71–84. arXiv: hep-th/9511154. DOI: 10.1016/0550-3213(95)00671-0.

[70] OKAMOTO K. Studies on the Painlevé equations: I.-Sixth Painlevé equation P VI[J]. Annali di Matematica pura ed applicata, 1986, 146: 337–381.

[71] GUKOV S. Gauge theory and knot homologies[J]. Fortsch. Phys., 2007, 55: 473–490. arXiv: 0706.2369 [hep-th]. DOI: 10.1002/prop.200610385.

[72] MACDONALD I G. Affine Hecke algebras and orthogonal polynomials: vol. 157[M]. Cambridge University Press, 2003.

[73] SEIDEL P. Lagrangian two-spheres can be symplectically knotted[J]. Journal of Differential Geometry, 1999, 52(1): 145–171. arXiv: math.DG/9803083 [math.DG].

[74] SEIDEL P. Fukaya Categories and Picard–Lefschetz Theory[M]. Zurich: European Mathematical Society, 2008. DOI: 10.4171/063.

[75] BANKS T, DOUGLAS M R, SEIBERG N. Probing F theory with branes[J]. Phys. Lett. B, 1996, 387: 278–281. arXiv: hep-th/9605199. DOI: 10.1016/0370-2693(96)00808-8.

[76] SEN A. F-theory and Orientifolds[J]. Nuclear Physics B, 1996, 475(3): 562–578.

[77] SAHI S. Nonsymmetric Koornwinder polynomials and duality[J]. Annals of mathematics, 1999, 150(1): 267–282. arXiv: q-alg/9710032.

[78] TERWILLIGER P. The Universal Askey-Wilson Algebra and DAHA[J]. SIGMA, 2013, 9, 047: 047. arXiv: 1202.4673 [math.QA]. DOI: 10.3842/SIGMA.2013.047.

[79] NOUMI M, STOKMAN J V. Askey–Wilson polynomials: an affine Hecke algebra approach[J]. Laredo Lectures on Orthogonal Polynomials and Special Functions, 2004, 111: C144. arXiv: math/0001033 [math.QA].

[80] STOKMAN J V. Difference Fourier transforms for nonreduced root systems[J]. Selecta Mathematica, 2003, 9: 409–494. arXiv: math/0111221 [math.QA].

[81] MACDONALD I G. Orthogonal polynomials associated with root systems[J]. 1987. arXiv: math/0011046.

[82] STOKMAN J V. Macdonald-Koornwinder Polynomials[G]//Encyclopedia of Special Functions: The Askey-Bateman Project: Volume 2, Multivariable Special Functions. Cambridge University Press, 2020. arXiv: 1111.6112 [math.QA].

[83] CHEREDNIK I. Double affine Hecke algebras, Knizhnik-Zamolodchikov equations, and Macdonald's operators[J]. International Mathematics Research Notices, 1992, 1992(9): 171–180. DOI: 10.1155/S1073792892000199.

[84] CHEREDNIK I. Double affine Hecke algebras and Macdonald's conjectures[J]. Annals of mathematics, 1995, 141(1): 191–216. DOI: 10.2307/2118632.

[85] CHEREDNIK I. Macdonald's evaluation conjectures and difference Fourier transform[J]. Inventiones mathematicae, 1995, 122(1): 119–145. arXiv: q-alg/9412016 [math.QA].

[86] CHEREDNIK I. Non-symmetric Macdonald's polynomials[J]. International Mathematics Research Notices, 1995, 1995(10): 483–515. arXiv: q-alg/9505029 [math.QA].

[87] CHEREDNIK I. Double affine Hecke algebras[M]. Cambridge University Press, 2005.

[88] NOUMI M. Macdonald-Koornwinder polynomials and affine Hecke algebras [J]. Surikaisekikenkyusho Kokyuroku, 1995, 919: 44–55.

[89] Van DIEJEN J. Self-dual Koornwinder-Macdonald polynomials[J]. Invent. Math., 1996, 126(2): 319–339. arXiv: q-alg/9507033.

[90] SAHI S. Some properties of Koornwinder polynomials[J]. Contemp. Math., 2000, 254: 395–411.

[91] STOKMAN J V. Koornwinder Polynomials and Affine Hecke Algebras[J]. Int. Math. Res. Not., 2000, 19: 1005–1042. arXiv: math/0002090 [math.QA].

[92] ASKEY R, WILSON J A. Some basic hypergeometric orthogonal polynomials that generalize Jacobi polynomials: vol. 319[M]. American Mathematical Soc., 1985.

[93] SAHI S. Raising and lowering operators for Askey-Wilson polynomials[J]. SIGMA. Symmetry, Integrability and Geometry: Methods and Applications, 2007, 3: 002. arXiv: math/0701134 [math.QA]. DOI: 10.3842%2Fsigma.2007.002.

[94] OBLOMKOV A, STOICA E. Finite dimensional representations of the double affine Hecke algebra of rank one[J]. Journal of Pure and Applied Algebra, 2009, 213(5): 766–771. arXiv: math/0409256.

[95] CAYLEY A, SALMON G. On the triple tangent planes of surfaces of the third order[J]. Cambridge and Dublin Mathematical Journal, 1849, 4: 118–138.

[96] REID M. Undergraduate Algebraic Geometry: vol. 12[M]. Cambridge, UK: Cambridge University Press, 1988.

[97] SHAN P, XIE D, YAN W. Mirror symmetry for circle compactified 4d $\mathcal{N} = 2$ SCFTs[J]. 2023. arXiv: 2306.15214 [hep-th].

[98] SHAN P, XIE D, YAN W. Modularity for $\mathcal{W}$-algebras and affine Springer fibres [J]. 2024. arXiv: 2404.00760 [math.RT].

[99] FLOER A. Morse theory for Lagrangian intersections[J]. Journal of differential geometry, 1988, 28(3): 513–547.

[100] FLOER A. Witten's complex and infinite-dimensional Morse theory[J]. Journal of differential geometry, 1989, 30(1): 207–221.

Acknowledgements

不知不觉，在复旦物理系已经度过了将近三年的时光，这三年的经历对我的影响无疑是巨大的。我有幸遇到了许多良师益友，在他们的影响下，我渐渐成为了更好的自己。

首先，最应该感谢的一定是我的导师绳田聪，他是我科研生涯的第一位领路人，将我从一个小白引入我喜欢的领域。在与他相处的过程中，令我印象最深刻的是，在经过多年的科研生涯之后，他依然保留着对知识本身的兴奋和执着。这种对科研的纯粹的态度是少见的，激励着我更加努力去追求梦想。

其次，我要感谢张宇泰同学。他具有极强的物理数学直觉和对知识的理解能力，对隐藏在物理背后的数学结构的把握有着出众的天赋。他对本研究之中的许多关键性理解做出了首要贡献，我非常感谢他对我的许多困惑的耐心解答。

在三年的学习生活之中，我还要感谢许多优秀的同伴。首先我要感谢庄舒同同学，他不一定是学习速度最快的，但他非常善于思考不同问题之间的关联，力求对知识理解透彻。此外，他在面对困难时的冷静乐观的态度以及理智的思考能力让我钦佩。其次我要感谢郑嘉豪同学，他务实的科研态度、对知识本身的热情以及对细节的把控让我印象深刻。在三年的学习生活之中，他在很多方面都给我提供了悉心帮助，对此我深表感激。然后我要感谢江加群同学，他善于发现隐藏在公式背后的规律，对学习和生活都充满了热情，从他身上我学到了许多优秀的品质。我还要感谢我的室友贺彬，他最让我钦佩的地方是，尽管他拥有充沛的知识储备，但却能够始终保持谦逊的学习态度，与他交流的过程总是让人受益颇丰且如沐春风。感谢很多次他陪我在寝室讨论物理问题至深夜，这些讨论总是让我的收获巨大。

最后，我必须要感谢我的家人。没有他们对我任性的理想的支持，我不可能继续在科研的道路上走下去。

复旦大学
学位论文独创性声明

本人郑重声明：所呈交的学位论文，是本人在导师的指导下，独立进行研究工作所取得的成果。论文中除特别标注的内容外，不包含任何其他个人或机构已经发表或撰写过的研究成果。对本研究做出重要贡献的个人和集体，均已在论文中作了明确的声明并表示了谢意。本声明的法律结果由本人承担。

作者签名：_____ 日期：_____

复旦大学
学位论文使用授权声明

本人完全了解复旦大学有关收藏和利用博士、硕士学位论文的规定，即：学校有权收藏、使用并向国家有关部门或机构送交论文的印刷本和电子版本；允许论文被查阅和借阅；学校可以公布论文的全部或部分内容，可以采用影印、缩印或其它复制手段保存论文。涉密学位论文在解密后遵守此规定。

作者签名：_____ 导师签名：_____ 日期：_____